Investigation of Shadow Matching for GNSS Positioning in Urban Canyons

Lei Wang

Space Geodesy and Navigation Laboratory
Department of Civil, Environmental and Geomatic Engineering
University College London (UCL)
England
2015

Supervisors:
Doctor Paul Groves
Professor Marek Ziebart

Thesis submitted for the degree of Doctor of Philosophy

I, Lei Wang, confirm that the work presented in this thesis is my own. Where information has been derived from other sources, I confirm that this has been indicated in the thesis.

Signature: .....

Date: .....

Abstract

All travel behavior of people in urban areas relies on knowing their position. Obtaining position has become increasingly easier thanks to the vast popularity of 'smart' mobile devices. The main and most accurate positioning technique used in these devices is global navigation satellite systems (GNSS). However, the poor performance of GNSS user equipment in urban canyons is a well-known problem and it is particularly inaccurate in the cross-street direction. The accuracy in this direction greatly affects many applications, including vehicle lane identification and high-accuracy pedestrian navigation. Shadow matching is a new technique that helps solve this problem by integrating GNSS constellation geometries and information derived from 3D models of buildings.

This study brings the shadow matching principle from a simple mathematical model, through experimental proof of concept, system design and demonstration, algorithm redesign, comprehensive experimental tests, real-time demonstration and feasibility assessment, to a workable positioning solution.

In this thesis, GNSS performance in urban canyons is numerically evaluated using 3D models. Then, a generic two-phase 6-step shadow matching system is proposed, implemented and tested against both geodetic and smartphone-grade GNSS receivers. A Bayesian technique-based shadow matching is proposed to account for NLOS and diffracted signal reception. A particle filter is designed to enable multi-epoch kinematic positioning. Finally, shadow matching is adapted and implemented as a mobile application (app), with feasibility assessment conducted.

Results from the investigation confirm that conventional ranging-based GNSS is not adequate for reliable urban positioning. The designed shadow matching positioning system is demonstrated complementary to conventional GNSS in improving urban positioning accuracy. Each of the three generations of shadow matching algorithm is demonstrated to provide better positioning performance, supported by comprehensive experiments. In summary, shadow matching has been demonstrated to significantly improve urban positioning accuracy; it shows great potential to revolutionize urban positioning from street level to lane level, and possibly meter level.

Acknowledgments

First and foremost, I would like to express my greatest appreciation to my supervisors, Dr. Paul D Groves and Prof. Marek K Ziebart. I would like to greatly appreciate my primary supervisor Dr. Paul D Groves for his creative guidance, constructive criticism, and his kind willingness to give his time so generously in weekly meetings and many other unscheduled discussions throughout the 4-year course of my PhD research. I'm especially grateful for his encouragement when my research faltered. His serious attitude and enthusiastic passion towards conducting excellent academic research deeply impressed and influenced me. I am also very grateful to my secondary supervisor Prof. Marek K Ziebart for his intelligent insights into the use of 3D city models, his strategic view on research methods, his amazing talent on presentations, his very valuable suggestions, constant encouragement, and providing the funding opportunity to me, which made it possible that I could enjoy the wonderful and life-changing PhD journey at UCL.

I'm very grateful to both of my examiners, Associate Professor Xiaolin Meng from the University of Nottingham and Senior Lecturer Jan Boehm from UCL, for their kind generosity in voluntarily providing their precious time in reading and examining the thesis, and for their valuable and constructive comments that results in a better thesis.

Special thanks should be given to a few individuals: Dr. Claire Ellul for her constructive advice in my upgrade examination and throughout my PhD; Dr. Ziyi Jiang for kindly helping me adapting to the life in London and for his help and wisdom in many aspects of life; Christopher Atkins, Santosh Bhattarai, Kimon Voutsis, Henry Martin and Haraldur Gunnarsson for their help on experiments; Hira Virdee and Haraldur Gunnarsson for suggestions in English of my papers; Dr.

Stuart Grey for his advice on 3D model rendering; Dr. John Momoh for his advice on thesis writing; Dr. Mojtaba Bahrami and Dr. Peter Stacey for their advice on GNSS algorithm development; Dr. Joe Bradbury for his help on 3D model processing; Prof. Xiaohong Zhang from Wuhan University for his constant encouragement and valuable insights into my research, Prof. Ruizhi Chen from Texas A&M University Corpus Christi for his constructive suggestions on my papers; Dr. Xingwang Yu for his help on BeiDou Navigation Satellite System (BDS) and Galileo orbit simulation; Dr. Toby Webb, Chia-Yuan (Naomi) Li, Debbie Walter, Dr. Li-Ta (Q-mo) Hsu, and Han Gao for their help in many ways; Prof. Jiming Guo, Prof. Weiming Tang, Prof. Caijun Xu, Prof. Jianchen Li, Prof. Jingnan Liu, and Prof. Xiaoji Niu who are all from Wuhan University for their recommendations, guidance, constant encouragement and valuable advices; Jie Wu, Yanxin Yu and Kun Liu for wonderful friendship. Assistance on experiments provided by Liz Jones and Dietmar Backes is greatly appreciated. Assistance on administration and IT provided by Lee Phillips, Mike Dunderdale and his brilliant team, Sarah Davies and Liselot Hertel is also very much appreciated.

I also acknowledge and appreciate the support of my sponsor, the UCL Engineering Faculty Scholarship Scheme and the Chinese Scholarship Council.

I would like to thank every members of the Space Geodesy and Navigation Laboratory, who made me felt at home and enjoyed the PhD journey. I would also like to thank staff in Department of Civil, Environmental and Geomatic Engineering of UCL for their immense contributions and support in many ways.

Contents

List of Figures

Nomenclature

3DCM Three dementional city models

ADOP Along-street dilution of precision

AM Amplitude modulation

API Application programming interface

BDS BeiDou Navigation Satellite System

BTS Base Transceiver Station

CDOP Across-street dilution of precision

CityGML City Geography Markup Language

CPT Conditional probability table

DAB Digital audio broadcasting

DEM Digital elevation model

DOP Dilution of precision

DR Dead reckoning

DTM Digital terrain models

ECEF Earth-centred, earth-fixed

ETRS89 European Terrestrial Reference System 1989

GEO Geosynchronous Eearth Orbit

GIS Geographical information system

GLONASS GLObal Navigation Satellite System

GPS Global Positioning System

GSM Global System for Mobile Communications, originally Groupe Spécial Mobile

HDOP Horizontal dilution of precision

ICD Interface Control Document

ID Identity

IDC International Data Corporation

IGS International GNSS Service

IGSO Inclined Geosynchronous Orbit

IOC Initial operational capability

IOV In-Orbit Validation

IR Infrared

ITRF International Terrestrial Reference Frame

ITS Intelligent transportation systems

LBA Location-based advertising

LBS Location-based services

LiDAR Light detection and ranging

LoD Level of detail

LOS Line-of-sight

MEO Medium Earth Orbit

MEO Middle Earth orbit

MF Medium frequency

NLOS Non-line-of-sight

NMEA National Marine Electronics Association

OSGB-36 Ordnance Survey Great Britain 1936

pdf Probability density function

PND Portable navigation devices

POI Point-of-interests

RAIM Receiver autonomous integrity monitoring

RF Radio frequency

RNSS Regional navigation satellite systems

SBAS Space-based augmentation systems

SDE Software development environment

SLAM Simultaneous localization and mapping

SPP Standard point positioning

TASS Tactical Automated Security System

TDOA Time difference of arrival

TOA Time of arrival

TRF Terrestrial reference frames

TRSS Tactical Remote Sensor System

WGS-84 World Geodetic System 1984

WLAN Wireless local area network

WSN Wireless sensor networks

Chapter 1.

Introduction

1.1. Brief motivation

All travel behaviour of people in urban areas relies on knowing their position. Consequently, positioning technologies have a wide spectrum of applications in land navigation, intelligent transportation systems (ITS), location-based services (LBS) and wireless sensor networks (WSN) (Rizos and Drane, 1998; Lewis, 2004; Kwon et al., 2007; Groves, 2013). In a land navigation system, for example, in order to navigate a user to a destination, a navigation system must keep updating the user's position. Both vehicle and pedestrian navigation rely on positioning systems. ITS provides improved transportation network operations. Transportation network monitoring, for example, incorporates positioning technologies for localizing probes (i.e. each vehicle). Dedicated fleets of vehicles, including FedEx, UPS trucks, taxis, or buses may be tracked for transportation network monitoring (Kwon et al., 2007; Moore et al., 2001; Herrera et al., 2010). The monitoring can then contribute to other important functions of ITS, e.g. traffic control. Location-based services (LBS), a fast growing technology sector, connects users with services according to their geographical location (Schiller and Voisard, 2004). Positioning technologies are essential in LBS, which includes asset tracking, tour guiding, friend & family finding, emergency reporting, location based advertisement, etc.. Sensor position is essential in a wireless sensor network (WSN), which often uses low-cost, low-power smart sensors, networked in large numbers, to monitor and control physical conditions of homes,

cities, and the environments (Mao et al., 2007). WSN has been used in defence and surveillance area and other tactical applications (Chee-Yee and Kumar, 2003), and in monitoring of machines, animals, vehicles and medical conditions (Lewis, 2004).

Requirements for positioning technologies can be specified from numerous perspectives, including accuracy, integrity, continuity and availability, depending on specific applications (Hegarty and Chatre, 2008).

Obtaining position has become increasingly easier thanks to the vast popularity of mobile devices. Since the price drop of mobile phones in mid-1990s (Shoval, 2008), the popularity of mobile phones encouraged research using people's position by exploiting cellular signals using Cell ID (Trevisani and Vitaletti, 2004) or signal strength (Ratti et al., 2006). Wi-Fi positioning has emerged in mobile devices, thanks to the high density of Wi-Fi access points in metropolitan areas and the large number of Wi-Fi enabled devices (Zandbergen, 2009). This includes both urban positioning in metropolitan scale (Cheng et al., 2005) and indoor positioning (Liu et al., 2007) using Wi-Fi positioning techniques. However, open-space Global Positioning System (GPS) provides better accuracy than Wi-Fi and cellular positioning (Zandbergen, 2009).

GPS, as a subset satellite constellation of global navigation satellite systems (GNSS), has been widely used in many of the aforementioned applications in urban environments, including land navigation (Groves, 2013; Farrell, 2008), intelligent transportation systems (ITS) (Herrera et al., 2010), Location-based services (LBS) (Agrawal, 2009) and wireless sensor networks (WSN) (Lewis, 2004).

However, in dense urban areas, known as urban canyons, the poor performance of GPS positioning still occasionally causes problems in vehicle and pedestrian navigation, location-based advertisement and gaming, and other location-based services. This is mainly because where there are tall buildings or narrow streets, the direct line-of-sight (LOS) signals from many, sometimes most, of the satellites are blocked. This is illustrated in Figure 1.1. Although combining other satellite navigation systems, e.g. GLObal Navigation Satellite System (GLONASS), a satellite navigation system developed by Russia, improves GNSS positioning performance in urban canyons, an urban canyon also affects the geometry as well as the number of the

available GNSS signals. Signals with lines of sight going across the street are much more likely to be blocked by buildings than signals with lines of sight going along the street. As a result, the signal geometry, and hence the positioning accuracy, will be much better along the direction of the street than across the street (Groves, 2011).

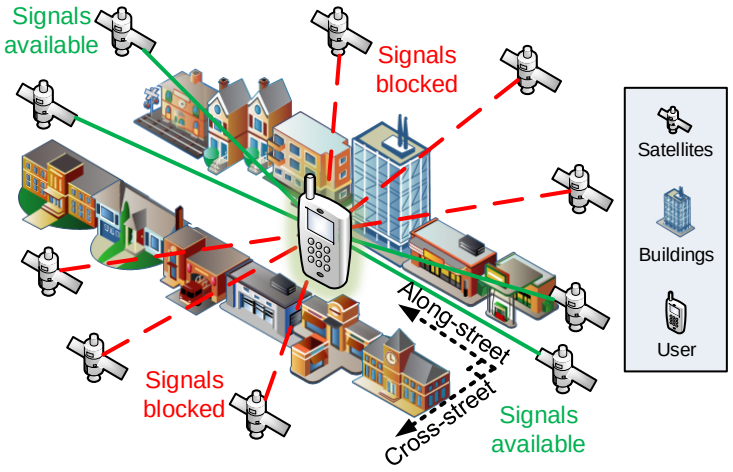

Figure 1.1.: Signal geometry of GNSS satellites in an urban canyon (aerial perspective)

Consequently, buildings in urban environments impose a vulnerability to low positioning accuracy in the cross-street direction. However, the positioning accuracy in this direction is vital to identifying traffic lanes for vehicles, and obtaining desired positioning performance for pedestrians, particularly when a user would like to know the correct side of the street. Identifying traffic lanes for vehicles is very important in many ITS applications, including driver's attention monitoring (McCall and Trivedi, 2004), lane departure warning (Kwon and Lee, 2002), and vehicle guidance (Heimes and Nagel, 2002; McCall and Trivedi, 2006). Knowing the correct side of the street for pedestrians can be important for step-by-step tour guiding for tourists and the visually impaired (Groves, Wang and Ziebart, 2012).

In order to improve navigation performance in highly built-up areas, a variety of navigation sensors have been used to enhance or augment GNSS. Typically, GNSS

is combined with map-matching algorithms and may be integrated with odometers for road vehicles. Whereas, for pedestrian users, GNSS may be combined with mobile phone signals, wireless local area network (WLAN, or Wi-Fi), inertial sensors, magnetic compass and barometers (Groves, 2013; Farrell, 2008). These multi-sensor approaches improve the robustness of the position solution, but do not meet the requirement for navigation in urban environments (Urmson et al., 2008), especially not the cross-street accuracy (demonstrated in Chapter 3).

Shadow matching is a new technique that helps solve this problem by integrating GNSS constellation geometries, information derived from 3D models of buildings and received signal strength and availability (Groves, 2011). This research therefore aims to use shadow matching in improvement of GNSS positioning accuracy in the across street direction, and, hopefully, enable some applications of GNSS that are now impractical.

The principle of shadow matching positioning was proposed (Groves, 2011), when the author's started the journey as a PhD researcher. There was no literature suggesting how such a principle of new positioning could be implemented in reality, which means this study needed to build a positioning system almost from scratch.

Thus the study first confirms GNSS's problem in urban areas from literature (Chapter 2) and from simulation (Chapter 3), then builds the fundamental architecture of the shadow matching technique (Chapter 4), after which focuses on improving two parts of the architecture where that are considered most important (Chapter 5 and Chapter 6), and finally adapts shadow matching for real-time scenarios and future practice (Chapter 7).

1.2. Objectives

The overall objective of this thesis is to explore the capability of a GNSS and Three dementional city models (3DCM) integrated positioning system, referred as shadow-matching system, in urban canyons. Five important issues are tackled in this thesis, namely the five main objectives. Detailed objectives of the report are summarised as follows:

1.2.1. Evaluation of GNSS positioning in urban environments

Can conventional GPS and GLONASS (using single-frequency pseudo-range measurements) meet the positioning requirements in urban environments? More specifically, in urban environments, how is the positioning performance different for pedestrians and vehicles, at traffic junctions and between junctions, and in the along-street and cross-street directions?

If GPS and GLONASS can not guarantee reliable positioning in urban canyons, does adding multiple constellations (Galileo and Beidou) solve this problem? In other words, can GNSS alone solve the positioning problem in urban canyons?

1.2.2. Shadow-matching system design

Following the principle of shadow matching, how to design a positioning system that uses knowledge of 3D city models, i.e. what are the different options in the overall design? What are the pros and cons of each of them?

1.2.3. Handling non-line-of-sight (NLOS) signals in shadow matching algorithm for urban environments

When signal reflection or diffraction occurs, how to handle the resulting mismatches between observation and predictions?

What is the optimum scoring scheme, given the constraints of the current visibility prediction algorithm, in a shadow matching algorithm for smartphones, and how to determine the parameters in this scheme?

1.2.4. Kinematic shadow matching algorithms

For kinematic applications, how to combine shadow matching information from multiple epochs to get a better position solution (particularly if

you have an ambiguous fix)?

How accurate positions can be obtained from kinematic shadow matching (compared with conventional GNSS and probability-based single-epoch shadow matching)?

1.2.5. Feasibility assessment of shadow matching techniques

Can the designed shadow matching algorithm run in real-time on a mobile device?

Is there a trade-off that has to be made between high efficiency and high accuracy?

Is it feasible to store enhanced map data for shadow matching on user's devices, or transmit over the mobile network? How much data storage is required per unit area?

How does the number of GNSS constellations impact shadow matching performance?

What is the shadow-matching performance difference between a smartphone versus a geodetic GNSS receiver?

1.3. Outline of thesis

This thesis consists of 8 chapters and one appendix and is organised as follows:

Chapter 2 first reviews a broad spectrum of location-related applications and discusses their requirements. Among these applications, land applications including land navigation, intelligent transportation systems (ITS), location-based services (LBS) and wireless sensor networks (WSN) are particularly discussed. This chapter then focuses on urban environments, presents advantages and limitations of GNSS-based and non-GNSS-based technologies in this context, which leads to the motivation for research on shadow matching, a new technique investigated in this work that complements conventional GNSS positioning.

Chapter 3 evaluates the performance of GNSS with 3D building models and verifies that stand-alone GNSS in urban canyons cannot provide reliable positioning solution, which agrees with the literature reviewed in Chapter 2. Simulation is conducted using an algorithm, with a visibility prediction model that considers both direct and diffracted signals, to quantitatively predict GNSS performance in urban areas using a 3D architectural city model. Experiments have been conducted to verify the simulation with real-world observations, and investigates the effects of diffraction modelling. The verified simulator was used to determine current and predict future GNSS performance in urban areas. Along-street and cross-street accuracy were also compared.

Chapter 4 presents possible options to design an algorithm that fulfills the shadow matching principle and discusses pros and cons of these options. A basic shadow-matching algorithm is designed and implemented. The implementation is then tested using both geodetic and smartphone grade GPS and GLONASS receivers. This chapter also acts as an entry point for the following chapters in the thesis on improvements of shadow matching algorithms.

Chapter 5 proposes strategies to handle non-line-of-sight (NLOS) signals in the shadow matching algorithm introduced in Chapter 4. Two rounds of improvements are investigated in this chapter. In the first round, signal visibility and diffraction in the scoring schemes are modelled against signal to noise ratio (SNR) by empirically setting thresholds. To improve this modelling, the smartphone GNSS signals should be better understood, thus a LOS/NLOS signal analysis with respect to SNR and elevations is then performed. This analysis inspires the second round of optimization, using Bayesian techniques, which leads to a probability-based shadow-matching algorithm. A comprehensive performance assessment is conducted to compare the probability-based shadow-matching algorithm in this chapter, the basic shadow-matching algorithm presented in Chapter 4 and conventional GNSS positioning using static smartphone GNSS measurements at 20 locations.

In Chapter 6, a new kinematic shadow-matching technique is presented. In this algorithm, pros and cons of different options of the position estimation schemes are discussed. Detailed algorithm descriptions of the selected scheme, a particle

filter, are then given. Real-world experiments are finally presented, comparing the performance between the conventional GNSS navigation solution, the single-epoch shadow-matching system solution as presented in Chapter 5, and the new kinematic shadow-matching system solutions.

Chapter 7 adapts shadow matching for practice from three aspects. The first aspect is whether the computation load of shadow matching is small enough for real-time positioning on resource limited mobile platforms, e.g. smartphones. For the first time, a smartphone-based real-time shadow matching positioning system is implemented as an Android application (app). The positioning performance of the real-time positioning system is assessed. The second aspect is to predict the future performance of shadow matching, in the context that emerging GNSS constellations, e.g. Galileo and BeiDou Navigation Satellite System (BDS), will be available by 2020. Quantitative predictions of future shadow matching performance from this perspective is also covered. The final aspect considers potential issues that may raise from large-scale deployment, including availability of 3D models, data storage and transfer requirements.

Appendix A describes an algorithm of line and triangle intersection determination that is used in this research, particular in Chapter 3.

1.4. Research output

1.4.1. Publications

JOURNALS

- Wang, L., Groves, P. D. and Ziebart, M. K. (2014), Smartphone Shadow Matching for Better Cross-street GNSS Positioning in Urban Environments. submitted to Journal of Navigation

- Wang, L., Groves, P. D. and Ziebart, M. K. (2013), GNSS Shadow Matching: Improving Urban Positioning Accuracy Using a 3D City Model with Optimized Visibility Scoring Scheme. Journal of Institute of Navigation, 60: 195–207. DOI: 10.1002/navi.38

- Wang, L., Groves, P. D. and Ziebart, M. K. (2012). Multi-Constellation GNSS Performance Evaluation for Urban Canyons Using Large Virtual Reality City Models. Journal of Navigation, 65, 459-476. DOI: 10.1017/S0373463312000082

CONFERENCE PROCEEDINGS

- Wang, L. (2014) Kinematic GNSS Shadow Matching Using a Particle Filter, Institute of Navigation (ION) GNSS+ Conference, Tampa, FL, USA

- Wang, L., Groves, P. D. and Ziebart, M. K. (2013) Urban Positioning on a Smartphone: Real-time Shadow Matching Using GNSS and 3D City Models, Institute of Navigation (ION) GNSS+ Conference, Nashville, TN, USA

- Wang, L., Groves, P. D. and Ziebart, M. K. (2013) Shadow Matching: Improving Smartphone GNSS Positioning in Urban Environments, Lecture Notes in Electrical Engineering, Proceedings of the Chinese Satellite Navigation Conference (CSNC), 245 (57), 613-621, Springer. DOI: 10.1007/978-3-642-37407-4_57

- Groves, P. D., Jiang Z., Wang L., Ziebart, M. K. (2012). Intelligent Urban Positioning, Shadow Matching and Non-Line-of-Sight Signal Detection, IEEE Aerospace and Electronic System Society Workshop, Netherland. DOI: 10.1109/NAVITEC.2012.6423047

- Wang, L., Groves, P. D. and Ziebart, M. K. (2012) GNSS Shadow Matching: Improving Urban Positioning Accuracy Using a 3D City Model with Optimized Visibility Prediction Scoring, ION GNSS 2012. Nashville, TA, USA

- Wang, L., Groves, P. D. and Ziebart, M. K. (2012) A Novel Solution to GNSS Navigation in Urban Canyons: Shadow Matching Using a 3D City Model, CSNC 2012, Guangzhou

- Wang, L., Groves, P. D. and Ziebart, M. K. (2011). GNSS Shadow Matching Using A 3-D Model of London. Proceedings of European Navigation Conference 2011, London, UK

MAGAZINES

- Wang, L., Groves, P. D., & Ziebart, M. K. (2013). Urban Positioning on a Smartphone: Real-time Shadow Matching Using GNSS and 3D City Models. Inside GNSS Magazine, 8 (6), 44-56 **(Cover Story)**
- Groves D. P., Wang L., Ziebart M. K. (2012). Shadow matching: Improved GNSS accuracy in Urban Canyons, GPS World, 23(2), 14 - 18 and 27-29 **(Cover Story)**

RELATED TOPICS

- Groves P. D., Wang L., Walter D., Martin H., Voutsis K., Jiang Z. (2014). Toward a Unified PNT Theory, Part I & II, The Four Key Challenges of Advanced Multisensor Navigation and Positioning, GPS World, 25(11), 25(12)
- Groves P. D., Wang, L., Walter D., Martin H., Voutsis K., Jiang Z. (2014) The Four Key Challenges of Advanced Multisensor Navigation and Positioning, IEEE/ION PLANS 2014 Conference, Monterey, CA, USA
- Groves, P. D., Martin H., Voutsis K., Walter D., Wang L. (2013) Context Detection, Categorization and Connectivity for Advanced Adaptive Integrated Navigation, ION GNSS+ 2013. Nashville, TN, USA
- Groves, P. D., Jiang Z., Wang L., Ziebart, M. K. (2012). Intelligent Urban Positioning (IUP) using Multi-Constellation GNSS with 3D Mapping and NLOS Signal Detection, ION GNSS, Nashville, TN, USA

1.4.2. Selected awards

- Student Paper Award, Sept 2014, Institute of Navigation GNSS+ Conference, Tampa, USA
- Best Paper Award (second author) in the Position Location and Navigation Symposium (PLANS), May 2014, Institute of Navigation (ION)/IEEE, Monterey, USA

- Best Presentation in Session Award , Sept 2013, Institute of Navigation GNSS+ Conference, Nashville, USA
- Young Scholars Award, May 2013, Chinese Satellite Navigation Conference (CSNC), Wuhan, China
- Best Presentation Award, Jun 2012, New Navigators Seminar, Royal Institute of Navigation (RIN), UK

1.4.3. Contribution to knowledge

There are a number of advances of this research compared with other investigations. The following contributions to knowledge are some major ones of them:

1. Chapter 3 (Wang et al., 2012*b*) firstly quantitatively verified that GNSS performance in urban canyon is worse in cross-street direction compared with along-street direction by simulating all four GNSS constellations (GPS, GLONASS, Galileo and Beidou) and verified with experiments. A number of other advances are detailed in Chapter 3.
2. A first demo and performance assessment of shadow matching by scoring candidate positions was implemented and published in Wang et al. (2011), more details can be found in Chapter 4.
3. A first implementation of a grid-based shadow matching is demonstrated and experimentally tested in Wang et al. (2012*a*), with details covered in Chapter 4.
4. Chapter 5 (Wang et al., 2014) independently proposed a signal strength-based Bayesian technique to train parameters in LOS/NLOS scoring schemes using large sets of experimental data, and comprehensively assessed shadow matching using a large set of data.
5. Chapter 6 (Wang, 2014*b*) independently proposed using a particle filter for kinematic shadow matching .

6. Among the literature, only Chapter 7 (Wang et al., 2013*c*) implemented a real-time demo of a shadow matching algorithm, which benefits partly from a system design of pre-processing 3D building models to generate building boundaries and partly from the optimization in the real-time Android application. This investigation is further described in Chapter 7, along with other advances;

7. Only the author's work experimentally tested shadow matching using both smartphone grade (Wang, 2014*b*; Wang et al., 2013*b*, 2014) and geodetic grade (Wang et al., 2011, 2012*a*) GNSS receivers, while others only use geodetic grade receivers.

Chapter 2.

Background

Localization in unfamiliar environments is commonly required in many application contexts. This chapter reviews a number of these applications and discusses their requirements for positioning systems and viable positioning technologies. Among these technologies, those using global navigation satellites are focused on, with a particular interest in their performance in urban environments. In addition to satellite positioning, characteristics of other positioning techniques commonly used for urban positioning are then reviewed. The limitations of the current performance of these positioning techniques motivates this investigation on 'GNSS shadow matching'.

A broad spectrum of location-related applications is introduced in Section 2.1, with emphasis on the role of the positioning system and the requirements for it. Section 2.2 reviews current GNSS positioning performance and problems in urban canyons. Other positioning methods, incorporating different sensors and data sources, are compared for their advantages and limitations in Section 2.3.

2.1. Application and requirements of land positioning technologies

Positioning technologies have a wide variety of applications in land navigation, intelligent transportation systems (ITS), location-based services (LBS) and wireless sensor networks (WSN) (Rizos and Drane, 1998; Lewis, 2004; Kwon et al., 2007;

Groves, 2013). People's activities are often dependent on knowing their locations. Yet, for hundreds of years, positioning methods stayed inaccurate, expensive and complex. However, development of wireless, electronics and information technologies has allowed a variety of location related services to improve quality of life (Agrawal, 2009). Location related services rely on positioning technologies in order to operate.

Requirements for positioning technologies can be specified from numerous perspectives, including accuracy, integrity, continuity and availability (Hegarty and Chatre, 2008). Different communities may use these terms to refer to different means in accordance with a specific context. Typical conventions within the navigation community are adopted in this thesis. A brief definition of each term is given here; for more detailed explanations and methods for computation, refer to Syrjarinne and Wirola (2008). Accuracy is probably the most used criteria which describes the error of a measured or estimated position with respect to the unknown true position. Integrity expresses on what level can the positioning system be trusted. Continuity is used to describe the reliability of the positioning system, which can be lost in cases of signal blockage or system fault. Availability describes the likelihood that the accuracy, integrity and continuity meet their requirements, depending on each application.

The requirements of these criteria for positioning technologies depend significantly on the specific application. For example, the 'accuracy' requirement varies from a few meters for a pedestrian navigation user, to a few hundred meters for cellular mobile advertising. From the perspective of integrity and robustness, airplane navigation requires much better performance than buses.

As well as varying between applications, requirements also vary with respect to the time frame of a given application. For instance, a vehicle navigation user requires a better heading solution when it is at a road junction than between junctions. This is because when a vehicle is at a junction, its direction can change significantly; whereas when it is between junctions, its direction is very unlikely to change. Another example would be an aeroplane also requires a much better overall positioning performance when landing or taking off than flying on course.

Among the aforementioned broad spectrum of applications, land applications for mobile devices are the major concern of this study. Thus, land navigation, intelligent transportation systems (ITS), location-based services (LBS), wireless sensor networks (WSN) are briefly introduced. In each application, the desired positioning performance and available positioning technologies are reviewed.

2.1.1. Positioning technologies in land navigation

A positioning system is a key component in a land navigation system. In order to navigate a user to a destination, a navigation system must keep updating the user's position. The updated user location is then used for decision making to navigate the user along the next part of the route. Requirements for a land navigation system vary for different navigation users. Land navigation using mobile devices can often be classified into two categories: vehicle navigation and pedestrian navigation.

Vehicle and pedestrian navigation have significantly different demands on positioning technologies. Vehicle navigation, which is relatively mature, is mostly outdoor. Research has shown that both motion constraint models (Dissanayake et al., 2001) and geometric road constraint models of vehicles can be used to improve positioning performance (Syed and Cannon, 2004). By contrast, a pedestrian may be both indoor and outdoor, on a road or a pavement, making it more difficulty to use constraint models to assist positioning (Gaisbauer and Frank, 2008). A pedestrian on a bus or car is classified as a vehicle user in this case. Furthermore, vehicle and pedestrian navigation also requires different scopes of operation. This difference results from the fact that pedestrians may demand indoor positioning while vehicles do not.

In terms of available positioning technologies, GNSS is often used in land navigation applications, thanks to its global 24-hour positioning capability. For example, in terms of positioning accuracy, GPS provides meters level accuracy in open sky areas (USA, 2014). To improve the positioning performance when GNSS blockage happens, a variety of navigation sensors can be used to augment GNSS. Road vehicles typically combine GNSS with odometers and map-matching, while pedestrians may combine GNSS with phone signals, Wi-Fi, Bluetooth Low Energy and/or dead

reckoning using inertial and magnetic sensors (Groves, 2013; Farrell, 2008).

2.1.2. Positioning technologies in Intelligent Transportation Systems (ITS)

Intelligent transportation systems (ITS) provide improved transportation network operations. According to a definition by the World Road Association, major functions of ITS network operations are network monitoring, maintaining road serviceability and safety, traffic control, travel aid and user information, and demand management (Miles et al., 2000).

Transportation network monitoring, for example, incorporates positioning technologies for localizing probes. Before the era of mobile internet, traffic monitoring relied heavily on static loop detectors, cameras, and radars (Herrera et al., 2010). The increased popularity of mobile phones enabled mobile phone equipped drivers to be treated as moving probes using cellular positioning technologies (Ygnace, 2011). GPS positioning was also investigated as a source of data for traffic monitoring by many research groups (Zito et al., 1995; Hall et al., 1996). Field tests have concluded that cellular phone tracking technologies provide less accurate positions (66% of the 3,756 probes had one or more points outside of a 200-meter accuracy range), whereas GPS provides much better accuracy (15 meter accuracy for 95% of the measurements); thus, GPS is more suitable for providing long sequences of time and position with high accuracy (Yim and Cayford, 2001). More specific research and tests have then been performed using dedicated fleets of vehicles equipped with GPS or automatic vehicle location (AVL) technology, including FedEx, UPS trucks, taxis, or buses (Kwon et al., 2007; Moore et al., 2001; Herrera et al., 2010). With the increasing popularity of smartphones equipped with GPS, GPS on smartphones are demonstrated to provide a real-time and accurate yet cost-effective way to monitor traffic information, leveraging existing cellar network for internet connectivity (Herrera et al., 2010). Differential GPS may further meet the demand of better accuracy in traffic monitoring (Jones et al., 1999). For example, Yim and Cayford (2001) found that in open sky environments, using consumer-grade GPS receivers, differential GPS offers 5 meter better accuracy than stand alone GPS, which has

15 meter accuracy, for 95% of the measurements. These studies have shown that with either sufficient number of traffic fixed detectors (e.g. loop detectors, cameras) or probes (e.g. GPS enabled devices), positioning technologies can supply sufficient information for traffic network monitoring, which is an essential function of ITS and contribute to other functions of ITS, e.g. traffic control.

2.1.3. Positioning techniques in location-based services (LBS)

Positioning technologies have a variety of applications in location-based services (LBS), including asset tracking, tour guiding, friend & family finding, emergency reporting, etc.. LBS, a fast growing technology sector, connects users with services according to their geographical location (Schiller and Voisard, 2004). Positioning systems, incorporating information technologies, communication technologies, wireless technologies, geographical information system (GIS), and mobile human-computer interaction, enable services to be performed to suitable potential customers (Brimicombe, 2010). Some examples of location-based services are categorized in Figure 2.1.

Positioning technologies have their technical characteristics, and thus limitations, refining them to certain location-based applications. The characteristics of commonly used positioning techniques are reviewed in Sections 2.2 and 2.3. Different applications have various requirements for positioning systems (D'Roza and Bilchev, 2003; Mountain and Raper, 2001). In location based games, for example, a positioning engine is used to enhance the game experience for players; thus, the requirements to positioning technologies are unique from other location based applications. Typically, for the purpose of embedding a virtual scene in the real world, three parameters are necessary: a coordinate of the device, the azimuth (direction) the device is facing, and the orientation (relative to the ground) (You et al., 2008). Thus, mobile augmented reality and multi-sensor data fusion (e.g. accelerometer, gyroscope and digital compass) are often used together to provide attitude with location, in location based games (Broll et al., 2008; Benford et al., 2004) and virtual reality gaming,

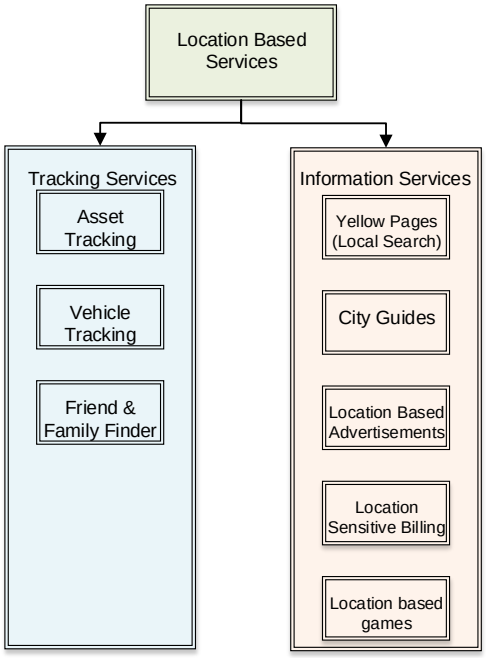

Figure 2.1.: Examples of the location based services. After: Agrawal (2009)

e.g. Oculus Rift (Luckey, 2014). In location based advertisement, however, accuracy requirements are variable from a few meters to hundreds of meters (Rashid et al., 2005). Many positioning techniques, including cellular phone positioning techniques, GPS, Bluetooth (Rashid et al., 2008), Bluetooth 4.0 and Wi-Fi (ILA, 2014) have been used in implementations of location based advertisement systems.

2.1.4. Positioning technologies in Wireless Sensor Network (WSN)

The development of wireless sensor networks (WSN) enables low-cost, low-power smart sensors, networked in large numbers, to monitor and control physical conditions of homes, cities, and the environments (Mao et al., 2007). WSN can be used in defence and surveillance area and other tactical applications (Chee-Yee and Kumar, 2003), including the Tactical Automated Security System (TASS) (Butler, 2002) and the Tactical Remote Sensor System (TRSS) (Lee et al., 2009). It has also been applied in monitoring of machines, animals, vehicles and medical conditions (Lewis,

2004).

Research has shown that, in some cases, for example, cellular network and wireless local area network (WLAN) can provide sufficient accuracy in WSN (Gustafsson and Gunnarsson, 2005; Guolin et al., 2005). Many outdoor WSN applications typically can accept an accuracy of 50 meters, while indoor applications require an accuracy of a few meters (Sayed et al., 2005). However, some other positioning techniques, including sensor fusion, may increase the quality of positioning in WSN, and thus enable more services, e.g. emergency call services with accurate location information (Gustafsson and Gunnarsson, 2005).

2.2. GNSS positioning in urban areas

The acronym 'GPS' is often used to refer any global navigation satellite systems. However, the word GPS should only be used to refer the global positioning system (GPS) operated by the United States. In this study, global navigation satellite systems (GNSS) is used instead to refer any global navigation satellite systems. Thanks to the fact that GNSS users can leverage free signals from satellites launched and maintained by various countries and organizations, GNSS positioning has been successfully and widely applied into many land applications. GNSS user equipment provides accurate positioning solutions with 24-hour availability and global coverage. GNSS often provides sufficient positioning accuracy in most open space, but has limitations in other environments, especially in urban environments (Montillet et al., 2007, 2009). This section reviews the current status of GNSS and then focuses on its performance in urban environments, which is of particular interest in this study.

2.2.1. Current GNSS status

GNSS consists of four constellations: GPS, GLONASS, Galileo and BDS; they are developed by United States, Russia, Europe Union and China, respectively. Some regional navigation satellite systems (RNSS) and space-based augmentation systems (SBAS) have been developed to boost satellite positioning in certain regions.

GPS is the most popular GNSS, because it was the first GNSS in full operation with 24 satellites (Block I/II/IIA), back to 1993 . Maybe equally importantly, GPS has been continuously updated, for example, by the modernization plan proposed in 1999 (Hofmann-Wellenhof et al., 2007). As a result, GPS has been pervasively adopted in many location-based applications. It has a minimum 24 satellite configuration to ensure there are at least four satellites, the minimum number of satellites to positioning, in view from any location on Earth. However, effectively, GPS now operates a 27-slot constellation, giving improved coverage throughout the world. In fact, There are normally even more than 27 operational satellites. For example, on 24th March 2012, there are 31 satellites in operation. Further details about GPS performance and specifications can be found in the official documents (USA, 2014). In addition, the modernization process continuously improves the performance of GPS. Figure 2.2 shows that the GPS signal-in-space user range error has decreased in the last 13 years. The signal-in-space user range error is the difference between a GPS satellite's navigation data (position and clock) and the truth, projected onto the line-of-sight to the user, as defined by (USA, 2014).

GLONASS is a Russian GNSS that is also currently in fully operational. There is also undergoing progressive renewal and modernization, resulting from substantial growth in Russia's economy. Satellite orbit information provided in navigation messages for GLONASS is in the Parametrop Zemp 1990 (PZ90.02) datum. The current GLONASS has a 24 satellite constellation; the latest status can be found on the official website (RussianFederalSpaceAgency, 2014).

Galileo, an emerging GNSS developed by the European Space Agency (ESA), has just finished the In-Orbit Validation (IOV) phase, and is getting into the initial operational capability (IOC) phase. The first two navigation satellites, GIOVE-A and –B were launched in 2005 and 2008. The first two of four operational satellites were launched on 21 October 2011. More detail can be found on the official Galileo website (EU, 2014).

BDS is the other emerging GNSS that plans to operate a constellation of 35 satellites by 2020. In August 2014, there are 16 satellites in orbit, consisting 6 Geosyn-

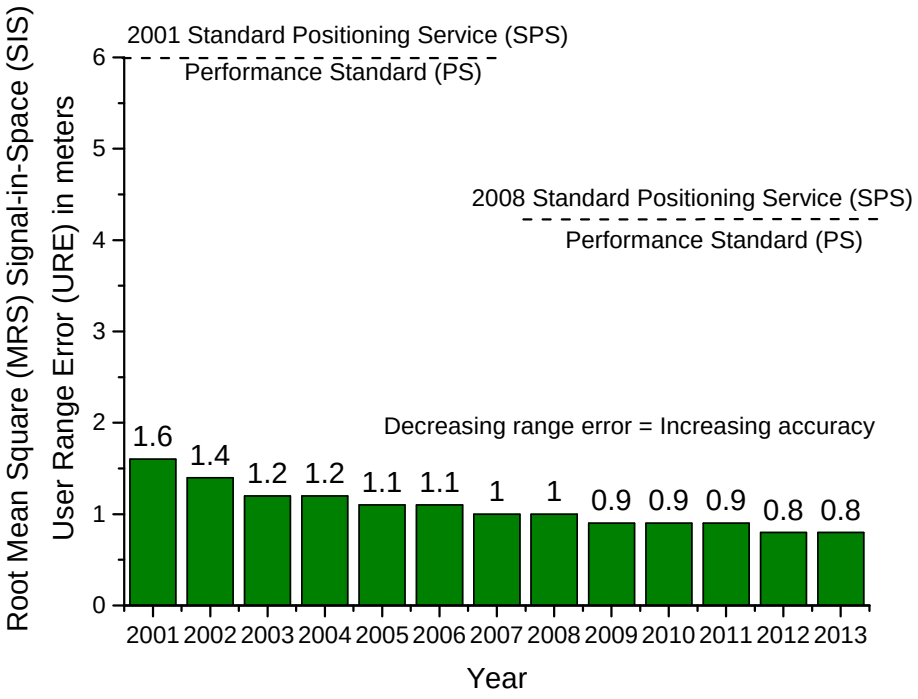

Figure 2.2.: GPS standard positioning service (SPS) signal-in-space performance, based on USA (2014)

chronous Earth Orbit (GEO) satellites, 5 Medium Earth Orbit (MEO) satellites and 5 Inclined Geosynchronous Orbit (IGSO) satellites, noting that GEO satellites only offers a regional service. The BDS navigation satellite system signal in space interface document was released in December, 2012. Detail of current status can be found on its official website (China, 2014).

2.2.2. Limitations of GNSS in urban canyons

Although GNSS is rapidly developing globally, as presented in the Subsection 2.2.1, there are certain GNSS-challenged environments where GNSS cannot provide sufficient performance. Deep indoors, underwater and tunnels are examples of where GNSS can be fully blocked; indoor/outdoor transition areas and urban canyons are challenged locations for GNSS. Amongst these locations, urban areas are of particular interest in this study. This is because both the rapid urbanizing process in many countries, and the increasing popularity of GPS-equipped mobile devices,

have boosted demands of location related applications in urban areas, as reviewed in Section 2.1.

In dense urban areas, known as urban canyons, the poor performance of GNSS positioning has remained a major problem in positioning. At least four satellites are required in view to compute a positioning solution; this is mainly because the user position has three dimensions that require three satellites in view, and the GNSS receiver clock suffers a considerable error that must be corrected using an additional satellite. Thus, four satellites are required to form a positioning solution using GPS satellites. Involving an extra satellite constellation (e.g. GLONASS) may require an extra satellite to estimate system time difference to complete a navigation solution, depending on the positioning strategy. GNSS constellations now can normally satisfy these basic requirements in open sky locations. However, in urban canyons, tall buildings block, reflect and diffract satellite signals. As a result, at some locations, there are insufficient signals for a navigation solution; while in other locations, a solution can only be formed if non-line-of-sight (NLOS) signals or multipath signals are used.

NLOS reception and multipath interference are the main sources that degrade GNSS accuracy significantly in urban canyons (Misra and Enge, 2010). Sometimes they are grouped together as 'multipath', but they are actually different phenomena that impose errors of different characteristics in a positioning solution. An NLOS signal appears when the direct line-of-sight signals are blocked; only a reflected signal is received; while multipath appears when both the direct line-of-sight signal and reflected signals are received. Their concepts are illustrated in Figure 2.3.

An NLOS signal exhibits significant positive biases, because the length of the path is always increased by reflection. Although typically the error is tens of meters, it is potentially unlimited. Multipath contaminates the direct signal by distorting the correlation peak in the correlation process in the receiver. The code tracking error, for example, can be up to half a code chip (GPS C/A code chip is about 150m). Thus, both NLOS and multipath impose significant bias in positioning using C/A code. Although there are many methods for correcting NLOS reception (Morrison et al., 2006; Ercek et al., 2005, 2006) and multipath interference (Jiang et al., 2011;

Groves et al., 2010; Farret et al., 2010; Nedic, 2009; Meguro et al., 2009; Viandier et al., 2008; Groves et al., 2013; Dodson et al., 2001; Roberts et al., 2002), they are difficult to be eliminated. In urban areas, NLOS and multipath mitigation can be assisted by using image or vision based augmentation technologies, which are transferred from mobile robot navigation or unmanned aerial vehicle navigation to land vehicle driving assistance (Heimes and Nagel, 2002; Enkelmann, 2001; Campoy et al., 2009; Bingham and Veth, 2009; Farley et al., 2008). For example, NLOS can be detected using an omnidirectional infrared (IR) camera (Meguro et al., 2009; Suzuki et al., 2011), or a fish-eye camera (Suzuki and Kubo, 2014) in urban areas. By detecting building boundaries, the image acquired from the camera is used to predict visible satellites and compare with received signal to mitigate NLOS.

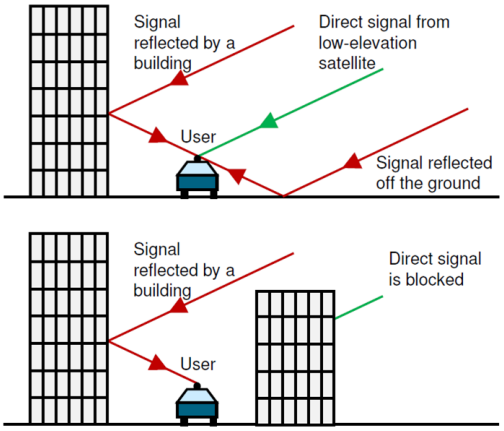

Figure 2.3.: A non-line-of-sight (NLOS) signal (bottom) and multipath signals (top) based on source: Groves (2013)

Many approaches can help increase GPS positioning performance. In this study, only those methods that are practical from the perspective of a user device are considered, rather than the whole navigation system including the space and control segments. Some solutions using stand-alone GPS but with assistance information (e.g. orbit and time information), high sensitivity or multipath interference mitigation are proved to help GPS positioning in urban canyons or indoor (Misra and Enge, 2010). However, the blockage caused by high buildings still increase vulnerability to stand-alone GNSS, preventing 24-hour reliable positioning in urban canyons, and

even worse indoors (Ji et al., 2010). More details about GNSS satellite positioning performance in urban canyons, especially accuracy and availability, can be found in Chapter 3. This accuracy and availability problem is simply because there are frequently not enough 'clean' signals from satellites to form a navigation solution in the challenging environments, i.e. deep urban canyons. Thus, GPS positioning performance in urban canyons needs improvement.

Besides GPS, GLONASS has increasingly become widely used by mobile devices to improve accuracy and integrity in recent years, because of its modernization in the last decade (refer to Subsection 2.2.1 for more detail). The emerging Galileo and Compass satellite systems, developing by European Union and China respectively, will present the opportunity to boost GNSS performance by adding more satellites in view (more details to be discussed in Chapter 3). This improvement is because generally, the more satellites in view, the more satellite positioning knowledge can be contributed to the positioning engine, and thus the more accurate the solution should be.

However, an urban canyon affects the geometry as well as the number of visible GNSS signals. Poor satellite geometry means the distribution of satellites in the sky is not optimized for similar positioning accuracy in all directions. For example, if most satellites are distributed in a line, then it is called poor satellite geometry, and the accuracy of GNSS positioning perpendicular to the line is much lower than that along the line. In urban canyons, signals with lines of sight going across the street are much more likely to be blocked by buildings than signals with lines of sight going along the street (refer to Chapter 3 for more detail). Thus the GNSS positioning accuracy in the cross-street direction is much lower than it in the along-street direction. This is also illustrated by Figure 1.1, and proven by pedestrian and vehicle simulations in Chapter 3.

2.3. Other related positioning techniques: advantages and limitations

In order to improve GNSS navigation performance in highly built-up areas, a variety of other positioning techniques, sensors and data sources have been used to enhance or augment GNSS positioning (Brimicombe, 2010). The range and accuracy of various signal based positioning technologies are compared in Figure 2.4. Road vehicles typically combine GNSS with odometers, and map-matching algorithms, while pedestrian navigation users may combine GNSS with mobile phone signals, Wi-Fi and/or dead reckoning using inertial sensors, magnetic compass and barometric altimeter (Groves, 2013; Farrell, 2008). This section briefly introduces research integrating these technologies and finds their limits in terms of cross-street positioning accuracy.

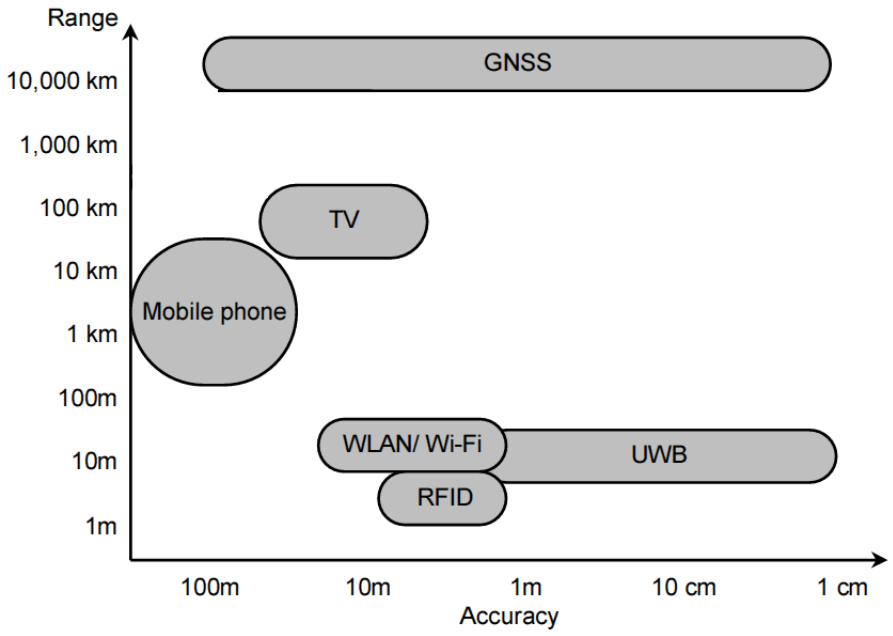

Figure 2.4.: Range and accuracy of signal-based positioning technologies for land positioning applications. Adapted from source: Groves, Ziyi, Wang and Ziebart (2012)

2.3.1. Map matching

Map matching integrates positioning solution from a positioning system with a digital road network to augment the performance of the positioning system (Quddus et al., 2007). Map matching has proven improved availability (Cui and Ge, 2003) and accuracy (Quddus et al., 2003) of the overall positioning solution.

Although it has been applied in pedestrians (Bernstein and Kornhauser, 1998; White et al., 2000), it is more often used in vehicles navigation (Greenfeld, 2002). For example, map matching has been used to improve lane-departure-warning, collision warning, and other vehicle safety systems (Joshi, 2001). In terms of the positioning technology, GNSS is often used in the vehicle positioning system (Greenfeld, 2002). Since dead reckoning (DR) using an odometer and magnetic sensors has been commonly used in vehicle navigation (Syed et al., 2008), research has also been conducted to explore application of map matching to enhance performance of such a GPS/DR positioning system (Krakiwsky et al., 1988) that integrates GPS and dead reckoning data, and a spatial digital database of the road network. Furthermore, road surface height information from a 3D city model/map has also been considered in the positioning engine to improve the position solution (Groves and Jiang, 2013).

Many algorithms have been applied in map matching. In order to integrate these information, a Kalman filter (Krakiwsky et al., 1988; Quddus et al., 2003) or a particle filter (Davidson et al., 2011) may be used. According to Quddus et al. (2007), there are at least 35 map matching algorithms published during the period 1989-2006.

Some literature focus on map matching in urban canyons, because of the difficulty of map matching in urban canyons where buildings block, reflect and diffract GPS signals. Various algorithms have been proposed. For example, Syed and Cannon (2004) proposed an algorithm based on fuzzy logic to cope with inaccurate measurements in urban areas; Zhang et al. (2007) proposed a map matchign algorithm that considers historical information, using road traverses and linear heading-change model, showing a better performance in urban canyons.

2.3.2. Wi-Fi positioning system

Wireless local area network (WLAN) technology, also known as Wi-Fi and IEEE 802.11, provides computer networking at radio frequencies around 2.4 and 5 GHz. Wi-Fi positioning has been emerged in mobile devices, thanks to the high density of Wi-Fi access points in metropolitan areas and the large number of Wi-Fi enabled devices (Zandbergen, 2009). This includes both urban positioning in metropolitan areas (Cheng et al., 2005) and indoor positioning (Liu et al., 2007) using Wi-Fi positioning techniques. However, tested over a number of sites, it is suggested that open-space GPS provides better accuracy than Wi-Fi and cellular positioning (Zandbergen, 2009).

There are generally two methods used in WLAN positioning: timing-based methods and signal-strength-based methods. In timing-based WLAN positioning, signals are normally measured and used for positioning at time of arrival (TOA). In situations where the access points in WLAN have unsynchronized clocks, another method using time difference of arrival (TDOA) measurement are often used. Generally, timing-based WLAN positioning methods exhibits relatively poor accuracy. This is mainly because timing resolution in WLAN is limited and, received signals are often subject to attenuation and reflection, especially in complex urban and indoor environments (Bensky, 2008). The basic service set identification (BSSID) is the MAC address of the Wi-Fi access point that can be used to identify each Wi-Fi access point. In both the timing-based and signal-strength-based methods, BSSID should be used to identify Wi-Fi access points.

Fingerprinting is the most widespread positioning technique used for high-accuracy ($<$ 5m) WLAN positioning technique (Bensky, 2008; Groves, 2013). The fundamental principle of fingerprinting is that the signal strength varies in different locations in an area covered by Wi-Fi signals, as illustrated in Figure 2.5. Signal strengths from different access points are highly related to the location of a Wi-Fi receiver.

There are two phases in Wi-Fi fingerprinting positioning. In the first phase, often called the survey phase or offline phase, a received signal strength fingerprint database is created over a grid mapped to the coverage area. In the second phase, which is often called the online phase, a positioning solution is made based on

comparison between real-time received signal strength with the signal strength map in the database.

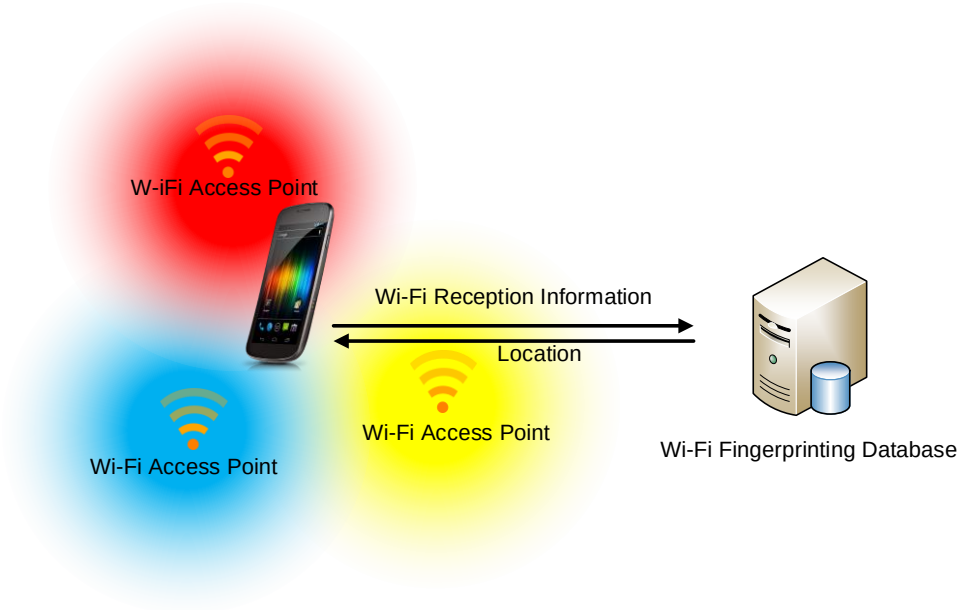

Figure 2.5.: Signal strengths from Wi-Fi access points vary according to locations

There are a few methods for fingerprint positioning based on database comparison. Two commonly known methods of them are database comparison by nearest neighbour search and Bayesian inference RSS location method. In the nearest neighbour algorithm, when matching the real-time Wi-Fi measurements with the pre-surveyed database, the estimated difference between the true position and each pre-surveyed location is determined by the difference of each of the received signal strength vectors (Bensky, 2008). The pre-surveyed location with the least difference is regarded as a best match, thus is deemed as the positioning solution. In the other method, i.e. the Bayesian inference RSS location method, a probability function is maximized at the positioning solution using Bayes' rules that express the relation ship between a prior and a posterior probabilities (Ito and Kawaguchi, 2005; Roos et al., 2002; Ladd et al., 2002). Detail of Bayesian filters that uses the Bayes' rules can be found in Chapter 6. Further detail of the mentioned Wi-Fi positioning methods can be

found in Bensky (2008).

2.3.3. Multi sensor and multi data source integration

In order to improve positioning performance, an increasing number of data sources can be integrated into a positioning system. An integrated positioning system may combines a set of sensors, including inertial measurement units (IMU), odometers, magnetometers, baro-altimeters, compact radio frequency (RF) motion sensors, and other sensors in addition to GNSS, to enhance positioning in dense urban areas (Godha and Cannon, 2007; Groves, 2013; Farrell, 2008; Zhou et al., 2009; Georgy et al., 2010; Farley et al., 2008; Groves et al., 2007).

Vision sensors have also been integrated for positioning. Light detection and ranging (LiDAR) can be used to capture urban 3D data (Boehm, 2009), and has proved able to provide independent positioning solution in urban environments, when integrated with 3D images and low-cost IMU (Susca and Inst, 2010). The LiDAR/IMU integrated system is reported to provide horizontal error of less than 10 meters, although a drawback being that a LiDAR system may be expensive. Location of buildings in georeferenced images has been determined using 3D CAD models, joint with low-cost GPS and a digital compass (Haala and Böhm, 2003).

Since the price drop of mobile phones in mid-1990s (Shoval, 2008), the popularity of mobile phones encouraged research on tracking people's positioning exploiting cellular signals using Cell ID (Trevisani and Vitaletti, 2004) or signal strength (Ratti et al., 2006). Simulations in a mobile positioning system based on Global System for Mobile Communications (GSM, originally Groupe Spécial Mobile) signals shows a 49 meter error with 4 GSM Base Transceiver Stations (BTS), and 26 meter error with 5 GSM BTS (Azaro et al., 2008).

Map matching can be considered as an integration of digital road network data and a positioning system, as reviewed in Subsection 2.3.1.

The inclusion of additional ranging signals transmitted from pseudolites (the term is derived from pseudo-satellite), ground-based generators and transmitters of GPS-like signals (Novakovic et al., 2009; Lei, 2009) has also been studied to enhance stand-alone GNSS. Commercial pseudolite positioning systems that are designed for

urban positioning include Locata (Barnes et al., 2003) and NextNav (Meiyappan et al., 2013). However, they are more expensive than smartphone-grade GNSS receivers.

Signals that are designed for purposes other than navigation has also been applied into positioning. These signals are thus named signal of opportunity. For example, digital audio broadcasting (DAB) signals (Palmer et al., 2011), TV signals (Rabinowitz and Spilker Jr., 2005) can both be used for positioning. For example, a positioning system that uses amplitude modulation (AM) radio broadcasts in the medium frequency (MF) band has been developed at UCL (Webb et al., 2010). Since both the transmitter position and the modulation format of these signals can be publicly available, these signals are often used as signal of opportunity. Yet, their positioning accuracy is normally less than GNSS, since they use lower bandwidth than GNSS satellites, but they may supplement GNSS in GNSS-challenged environments.

These alternative positioning approaches improve the robustness of the position solution, because new sources of positioning knowledge that are parallel to GNSS are involved in integrated navigation solutions; but the multi-sensor integration does not meet the requirement for navigation particularly in urban environments (Urmson et al., 2008). In addition, extra performance also brings extra cost and extra hardware. More importantly, there is no evidence that any of these sensor and data source integration techniques can particularly improve positioning accuracy in the cross-street direction, when very small or no extra cost is desired. However, the positioning accuracy in this direction is vital to identifying traffic lanes for vehicles and obtaining desired positioning performance for pedestrians, particularly when a user would like to know the correct side of the street. Identifying traffic lanes for vehicles is very important in many ITS applications, including driver's attention monitoring (McCall and Trivedi, 2004), lane departure warning (Kwon and Lee, 2002), and vehicle guidance (Heimes and Nagel, 2002; McCall and Trivedi, 2006), etc.. Knowing correct side of the street for pedestrians can be important for step-by-step tour guiding for tourists and the visually impaired (Groves, Wang and Ziebart, 2012).

Thus, other approaches should be investigated to improve positioning accuracy in cross-street direction. In this thesis, the approach, known as shadow matching (Groves, 2011), has been researched. The technique uses 3D city models to improve GNSS performance in urban canyons.

Chapter 3.

Multi-constellation GNSS Performance Evaluation for Urban Canyons Using 3D City Models

This chapter investigates the use of 3D building models to predict satellite visibility and verifies that stand-alone GNSS in urban canyons cannot provide reliable positioning solution. There are two main objectives of this chapter. Firstly, since satellite visibility prediction is a pre-requisite for implementing shadow matching algorithms, it needs to be developed and tested. Secondly, the current and future GNSS performance needs to be examined to establish whether multi-constellation GNSS alone can solve the positioning problem in urban canyons, particularly in the cross-street direction. In this work, a visibility prediction model that considers both direct and diffracted signals has been developed to predict GNSS performance using a 3D architectural city model. Section 3.1 presents classification and generation of a 3D city model and its application in GNSS; Section 3.2 describes the satellite visibility determination algorithm. Section 3.3 compares the simulation with real-world observations to validate the simulation, and investigates the effects of diffraction modelling. Section 3.4 then uses the verified simulator to determine current and predict future GNSS performance in urban areas and analyses the results in terms of availability and integrity. Two sets of simulations representing pedestrian and vehicle routes in central London were selected to evaluate GNSS positioning perfor-

mance using different combinations of constellations. Along-street and cross-street accuracy are also compared. Finally, Section 3.5 summarizes the main findings of this chapter, discussing the imiplication for shadow matching and for other potential applications.

This chapter is based on a paper published in Journal of Navigation (Wang et al., 2012*b*).

3.1. 3D city models and it application in GNSS

3D city models are digital representations of buildings and other objects in cities. It is widely used in urban planning, navigation systems, intelligent transportation systems (ITS), noise modelling, etc. There is an increasing number of technologies available to generate 3D models.

To obtain 3D information of the earth's surface, digital aerial photogrammetry and laser scanning are often used. Aerial photogrammetry has been used widely with image matching techniques to generate digital terrain models (DTM), though automation of this process has been a problem hard to solve. On the contrary, aerial laser scanning is proved to be very effective in automated digital surface model construction, though it is less suitable to measure accurately for a single object. (Brenner, 2005). Therefore, when aiming for highly automated and accurate 3D information collection, it is promising to combine the two technologies. After 3D information is captured in an urban area, extraction of buildings can be conducted to generate 3D building models.

Level of detail (LoD) is often used 3D modelling to describe the level of complexity a 3D object representation has. It is a concept borrowed from computer graphics to reduce geometrical complexity of visualized objects according to the distance between objects and the user. In the domain of 3D city modelling, the convention in the City Geography Markup Language (CityGML) encoding standard is often used (Kolbe et al., 2005). It should be noted that the CityGML encoding standard has been adopted as OGC standard in 2012 (Gröger et al., 2008). Five levels of LoD are characterized in CityGML, according to the level of object details, differing

accuracies and minimal dimensions of objects. Examples of the five levels can be found in Figure 3.1, and more details on LoD can be found in the official CityGML documentation (Gröger et al., 2008).

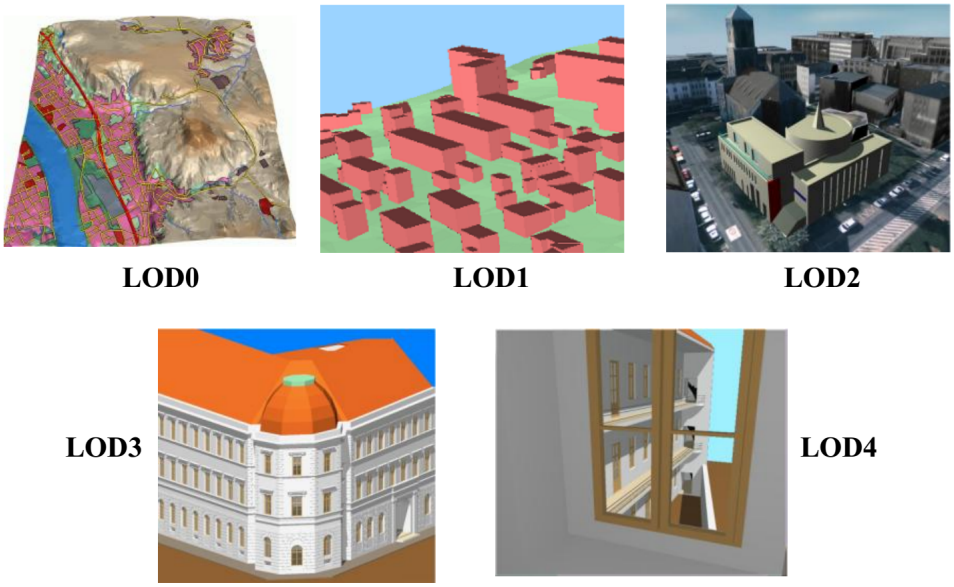

Figure 3.1.: The five levels of detail (LOD) defined by CityGML (source: Gröger et al. (2008))

There is an also increased availability of digital 3D city models, both in terms of number of cities coveraged and higher level of details (Guercke et al., 2009). To name a few examples of among them, Google Maps 3D, Apple 3D Maps, Microsoft Bing Maps 3D, Nokia Here 3D Maps and Edushi 3D Maps are commercially available, while Open Street Maps 3D is available free of charge. This trend is driven by applications of 3D building models in the construction industry, urban planning, gaming, defense and internal security (Dowman and Arora, 2012).

In the navigation community, 3D models have been actively used to evaluate the navigation performances of GNSS in terms of availability, coverage, using simulations of many major cities in the world. GPS availability has been predicted using 3D models of Tokyo, Japan and London, UK (Bradbury, 2007; Steed, 2004; Suh and Shibasaki, 2007). Combinations of GPS and Galileo LOS availability have been predicted in Delft and Schiphol airports in the Netherland (Kleijer et al., 2009;

Tiberius, Christian and Verbree, 2004). In addition to GPS and Galileo, GLONASS was also included in portfolio of GNSS constellations evaluated in Hong Kong, China and Daejeon, Kerea (Kim et al., 2009; Ji et al., 2010). Among this research, some focused only on LOS and NLOS prediction (Kim et al., 2009; Ji et al., 2010; Kleijer et al., 2009), while others also included diffraction modelling (Suh and Shibasaki, 2007; Bradbury, 2007). The techniques used in this research are typically 3D ray tracing or ray intersection, which is an established field in computer graphics (CG) community, and can be optimized for faster speed using graphics hardware (Purcell et al., 2002).

3D city models have been used to detect and eliminate NLOS GNSS signals, improving the positioning accuracy (Francois et al., 2011; Groves, Ziyi, Wang and Ziebart, 2012; Obst et al., 2012; Peyraud et al., 2013; Betaille et al., 2013). By modelling the path delay as a function of user position, NLOS signals can also be used for position determination (Bourdeau and Sahmoudi, 2012; Suzuki and Kubo, 2013).

However, for navigation purpose, signal availability prediction is only an factor, among many others, that influences reception of GNSS signals on users' devices. Real-world GNSS reception is difficult to be predicted, especially in urban areas. Signal obstructions, reflections and diffractions can be caused by both permanent and temporary objects. Permanent objects are likely incorporated in the 3D city models, whereas temporary objects are not. For the purpose of navigation, one important question to answer comes from the fact that pedestrian and vehicle GNSS users suffer signal degradation with different characteristics, which has not been investigated before. Furthermore, how GNSS accuracy is degraded differently in different horizontal directions relative to the street direction has not been examined. Moreover, to the author' knowledge, little research has modelled the effect of the emerging Chinese system – BDS on the overall GNSS navigation performance in urban canyons using 3D city models. Finally, and most importantly for this thesis, the current and future GNSS performance needs to be examined to justify whether multi-constellation GNSS can solve the positioning problem in urban canyons on its own, particularly when considering positioning accuracy in different directions. The

aim of this chapter is to answer these research questions.

3.2. Satellite visibility determination

Determining satellite visibility first requires data preparation to ensure 3D building models, GNSS satellites and user route locations are expressed in a common reference frame. Secondly, a satellite visibility determination algorithm is designed and developed for testing. This section describes how these are achieved.

3.2.1. Handelling city models

A software toolkit is developed for this study to store and process 3D city model data in Virtual Reality Modelling Language (VRML), an international standard format. It is a routine function for 3D model software to transform other formats to VRML. Buildings in VRML format are represented by structures, which in turn compromise polygons (normally triangle meshes). The format of the 3D city models can be any other formats, as long as the structures are present.

Throughout this work, a real 3D city model of part of central London (around Aldgate) supplied by ZMapping Ltd has been used. The model has a decimetre-level of detail and is verified by surveying to have decimetre-level accuracy (Bradbury, 2008).

3.2.2. Data preparation

Data sets for simulation consist of GNSS satellite orbits, building geometries from the 3D city model and user routes. Four GNSS systems, comprising GPS, GLONASS, Galileo and BDS, have been deployed in the simulation. The GPS and GLONASS satellite positions are computed from the satellite broadcast ephemeris data published online by the International GNSS Service (IGS). Galileo orbits are synthesized using the description in the Space Interface Control Document (ICD) GJU (2006). Orbits of the BDS system, whose full network is due to be completed in 2020, are generated from an unofficial description of the full global system (VanDiggelen, 2009).

Building geometries are extracted from the city model VRML file. User routes are generated with reference to the city models using Rhinoceros, a 3D modelling tool (Rhinoceros, 2014).

It is imperative to express all geometric information in a common coordinate frame. Thus, coordinates of the satellites, user positions and model data, are transformed into an earth-centred, earth-fixed (ECEF) datum, World Geodetic System 1984 (WGS-84).

It should be noted that WGS-84 has dual meanings. Generally, it means a geodetic datum used in GPS positioning that defines a Cartesian coordinate system and an associated ellipsoid to represent the Earth, with its origin at the centre of mass of the Earth. Each Cartesian coordinate can be transferred into a geodetic coordinate. This theoretical definition of the WGS-84 datum has to be realized in practice as a terrestrial reference frame (TRF). There are different WGS-84 realizations, each realizing a slightly different datum, although all referred to as 'WGS-84'. More specifically, WGS-84 may also mean the WGS-84 broadcast TRF that is the coordinate system broadcast by GPS satellites to GPS receivers. In this thesis, the term 'WGS-84' is used for this specific meaning as a TRF, and the term 'WGS-84 datum' is used to refer to the general theoretical definition.

Similar to the WGS-84 TRF, International Terrestrial Reference Frame (ITRF), European Terrestrial Reference System 1989 (ETRS89) and Ordnance Survey Great Britain 1936 (OSGB-36) are alternative TRFs, using slightly different ellipsoids to serve global, European and United Kingdom regions, respectively. Coordinate transformations between these different TRFs are achieved by applying a translation and rotation to their Cartesian coordinates. Detailed explanations of the transformation can be found in Ordnance Survey's documentation (Mark Crossley, 2012).

Satellite orbit data for GPS is already expressed in WGS-84; whereas satellite orbit data for GLONASS have been transformed from the Parametrop Zemp 1990 (PZ90.02) datum into WGS-84. The Grid InQuest 6.0 DLL (Quest-Geo-Solutions-Ltd, 2004) was used to transform the 3D city model data from the OSGB-36, used in the UK and Ireland, to the ETRS. The coordinates are is further transformed into ITRF 2005, which is within centimetres of WGS-84.

3.2.3. Visibility determination algorithm

A building in 3D city models can be represented by a number of triangles. Determining visibility of a satellite with respect to a user can be regarded as testing whether the user-satellite line-of-sight (LOS) intersects such a triangle. Thus, satellite visibility can be determined using a line and triangle intersection determination algorithm, as described in Appendix A. In a simple satellite visibility determination algorithm, each detailed building structure (comprising about 100,000 surfaces) within the 3D city model is tested for blockage of the user-satellite LOS vector. Moreover, each of these tests is applied to every satellite above the elevation mask angle in up to four GNSS constellations, and all parts of the 3D models. An elevation mask angle is routinely used in GNSS processing algorithms to ignore satellites whose elevation angle is below the specified angle, in order to prevent low-elevation satellites from degrading the GNSS solution. This is because low-elevation satellites are prone to larger atmospheric errors.

This basic approach consumes far too much processing power for a large batch of simulations. Consider in this simulation there are a number of satellites each moving, but all for visibility simulation at a limited number of discrete points, where a pedestrian or vehicle user can be. Therefore, in the satellite visibility determination algorithm used for this study, the following change is made to improve the efficiency.

Instead of using the city model to compute the visibility of each satellite directly, it is useful to determine the boundary of the buildings from the user's perspective at each user location. A sky plot of the building boundary in terms of elevation and azimuth is thus obtained. Then, satellite visibility is easily determined by comparing the satellite's elevation with the building boundary's elevation, at the same azimuth. This approach is more efficient where a great number of satellite visibility tests are performed at the same location. For real-time visibility determination, building boundaries may be pre-computed and stored for a grid of possible user locations. This information is also useful for shadow matching, as discussed in more detail in Chapter 4. This strategy will also significantly benefit real-time shadow matching, detailed explanations and discussions to be provided in Chapter 7.

In this approach, the building boundary is determined at a number of different azimuths, spaced at regular intervals and spanning 360°. For each azimuth, the building boundary is the highest elevation at which the LOS from a virtual satellite at that azimuth is blocked. This is determined using bisection: firstly the visibility of a virtual satellite at a 45° elevation is tested. If it is blocked, then the higher elevation region is refined in bisection, and the next test is performed at an elevation of 45°+45°/2=67.5° of elevation; otherwise, the satellite is visible and the lower elevation region is refined, so the next test is at 45°−45°/2=22.5° of elevation. The bisection process continues until the boundary has been determined to within a 1° elevation resolution. As a result, seven satellite visibility tests must be performed at each azimuth.

With a 1° azimuth resolution, which is relatively high, 7 * 360 = 2520 satellite visibility tests are required to determine the building boundary at each user location, which still imposes a considerable computational load. Therefore, lower azimuth resolutions can be considered if computation power is a concern. Figure Figure 3.2 compares the building boundaries obtained with 2°, 10°, and 30° azimuth resolutions. A compromise azimuth interval of 10° may be used in implementations where the pre-processing time is limited. Then, this approach is more efficient than the basic approach, requiring 7 * (360°/10°) = 252 satellite visibility tests to be performed at each location. The building boundaries can then be used for any satellite visibility prediction at the same location at any epoch. There is a trade-off between computation load and satellite prediction accuracy.

The software toolkit for all data pre-processing and the satellite visibility determination was developed in C++. Figure 3.3 shows the software flowchart.

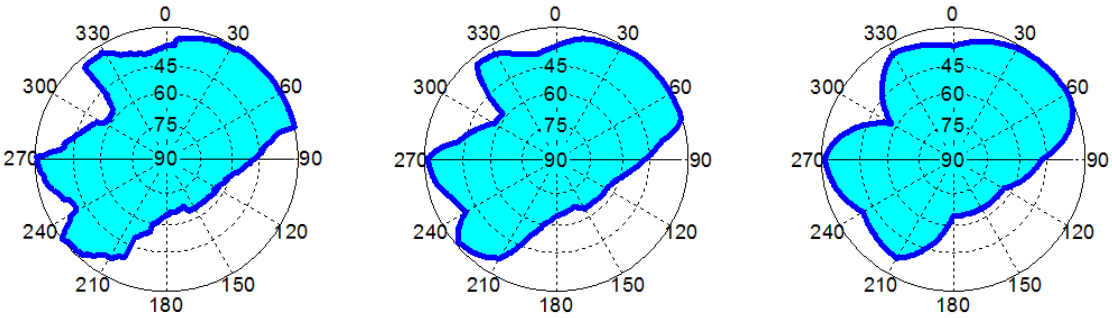

Figure 3.2.: Sky plot of building boundaries from the perspective of GNSS users with different azimuth resolutions. (The dark blue lines represent the roof and edge boundary of the buildings surrounding the user; the light blue area represents the visible sky)

3.3. Experimental verification

3.3.1. Experimental settings and results

Experiments have been carried out to compare the model-predicted satellite visibility with real-world observations. Two two-hour GNSS data collection sessions were conducted in urban environments (named test points 1 and 2). To give an example, views of the real urban environment and the city model at test point 2 are shown in Figure 3.4.

Accurate positions of the test sites were determined by differential carrier phase GNSS positioning using four Ordnance Survey reference stations within 50 km.

A comparison is made between observed and predicted satellite visibility every 30 seconds. Figure 3.5 and 3.6 present the comparisons between real and predicted satellites visibility for test points 1 and 2, respectively. The building boundary for prediction was determined using a 1° azimuth interval. In these two figures, G denotes GPS satellites and R refers to GLONASS satellites.

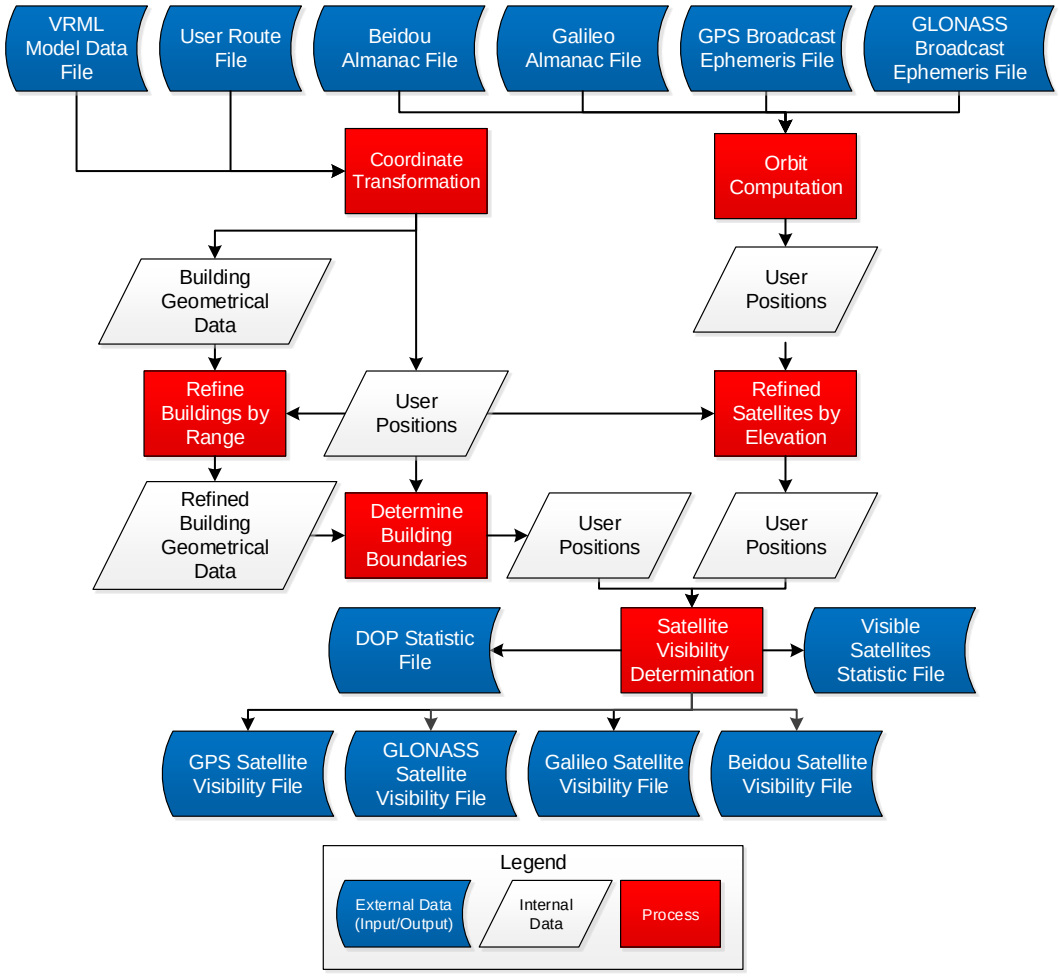

Figure 3.3.: Software flowchart for satellite visibility determination

The results show that in most cases, the predicted satellite visibility agrees with the experimental observation (blue and grey dots in Figure 3.7 and 3.8). However, there are a significant number of cases where they are disagree (shown as green and red dots). Reasons for predicting a signal that is not observed include new buildings that are not in the database, trees and street furniture. All of these were observed at the test sites. Obstruction of a signal by a small object can account for many of the relatively short interruptions to signal tracking seen in the test data.

Sometimes a signal that is predicted invisible is observed. The reasons include signal diffraction, reflection via non-line-of-sight (NLOS) paths, city model precision limitations, and demolished buildings. NLOS signals may be neglected as they

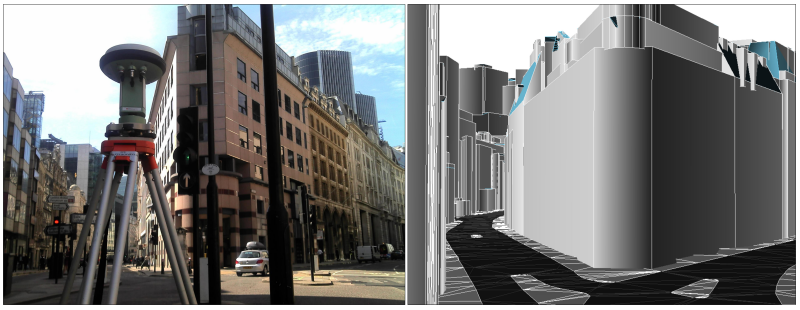

Figure 3.4.: View from test point 2: the 3D city model (right) and the real environment (left)

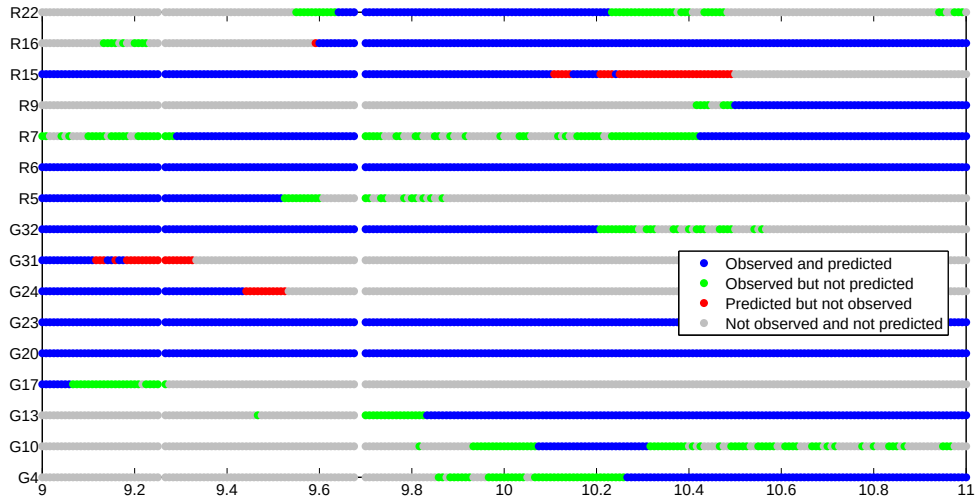

Figure 3.5.: Comparison of observed and predicted GPS and GLONASS satellite visibility at test point 1

normally have large range biases so may be filtered out of the position solution when any consistency checking algorithms are performed. Furthermore, for the purposes of predicting GNSS availability across a range of time and locations in urban environments, the effects of demolition and construction of buildings may be assumed to cancel. The effect of city model precision limitation may also be assumed to cancel. However, diffracted signals have relatively small biases, and thus they can be used in non-precision positioning solutions. The intermittent reception observed for many of the unpredicted signals is characteristic of diffraction (Bradbury, 2008). Therefore, The diffraction interference was investigated further.

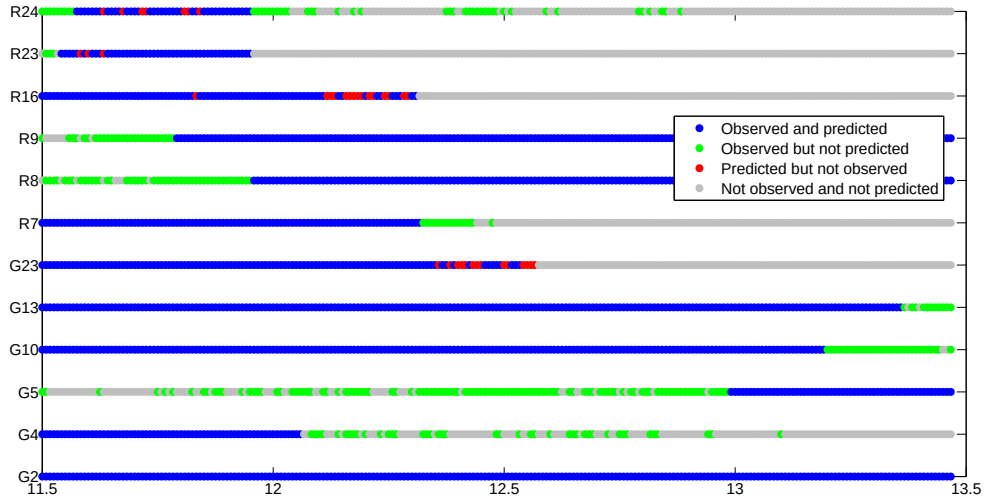

Figure 3.6.: Comparison of observed and predicted GPS and GLONASS satellite visibility at test point 2

3.3.2. Diffraction modeling

Diffraction occurs at the edge of a building (or other obstacle) when the incoming signal is partially blocked, noting that the path taken by a GNSS signal is several decimetres wide. There are two approaches to predicting the effect of diffraction on satellite visibility using a 3D city model. The first one would be to numerically determine the diffraction field based on every physical factor, including the angle of incidence of the signal, the weak signal tracking ability of GNSS user equipment, and the detailed material properties information of the building, which is highlighted as important for accurate prediction (Fisher et al., 2002). This method is impractical for our purpose because the necessary information about the building materials and antenna characteristics is difficult to obtain and the computational complexity is high. The second, much simpler, approach has been adopted here. This simply extends the building boundary used for satellite visibility determination by adding a diffraction region to model the diffraction effect around building edge. Thus, wherever the LOS intersects the diffraction region, the signal is classified as potentially diffracted instead of blocked (Bradbury et al., 2007; Walker, Rodney and Kubik, 1996). Both horizontal and vertical edges are considered for diffraction modelling.

Here, a 3^{o}-wide diffraction region was modelled.

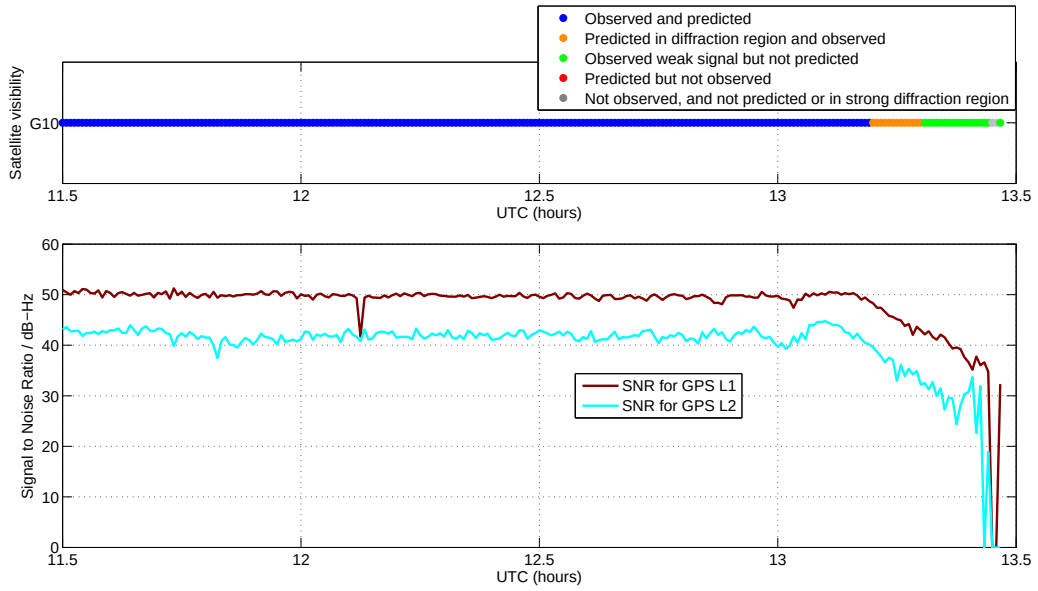

Figure 3.7.: Comparison between measured signal to noise ratio (SNR) and GNSS signal availability for GPS PRN 10 at test point 2 (Diffraction considered)

Figure 3.7 and 3.8 show that using the implemented diffraction model, the satellite visibility prediction is closer to the real observations. However, this diffraction model can only predict strong diffraction, when the signal to noise ratio decreases by no more than 10 dB-Hz from its normal value. However, very weak signals are less useful for navigation. Figure 3.8 also shows that the signal characteristics in an urban area can sometimes be very complex. However, the model still successfully predicted the strongest signals.

Figure 3.9 and 3.10 show that the diffraction model works reasonably well for most other satellites in the experiments, increasing the reliability of the satellite visibility prediction.

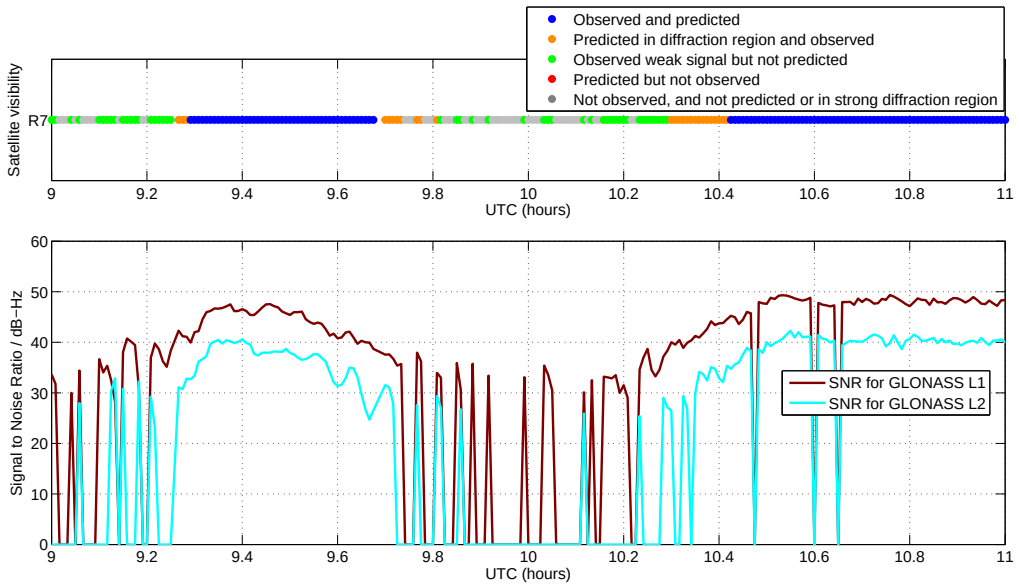

Figure 3.8.: Comparison between measured signal to noise ratio (SNR) and GNSS signal availability for GLONASS 7 at test point 1 (Diffraction considered)

3.4. Performance prediction for pedestrians and vehicles

This section describes the simulations conducted to predict multi-constellation GNSS performance in urban canyons. Subsection 3.4.1 describes the design and configuration of the simulation. The results are then presented and analysed within subsections 3.4.2 and 3.4.3, focusing on direct LOS signal availability and dilution of precision (DOP), respectively. DOP, as an indicator of satellite geometry, is used to analyze positioning accuracy in different directions (along-street and across-street). In urban environments, the real-world positioning performance can be affected by many factors, including signal reflection, diffraction, blockage of human body, surrounding vehicles, trees or other objects. It is unrealistic to model all these factors. Thus, given that a perfect modelling of GNSS performance in urban canyons is not practical, only the dominant factor in urban canyons, building blockage of LOS, is modelled in this study. It is assumed that decreased signal availability caused by objects blockage and increased signal availability caused by reflection and diffraction

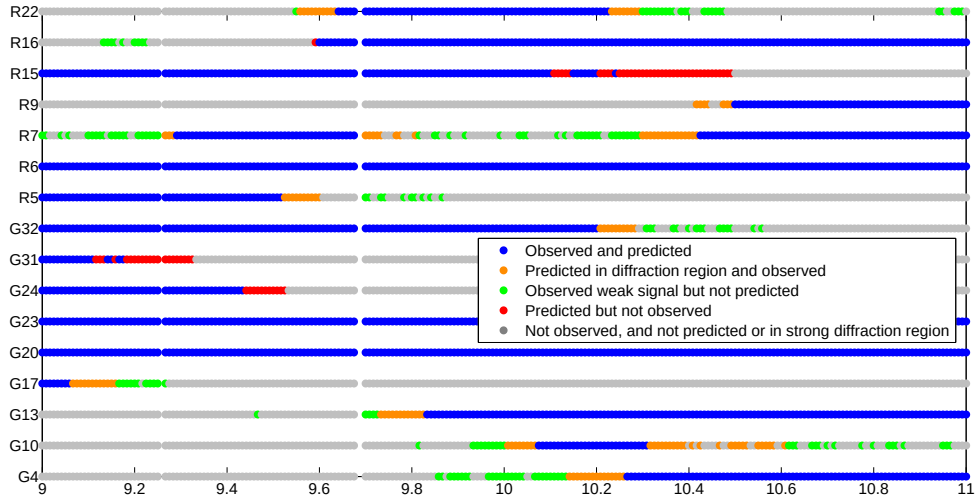

Figure 3.9.: Comparison of observed and predicted GPS and GLONASS satellite visibility at test point 1 with diffraction model

can be canceled out. Under this assumption, DOP of LOS is used to indicate the accuracy difference of different directions.

3.4.1. Simulation design and configuration

Two routes, representing vehicle and pedestrian motion were generated to evaluate GNSS navigation performance by simulation in urban environments. Both routes pass through the same environment with the pedestrian route closer to the buildings, as shown in Figure 3.11.

There are four important requirements of any navigation system: accuracy, availability, continuity and integrity (Misra and Enge, 2010; Groves, 2013). For both routes, availability and integrity are evaluated using the 3D city model. Comparisons were then made between different scenarios with various satellite constellations in operation.

The particular area from the London city model chosen for the simulations is around Lloyd's of London and Aldgate where there are tall buildings, as shown in Figure 3.11.

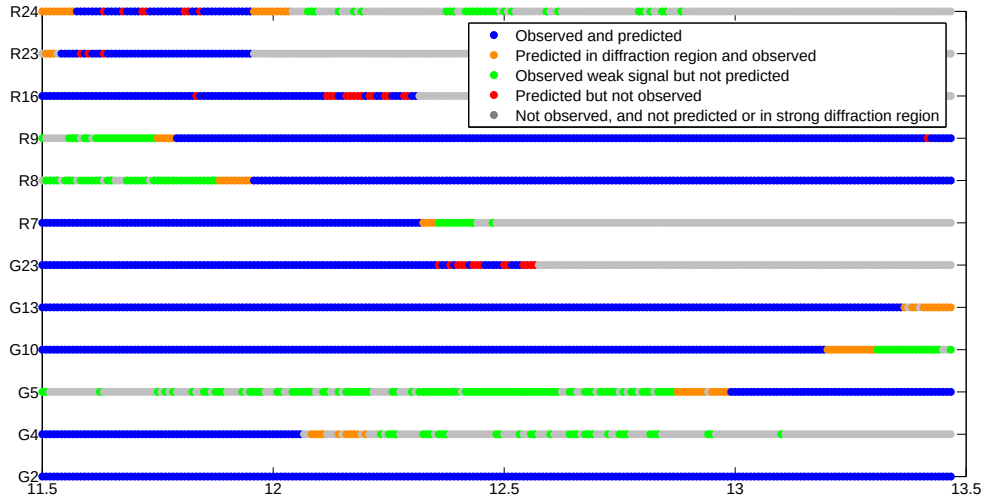

Figure 3.10.: Comparison of observed and predicted GPS and GLONASS satellite visibility at test point 2 with diffraction model

Figure 3.11 shows the simulated pedestrian and vehicle routes, which are represented by the yellow and red line, respectively. The locations used for GNSS satellite visibility determination are labelled using point identities (IDs). P represents the pedestrian route, while V denotes the vehicle route. In order to simulate a representative range of urban environments, alternate test points were located at road junctions and between junctions on both routes.

The pedestrian route was generated by simulating a receiver located on the pavement. The vehicle route comprises the left traffic lane of the road, when travelling from V1 to V23. The user antenna height modelled along the pedestrian route is based on the assumption that when people use a GNSS-equipped mobile phone or other portable navigation devices (PND), they normally hold it in front of their chest. This is assumed to be 1.5 m above the ground. For the vehicle route, the GNSS antenna is assumed to be 1 m above the ground.

For both the pedestrian and vehicle routes, four GNSS constellation scenarios were simulated. They comprise GPS alone, GPS and GLONASS, multi-constellation GNSS in the year 2014 and multi-constellation GNSS in 2020. The GNSS in 2014 scenario comprises the predicted GNSS operational status in 2014 (note that the GNSS operational status in 2014 was predicted in 2011), when GPS and GLONASS

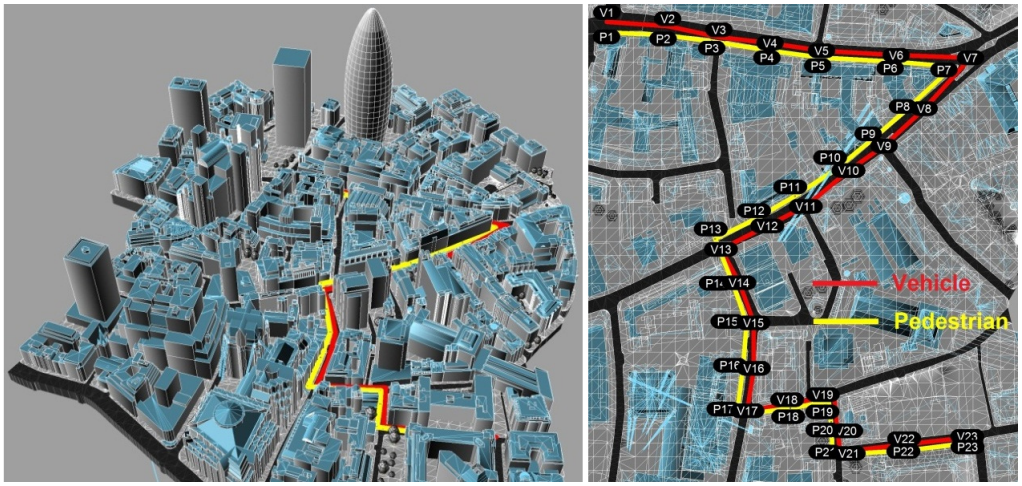

Figure 3.11.: Routes representing vehicle and pedestrian motion (perspective view in the left; top view in the right)

was assumed to be fully operational, while Galileo was predicted to have 9 satellites in operation. The regional deployment of BeiDou Navigation Satellite System (a.k.a. Beidou or Compass) to serve Asia should be completed, which will comprise 5 geosynchronous Earth orbit (GEO) satellites, 3 inclined geosynchronous satellite orbit (IGSO) and 4 middle Earth orbit (MEO) satellites. This was based on the public announcements and plans as in 2011. However, it turned out in 2014, the Galileo has 4 in-orbit validation (IOV) satellite (GSAT0101) available and Beidou has 16 satellites (6 GEO, 5 MEO and 6 IGSO). Thus, the scenario simulated for 2014 should correspond to actual performance at some point in 2015. The GNSS in 2020 scenario assumes that all four constellations will be fully operational as currently scheduled. The elevation mask angle was set at 10° in all simulations.

The accuracy of GNSS position estimates basically depends upon: (i) The number of satellites in view and their geometry and (ii) the accuracy of the range and range rate measurements (Misra and Enge, 2010). In this work, the performance of GNSS in urban environments is evaluated using the number of satellites in view and the dilution of precision (DOP), both of which have been analysed for all of the simulation scenarios described.

To minimize biases on the results that can arise from randomly chosen epochs, all simulations were repeated at epochs every 15 minutes over one sidereal day. Thus,

96 epochs were simulated for each of the eight scenarios. The day selected was 7th September, 2011.

3.4.2. Performance evaluation based on satellite numbers in view

Figure 3.12 shows the number of satellites in view, averaged over a 24-hour span, across all epochs at each user location, including useful diffracted signals. To enable contributions of different GNSS constellations to be compared, the four colour bars represent the additional average number of satellites for each successive scenario. Thus, the total is obtained by summing the appropriate number of colour bars. As shown in Figure 3.11, user locations with even point IDs are between junctions and those with odd point IDs are at junctions.

As expected, the histograms in Figure 3.12 indicate that with more satellite constellations operational, more satellites will be in view in city canyons. With only GPS used, the average number of visible satellites is less than 4 at many locations, which is not sufficient to provide a positioning solution. Even the combination of GPS and GLONASS fails to provide an average of more than 5 visible satellites at a few locations. However, with the addition of Galileo and Compass, the average visibility including diffracted signals is at least 8 satellites, except at pedestrian Point 10, which is close to a tall building. These results illustrate the poor GNSS performance that can arise obtained in challenging urban environments due to buildings blocking the satellite signals and show the potential benefit of the new GNSS constellations.

Figure 3.13 shows how the different constellations contribute to GNSS availability averaged across all the urban environments considered. It is apparent from the chart that GNSS signal availability will increase significantly if all of the additional satellites proposed for launch by 2020 become operational.

To compare the performance of individual GNSS constellations, in other words,

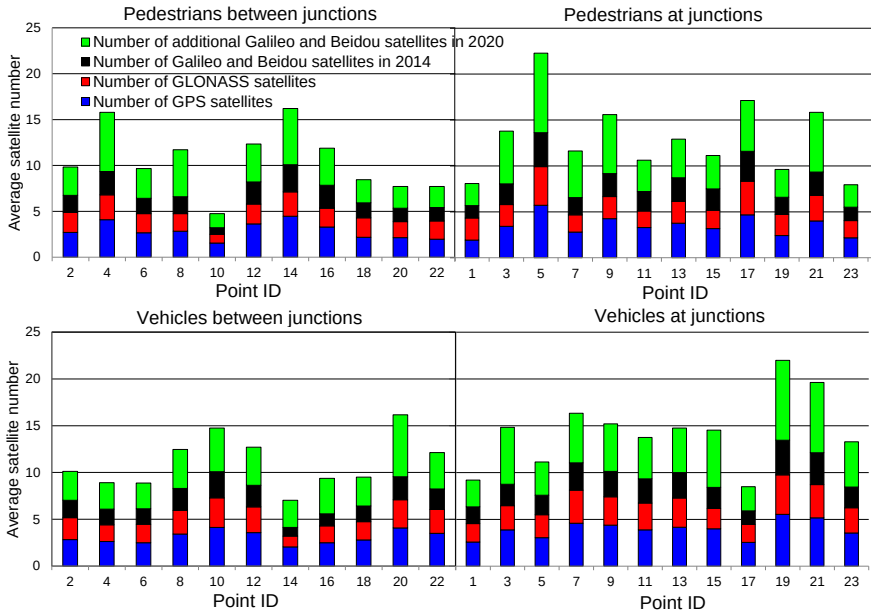

Figure 3.12.: Daily average number of satellites in view for the pedestrian route (top) and the vehicle route (bottom)

the performance of GNSS now and in the future, a simple statistical analysis was conducted based on data from both pedestrian and vehicle routes. Figure 3.14 shows the relationship between the type of user location and GNSS signal availability for each GNSS constellation scenario. As expected, there is a clear trend that the number of satellite in view increases with the number of satellites in operation. Interestingly, the figure also shows consistently fewer number of satellites in view for the pedestrian scenarios compared with the vehicle scenarios, as well as fewer satellites in view for locations between junctions than locations at junctions. The difference may be caused by the pedestrian route being close to the buildings, resulting in more signals being blocked by surrounding buildings. Similarly, the locations between junctions are typically surrounded by more buildings than the locations at junctions.

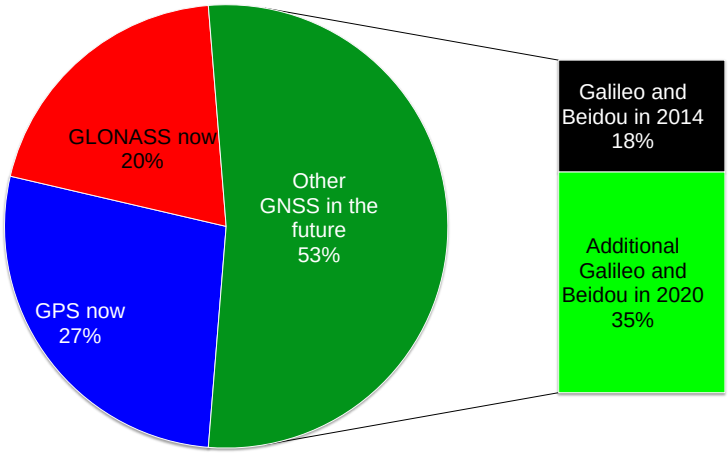

Figure 3.13.: Average contribution of each constellation to the number of satellites in view for the 2020 scenario across all pedestrian and vehicle locations

As GNSS user equipment normally needs at least four satellites to provide a navigation solution, GNSS availability is assessed by determining the percentage of time for points on each route when at least four satellites are directly in view with each combination of GNSS constellations. Furthermore, to evaluate the integrity of GNSS in an urban environment, the percentage of time when at least 5 satellites are directly in view has also been determined. This is because at least five satellites are required for receiver autonomous integrity monitoring (RAIM) (Wang and Hewitson, 2006; Ochieng et al., 2002).

For both the pedestrian and the vehicle routes, Figure 3.15 compares the percentage of time over a day when GNSS is available for a positioning solution and for RAIM under each simulation scenario. The average availability across all locations in each category is shown along with the percentage of time at which each criterion is met simultaneously at all locations within that category.

It can be seen from the charts that the availability of both a position solution

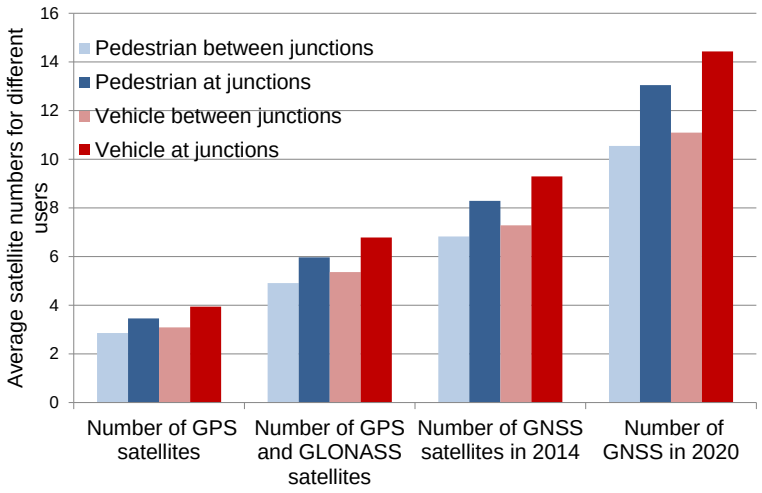

Figure 3.14.: Average satellite numbers with respect to different type of user locations

and RAIM is notably better for a vehicle-based user than for a pedestrian user. However, even for the vehicle route, all four GNSS constellations are required for close to 100% positioning availability and high RAIM availability. Performance is unreliable even for the GNSS in 2014 scenario. Performance along the pedestrian route is normally poorer, particularly at points between junctions. Therefore, even with four fully-deployed constellations, robust and reliable pedestrian positioning in challenging urban environments cannot be achieved using conventional GNSS positioning alone.

3.4.3. Performance evaluation based on dilution of precision

For this study, only the horizontal performance is studied as this is the main concern of GNSS users in urban canyons. The DOPs investigated in this work are the horizontal DOP (HDOP), the along-street DOP (ADOP) and the cross-street DOP (CDOP). Along-street is defined as the direction along the street which the GNSS user is on. Cross-street is the perpendicular direction across the street. In an urban canyon, most satellite lines of sight will be much closer to the along-street direction

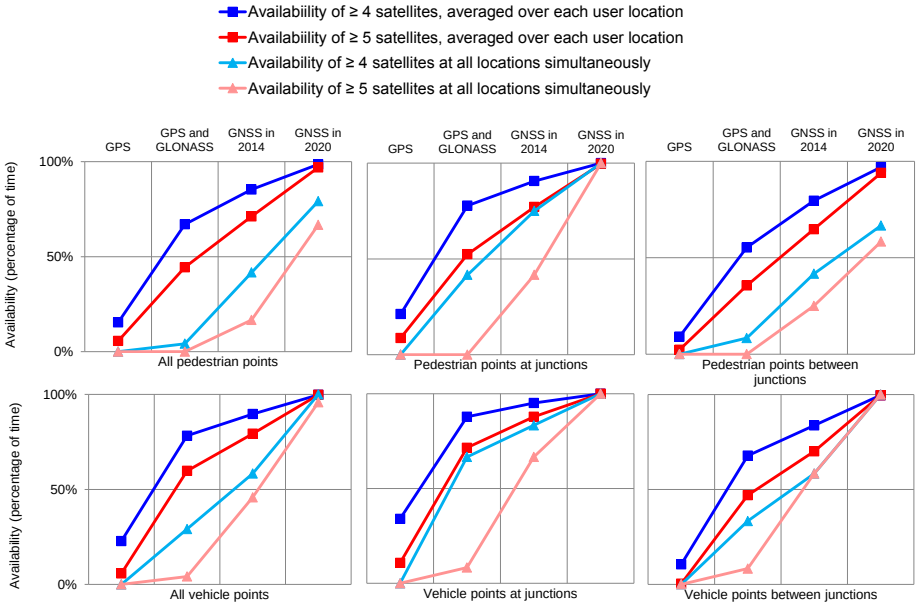

Figure 3.15.: Percentage of time when the number of satellites is enough for positioning (4 or more satellites) and for RAIM processing (5 or more satellites)

than the cross-street direction.

The aim is to compare the positioning accuracy in the along-street and across-street directions. The accuracy can be modeled by multiplying the ranging error with a correspondent DOP value (Misra and Enge, 2010). The ranging error varies considerably depending on the environment, receiver design and whether differential techniques are used. Thus it is assumed that the pedestrian and vehicle GNSS users uses the same GNSS receiver, use the same positioning technique, and are simulated at the same time. Under this assumption, the range error is the same for them, and only DOP is used as an indicator of accuracy prediction.

The horizontal, along-street and cross-street position solutions are compared in terms of their DOP value. It is considered acceptable when the corresponding DOP is below 5.0. For each simulation scenario, Figure 3.16 shows the average percentage of time when criteria are met over each user location and the percentage of time the

criteria are met at all locations simultaneously. DOP is calculated as described in Misra and Enge (2010) and Groves (2013).

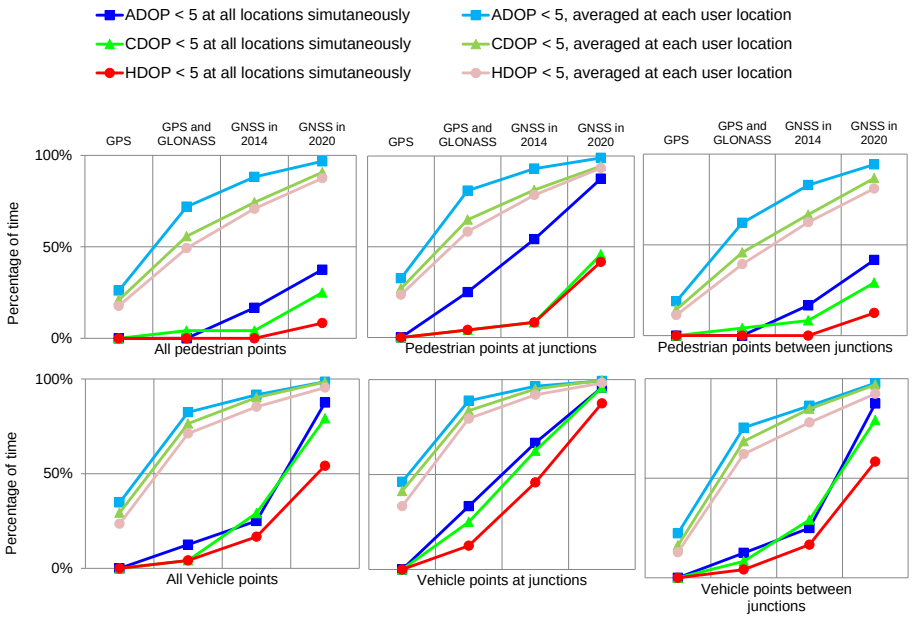

Figure 3.16.: Percentage of time when the HDOP, along street DOP and cross street DOP are below 5, for each scenario

Figure 3.16 shows that, on average, the along-street DOP is smaller than the cross-street DOP as would be expected from the geometry of the unblocked signals. This is more significant for the pedestrian route. For the locations between junctions the overall precision is poorer than at the junctions. For all of the simulation scenarios, the DOP criteria are met more often along the vehicle route than the pedestrian route. This is consistent with the availability results presented in the previous section. Even with all four constellations, the HDOP criterion is met across the whole route simultaneously only 69.1% of the time for the pedestrian route and 90.4% of the time for the vehicle route.

3.5. Summary and discussion

This chapter prepares for GNSS shadow matching positioning by verifying the satellite visibility determination algorithm, and quantitatively demonstrating the inadequacy of multi-constellation GNSS positioning in urban canyons, particularly in the cross-street direction, thus demonstrating the need of shadow matching.

A satellite visibility determination toolkit has been developed for predicting GNSS performance in urban environments using 3D building models. The capability to determine satellite visibility using 3D models is a pre-requsite of shadow matching. The toolkit was verified at two test points with field trials. Comparison of satellite visibility between prediction and observation demonstrated that direct line-of-sight signals can be predicted using the 3D city model and the toolkit. However, due to the complexity of the environments, diffracted and reflected signals were also observed that the original model did not predict. As diffracted signals are potentially useful in positioning, the simulation has been modified to predict them. Verification with real observations shows that the implemented diffraction model successfully predicted most of the strong diffracted signals.

Positioning performance using different combinations of GNSS, including GPS, GLONASS, Galileo and Beidou has been evaluated by simulation using a 3D model of London. Solution availability, RAIM availability and precision at different directions have been assessed for both pedestrian and vehicle routes within a urban environments. Positioning performance using GPS and GLONASS was found to be unreliable at some of the locations evaluated. Performance using all four GNSS constellations was predicted to be much better, but still unreliable at a few of the locations. Performance was better along the vehicle route than the pedestrian route, which is closer to the buildings; and was better at junctions than between them, where there are typically more close-distant buildings. When both Galileo and Beidou systems will be operational in the year 2020, the number of available GNSS signals in urban environments will be doubled. However, even with four constellations, GNSS performance will still be unreliable at some urban locations in 2020.

Finally, positioning precision was found to be generally poorer in the cross-street direction than in the along-street direction, because the buildings constrain the

satellite signal geometry. Thus, other techniques are needed to complement GNSS in the cross-street direction. One of these solutions is GNSS shadow matching, which can potentially improve the across-street positioning accuracy by comparing the observed GNSS signal availability with that predicted using a 3D city model (refer to Chapter 4 for more details).

Based on the comprehensive simulations, to ensure a reliable positioning service in urban canyons, conventional GNSS should be augmented with other techniques. There are a number of methods, including combining GNSS with other signals, sensors and data sources in an integrated navigation system (refer to Chapter 2 for more details).

For many applications, the modelling technique presented in this work could also be used to predict the best route through a city at a given time, or the best time to perform GNSS positioning at a given location. This technique could also be applied to GNSS signals prediction in mountainous area by using a digital elevation model (DEM) instead of a city model.

Chapter 4.

A Two-phase Shadow Matching Algorithm

The overall principle of the shadow matching positioning technique is to match GNSS signal observations with predictions determined using 3D city models to improve positioning in urban areas (Groves, 2011). Building on the work of experimentally verified visibility determination algorithm in Chapter 3, the shadow matching technique is introduced in this chapter. There are a variety of options for designing a detailed algorithm that fulfills this principle. The scope of this chapter focuses on discussing the pros and cons of these options, and proposes a shadow-matching algorithm that is optimized in terms of architecture. This chapter also acts as an entry point for the following chapters in the thesis on detailed optimizations of shadow matching algorithms. A preliminary but complete version of the shadow-matching algorithm is then designed and implemented. The implementation is then tested using geodetic grade and smartphone GNSS receivers, comparing the impact on the shadow matching technique of different GNSS measurement qualities.

4.1. Introducing shadow matching research

This section reviews the principle of the shadow matching positioning technique and its development history.

4.1.1. The principle of shadow matching

The earliest concept similar to shadow matching is found at the end of a paper in its discussion section (Tiberius, Christian and Verbree, 2004). The concept follows a fingerprinting principle that compares line-of-sight (LOS) availability predicted using 3D models with received signals to determine the user's location. Recently, another work named 'power matching' (Saab and Kassas, 2006) was also found using similar principle with shadow matching. This work focuses on signal power prediction of direct LOS and diffracted signals, and then matches it with received signal strength. However, these concepts was not developed further by their authors.

The shadow matching positioning principle was first proposed and the name 'shadow matching' was first introduced in Groves (2011). The principle of shadow matching combines two commonly known principles together: GNSS signal availability determination using 3D building models and the fingerprinting-like positioning techniques. At UCL, the concept of 'shadow matching' was proposed and tested with mathematical modelling, to improve cross-street GNSS positioning accuracy, based on knowledge derived from 3D building models. Following the work in Groves (2011), the author's investigation on shadow matching embarked.

The principle of shadow matching is simple. Due to obstruction by buildings in urban canyons, from many GNSS satellites will be receivable in some parts of a street, but not others. Figure 4.1 illustrates this, noting that the boundary between the two regions is fuzzy due to diffraction effects at building edges (Bradbury, 2007). Where each direct signal is receivable can be predicted using a 3D city model. Consequently, by determining whether a direct signal is being received from a given satellite, the user can localize their position to within one of two areas of the street. By considering other satellites, the position solution may be refined further. At each epoch, a set of candidate user positions is generated close to the user's low-accuracy conventional GNSS positioning solution. At each candidate user position, the predicted satellite visibility is matched with the real observations. The candidate position that has the best match between the prediction and the real observations can be deemed the shadow matching positioning solution. This process can be

conducted epoch by epoch, so the GNSS user can be either static or dynamic.

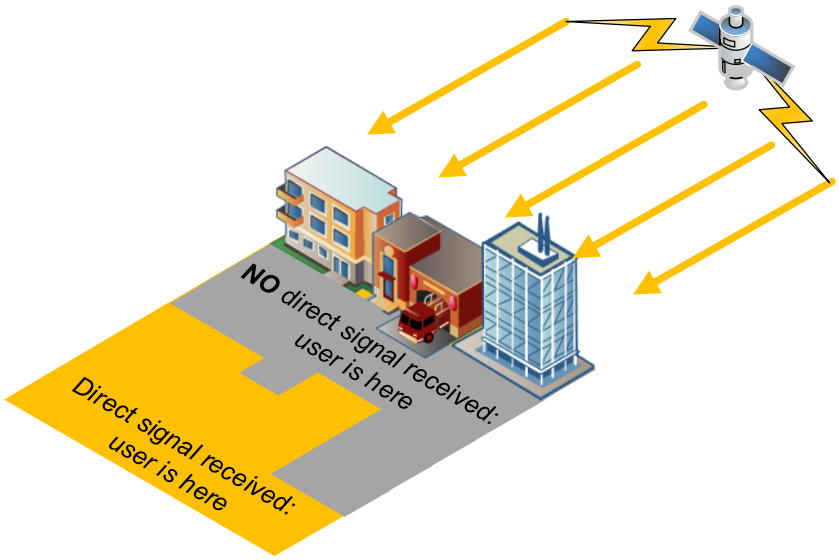

Figure 4.1.: A satellite casts shadows on the ground, adjacent to buildings, to demonstrate the concept of shadow matching

4.1.2. A development history of shadow matching

At UCL, shadow matching was first proposed and demonstrated by mathematical modelling (Groves, 2011). A preliminary shadow-matching algorithm was developed and verified with experimental data, instead of simulation (Wang et al., 2011). This was also the first shadow matching algorithm that evaluates Research degree of matching by scoring at candidate positions. The potential of using shadow matching to identify the correct side of the street was demonstrated. Then, an improved scoring scheme has been proposed to account for the effects of satellite signal diffraction and reflection. A full search grid of candidate positions was also implemented, and experiments were conducted at over 20 locations (Wang et al., 2013*a*, 2012*a*). Furthermore, shadow matching has been adapted to work with post-processed smartphone GNSS data (Wang et al., 2013*b*). For the first time, a real-time prototype system has been developed for the Android mobile operation system, which demon-

strates the efficiency of the shadow-matching algorithm (Wang et al., 2013*c*). A Bayesian approach is then used for estimating matching probability in the presence of weak signals, and comprehensive performance assessment of smartphone GNSS shadow matching has demonstrated the improvements and predicted performance with four GNSS constellations (Wang et al., 2014). With previous research focusing on static shadow-matching positioning algorithms, kinematic shadow-matching positioning is tackled using a Kalman filter and a particle filter (Wang, 2014*b*). Overall, the research at UCL has shown that, in urban canyons, shadow matching is more accurate in the cross-street direction than the conventional GNSS positions (compared in the sense of using a typical navigation GNSS receiver, which uses pseudo-range code-based, non-differential GNSS data), verifying its potential to complement conventional GNSS.

In parallel with the author's research, other research groups have also conducted research on shadow matching or a similar concept. They are Yozevitch et al. (2012, 2014) and Suzuki and Kubo (2012). Building on the work at UCL, recently, Isaacs et al. (2014) also implemented a version of shadow matching. Different versions of shadow matching have been implemented by different groups. For instance, in terms of the way the 3D model is used, a grid-based approach (refer to subsection 4.2.1) is used in the author's work (Wang et al., 2012*a*) and later combined with a particle-filter approach (Wang, 2014*b*); whereas Yozevitch et al. (2012) uses a zone-based approach (refer to subsection 4.2.1), Suzuki and Kubo (2012) also uses a particle-based approach, though their main focus is static surveying instead of kinematic navigation. Detailed comparison of these different options is discussed in Section 4.2. Since signal strength can be attenuated due to a variety of reasons, modelling it using a probability theory is more appropriate than manual set parameters, and is thus used in Isaacs et al. (2014) and Wang et al. (2014). Simultaneous localization and mapping (SLAM) is used in Isaacs et al. (2014) to feed shadow matching results back to the 3D maps. Following an idea similar to shadow matching, 3D models of lamp posts were specifically used for positioning on open field roads (Yozevitch et al., 2014).

4.2. Shadow matching implementation options

This section discusses different options for implementing the shadow matching technique into algorithms. Comparisons from two perspectives are made in this section. The first comparison is conducted between a shadow-based and a point-based shadow matching algorithm, while the second comparison concerns the trade-offs between cloud computing and local processing.

4.2.1. Zone-based or point-based shadow matching

There are two major different approaches to the design of a shadow matching algorithm, a zone-based approach and a point-based (e.g. grid-based) approach. A zone-based approach is adopted in Yozevitch et al. (2012), which uses the 3D models to compute satellite shadows, cast by the buildings, for each satellite, and then compares this with observations to eliminate un-matched points inside a search area, resulting in a matched zone. In contrast, the point-based approach reverses the focus of computation: instead of calculating where the perfect matching zone is, the satellite signal visibility at a grid of point locations is first calculated using 3D models. This is then compared with GNSS measurements to assign each location with matching scores. Locations with higher degree of match can be used to estimate user's location. This approach is adopted in this author's work Wang et al. (2012*a*), Suzuki and Kubo (2012) and Isaacs et al. (2014).

These two approaches are essentially two forms of the same shadow matching concept that should be equivalent in terms of making use of knowledge derived from the 3D city models. A shadow-based approach starts with calculating the satellite signal shadow cast by buildings, which may be more straightforward, since it computes the 'shadow' first in the 'shadow matching'. It may also be straightforward to leverage GPU hardware acceleration, e.g. using OpenGL shaders (Shreiner et al., 2013) to speed up shadow computing, since shadow mapping is routinely supported by graphic cards (Purcell et al., 2002). A point-based shadow matching algorithm focuses on each candidate point (user's potential location), which is naturally required, e.g. in a particle filter, to determine each particle's weight. These

two approaches should give equivalent results in an ideal world. However, in the real world, the zone-based approach struggles when there is not 100 percent match between predictions and observations. Thus, the grid-based approach proposed in Wang et al. (2012*a*) is better from this perspective.

Though Suzuki and Kubo (2012), Isaacs et al. (2014) and this author's work all use a point-based approach, they have a difference in terms of 'which points' are used in satellite visibility determination. Suzuki and Kubo (2012) and Isaacs et al. (2014) first generate a number of particles in a particle filter, based on an initial position, and then use the 3D models to compute satellite visibility at each of these randomly generated locations. Some of the author's work also uses a particle filter (Wang, 2014*b*), but most of the author's work (Wang et al. (2012*a*, 2013*c*); Wang (2014*b*); Wang et al. (2013*b*, 2014)) opt to use a grid-based method (to be explained in more detail in Section 4.3) first, before applying any positioning algorithm, e.g. a k-nearest neighbor method (Chapter 4), a Kalman filter (Wang, 2014*b*) or a particle filter (Chapter 6). This method separates the 3D model related computation from a matching algorithm by pre-determining building boundaries using the 3D models at a regularly spaced grid of points.

The motivation of this author's grid-based method comes from two reasons. The first is that random particles may be too close to each other (e.g. a few centimeters or decimeters) compared to the 3D model's resolution. In other words, it is a waste of processing resources to compute satellite visibility for every single particle, once the particles are too close to each other. A grid-based method solves this issue by pre-defining the grid spacing, thus avoiding over-exploiting the 3D models beyond its accuracy limit.

The other reason for using a grid-based method comes from concerns raised when considering real-time, as oppose to post-processed, applications. For post processing navigation, using a grid-based method does not affect correctness of the results. Example user cases may include user location tracking, in which case users' location can be determined off-line after users' travel behavior. However, when it comes to real-time scenarios, the heavy computation of processing 3D models has to be conducted on the fly, i.e. at the time when positioning request is fired, if a grid-based

method is not used. For mobile devices, this means the device's battery would be drained faster and acquiring a positioning solution becomes slower. Whereas, a grid-based method allows all computations that involve 3D models to be pre-processed only once and the stored results, in the form of building boundaries (see Subsection 3.2.3), are used when needed (on-the-fly). This saves time and battery consumption for the real-time applications. A potential drawback of this building boundary approach is that the building boundaries (i.e. the intermediate pre-processed data) may require more storage space than the original 3D model. This trade off is regarded as plausible since without using the grid-based method, certain amount of 3D model data also has to be cached on user's devices, and caching itself also is the normal practice that many map applications (Google Maps, Apple Maps) use for their map layers. The data required for shadow matching can be regarded one of these layers, together with other layers, e.g. base vector maps, satellite image maps, roads, rivers and point-of-interests (POI).

4.2.2. Cloud computing or local processing

There are two system architecture options to convey shadow matching techniques - run the algorithm locally on the device, or, on a cloud. A discussion of storage requirements of a local processing approach and data transfer requirements of a cloud computing approach is presented in Wang et al. (2013*c*). A cloud computing approach for shadow matching is also mentioned in Isaacs et al. (2014).

The local processing approach and cloud computing approach are illustrated in Figure 4.2 (a) and (b), respectively. In approach (a), shadow matching is performed on the device, which pre-store the 3D city models or retrieve the model data from a remote server. It is assumed in this approach that no building boundary is pre-processed. This approach has a simple system structure, but requires a great amount of computation load and thus power consumption from the device. Depending on the computation capability of a mobile device, this process may take considerable amount of time. Thus, approach (a) is not particularly suitable for mobile devices. In approach (b), the device does not store 3D city models, leaving all shadow matching processing to the cloud. The device only measure GNSS signals as it already does in

conventional GNSS positioning, and sends its initial position and GNSS observations (this may include signal strength measurements) to the cloud server. Once the shadow matching positioning process is finished, the solution can be sent back to the user devices, which may integrate the solution with other positioning methods. In this approach (b), the server handles most of the computation, so the device reduces computation load and saves battery life. The device also saves storage since no 3D models nor intermediate data needs to be stored on it. However, the main drawback of this approach is that the computation cloud is significantly more complex than that in approach (a); and more importantly, the user has to tolerate unpredictable delays (e.g. network delays and server response delays), which may be the main bottle neck in the overall shadow matching positioning process.

The third approach, namely (c) in Figure 4.2, assigns most of the computationally intensive work to the cloud server which could pre-process building boundary generation, and pre-store or transfer the results (enhanced maps for shadow matching) to the device. The shadow matching application on the mobile device can then use the building boundary received from the server to conduct shadow matching with much less computation load. Using building boundary data for shadow matching, the user devices do not need to store or directly interact with the 3D city models, instead, only the useful information from the 3D models, i.e. the building boundaries, are used. Thus, the user devices are released from the most heavy computation involved in the shadow matching technique. Compared with approach (a), this approach leaves the less real-time processing load for the mobile device; compared with approach (b), this approach does not completely rely on the server, which may or may not always be fast and reliable. Furthermore, if the 3D models are copyrighted (as they normally are) and only allowed to be stored on the server rather than distributed to each user, this problem can be eliminated using the approach (c). Thus, approach (c) is designed and selected in this thesis.

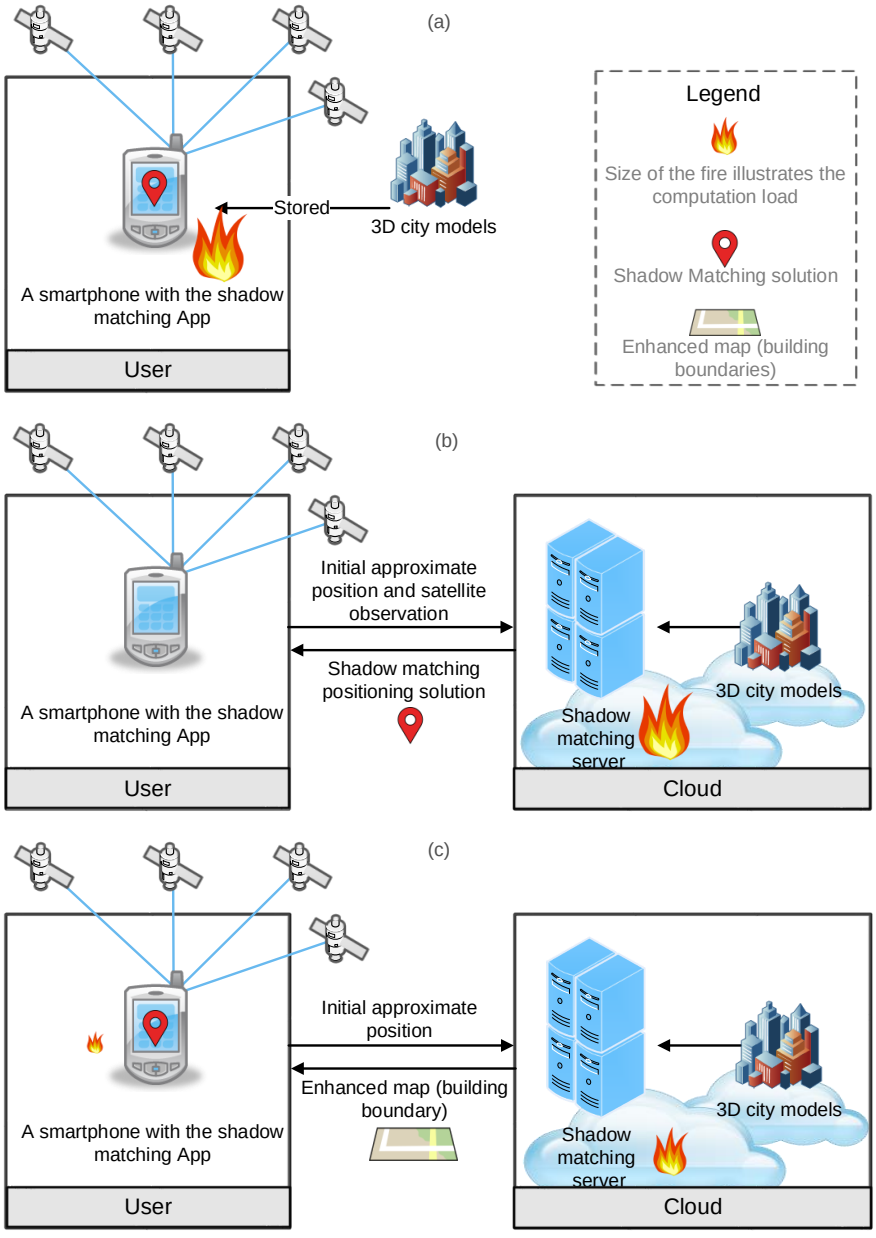

Figure 4.2.: Choices of system archetectures for shadow matching

4.3. A six-step shadow matching algorithm

This section introduces a basic but complete version of the shadow matching algorithm that is developed further later in this work. In this version, there are six steps to follow, each of them are described in details in the following subsections.

4.3.1. The overall shadow matching system

In this work, the shadow-matching algorithm has two phases – the offline phase (preparation) and the online phase (real-time positioning), consisting of six steps, as illustrated in Figure 4.3. An off-line phase is performed to generate a grid of building boundaries (an enhanced map for shadow matching). In the beginning of the online phase, the user position is first initialized, for example, using conventional GNSS positioning solutions. In the third step, the search area for the shadow-matching position solution is defined. Forth step predict the satellite visibility at each grid position using the building boundaries generated from the 3D city model in the offline phase. Fourthly, the similarity of satellite visibility between predictions and observations is evaluated using a scoring scheme to generate a score for each grid point in the search area, from which grid positions with best matches are found. Finally, the shadow-matching positioning solution is generated by a positioning algorithm (e.g. a modified k-nearest neighbours algorithm that averages the grid points with the highest scores). Each of the steps is described in more detail below.

4.3.2. Step 1: building boundary generation (offline phase)

In the off-line phase, building boundaries at a grid of locations are generated. A building boundary means from a GNSS user's perspective, the building's edge determined for each azimuth (from 0° to 359°) as a series of elevation angles. Figure 3.2 illustrates building boundaries with different resolutions. The results from this step show where the building edges are located within an azimuth-elevation sky plot. Once the building boundary has been computed, it may be stored and reused easily

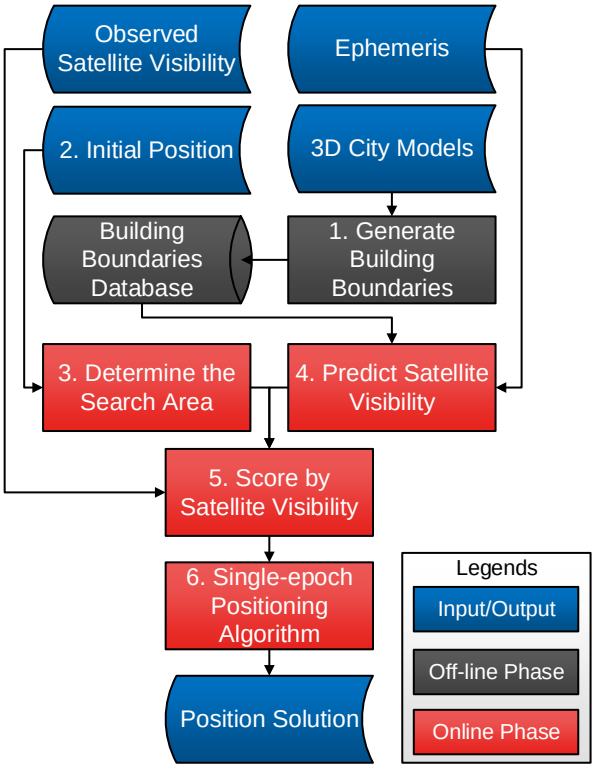

Figure 4.3.: A two-phase 6-step flowchart of the shadow matching algorithm

in the online phase to predict satellite visibility by simply comparing the elevation of a satellite with the elevation of the building boundary at the same azimuth.

To determine the building boundaries, 3D city models are used to determine visibility of virtual satellites at each azimuth and elevation angle. Details of literature, algorithm and experimental verification of satellite visibility determination in building boundary generation is described in Chapter 3.

Briefly mentioned in the Subsection 4.2.1, the design reasons for the off-line phase are discussed in more details here. From the perspective of mobile devices, limited computational power, memory and battery life introduces great concern on performance. To overcome these limits, the off-line phase is designed to move the most computationally intensive tasks from the mobile devices to the server (or cloud), as discussed in Subsection 4.2.2. This algorithm design exchanges real-time computational load for a one-off processing requirement at the server side. Specifically, this is achieved by representing the 3D model in a specially designed form - building

boundaries at a grid of positions. The observation behind the strategy is that the vast amount of data in a 3D city model is not of direct interest to the shadow-matching algorithm, only where the edges of the buildings are located from a user's perspective matter. Thus, utilizing this knowledge, only building boundaries at each candidate positions are abstracted from the 3D model. This method saves computation load because individual mobile devices do not need to compute the building boundaries on the fly. Instead, they can simply request building boundaries at a certain range of locations, or cache/store building boundaries for a desired region.

In building boundary generation, only buildings that are close to the candidate position and in the direction of interest are tested. Figure 4.4 illustrates the process and Figure 4.5 shows this refined search area. It should be noted that the parameters used in this example are manually selected based on knowledge of the 3D city model used in this work. Appropriate changes should be made if using another type of city model. The time required to generate building boundaries at a 500m by 500m grid of points (with 1m spacing) was 10 hours using a processor of ~3GHz.

Chapter 7 uses examples to discuss the practical side of how the size of building boundary data is related to the size of covered region.

4.3.3. Step 2: position initialization (online phase starts)

In the second step of a shadow-matching algorithm, an initial position should be acquired. This initial position is considered to be with low accuracy (e.g. a few tens of meters). It may, for example, come from standard point positioning (SPP) using GNSS pseudo-ranges, as is the normal practice in conventional GNSS positioning. Consistency checking may be used to identify non-line-of-sight signals and remove them from the position solution (Groves et al., 2013). Other available positioning methods (e.g. Wi-Fi) may be introduced into this step when the GNSS SPP is poor or unavailable. If the initial position comes with an associated accuracy, e.g. an error covariance matrix or a confidence region, this information may be used in the next step to better define the search region.

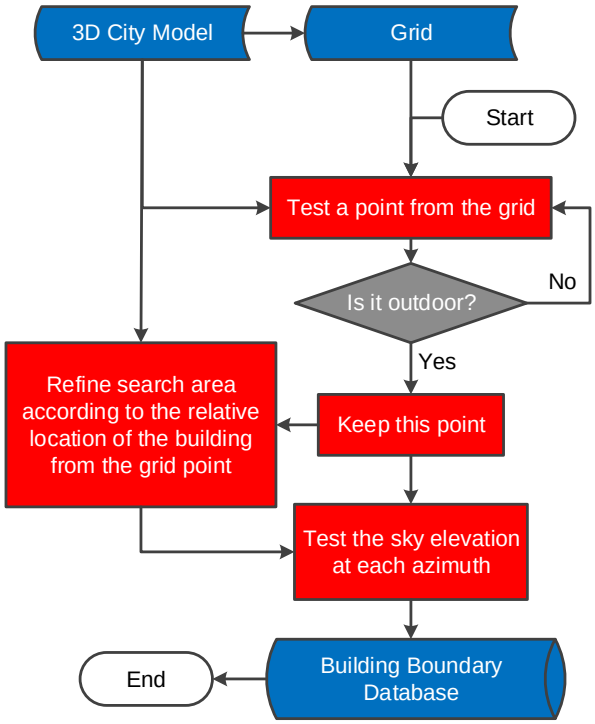

Figure 4.4.: The process that generates the grid of building boundaries

4.3.4. Step 3: search area determination

The third step defines the search area in which candidate positions are located for the shadow-matching position solution. A search area is defined based on an initial position generated in the second step. For example, the search area may comprise the area within a fixed-radius circle centred at the initialized position. Indoor locations can be excluded from the search area where the building boundaries grid is generated in the offline phase. The circle radius can be determined empirically. For example, a circular search area with a 40-metre radius is used in most of the author's work, which means it is assumed that the accuracy of initial position is within 40 metres. This is an empirical value learned using the smartphone GNSS tested in this work. A different radius can be used in another implementation and the bigger the radius of the search area is, more computation load is required to consider these areas. Clearly, there is a trade-off between saving computation power and increasing possibility of having the true position out of the search area. Having a bigger search area may

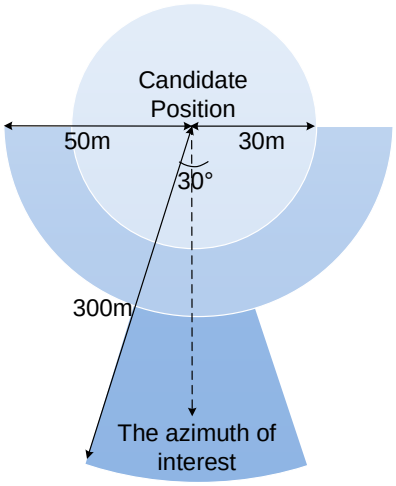

Figure 4.5.: The optimization used in building boundary generation by refining city models according to location of a candidate user position and an azimuth of interest. (Aerial perspective, the figure is not drawn to scale)

also cause greater ambiguity, to be discussed in more detail in Chapter 6. More advanced algorithms can be developed to use the knowledge from the initialization process to optimize the search area, e.g. vary the size and direction, or use a discrete description (e.g. particles, to be explained in more detail in Chapter 6) of its search area based on an assessment of the quality of the initial position.

The idea of a search region is illustrated in Figure 4.6, with the green area representing the search area centred at the initial position and the grid representing positions where building boundaries are available.

For example, Chapter 6 uses the error distribution information of the shadow matching result from the last epoch to estimate the current shadow matching 'search area' in a particle filter. Another example would be when the initial position is generated using a conventional GNSS solution, the satellite signal geometry, and hence the positioning accuracy, will be much better along the direction of the street than across the street. This is because an urban canyon affects the geometry of the available GNSS signals. Signals with lines of sight going across the street are much more likely to be blocked by buildings than signals with lines of sight going along the street, as demonstrated in Chapter 3. The search region in shadow matching can be

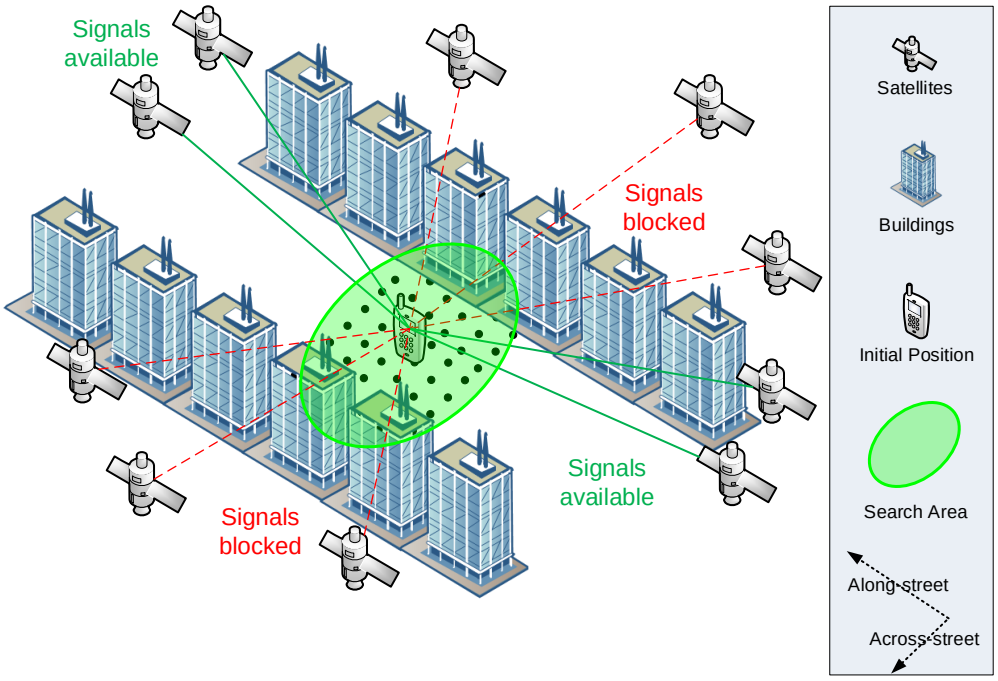

Figure 4.6.: A search region in the shadow matching algorithm

adjusted to account for this information. The conventional GNSS solution has lower across-street accuracy and higher along-street accuracy, which is complementary to shadow-matching solution.

4.3.5. Step 4: satellite visibility prediction

To predict satellite visibility, each satellite's elevation is compared with the building boundary elevation at the same azimuth. Where a satellite elevation is below the building boundary, the buildings block any satellite signals, assuming there are no holes in them allowing signals to travel through. Thus, the satellite is predicted to be visible if the satellite is above the building boundary; otherwise, the satellite is predicted to be invisible. This satellite visibility prediction concept is illustrated in Figure 4.7. The visibility is given by

$$V_{s,p} = \begin{cases} 1 & \theta_{nu}^{as} \geq \theta_{nu}^{pb}(\psi_{nu}^{as}) \\ 0 & \theta_{nu}^{as} < \theta_{nu}^{pb}(\psi_{nu}^{as}) \end{cases} \tag{4.1}$$

where $V_{s,p}$ denotes the predicted visibility of the satellite s at the candidate position p, 1 means visible and 0 means invisible; θ_{nu}^{as} denotes the elevation of satellite s, a denotes the user antenna, n denotes the local navigation frame, and u denotes line-of-sight unit vector; and $\theta_{nu}^{pb}(\psi_{nu}^{as})$ denotes the elevation of the building boundary at azimuth φ, from the perspective of the user position. Similar naming conventions are used in Groves (2013).

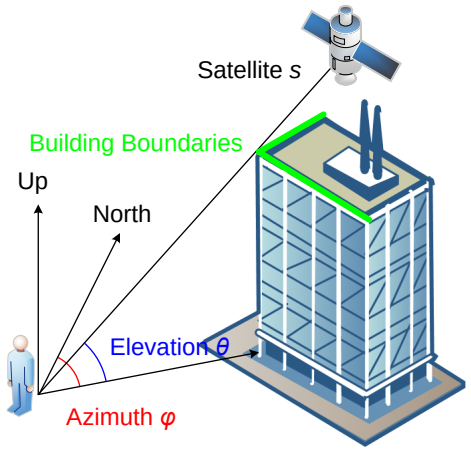

Figure 4.7.: Compare elevation of building boundaries with a satellite at the same azimuth

4.3.6. Step 5: satellite visibility scoring

In the fifth step, there are two stages for calculating a satellite visibility score: satellite scoring and candidate position scoring. Firstly, each satellite above the elevation mask angle is given a score, calculated based on the predicted visibility (obtained in the last step) and the observed visibility, using a scoring scheme. Secondly, the position scoring function is used to evaluate for each possible user position the overall degree of match between predicted and observed satellite visibility.

An example satellite scoring scheme SS_{22} is shown in Figure 4.8. Only direct line-of-sight (LOS) signals are considered using this scoring scheme. The diffraction effect could also be modelled. For example, a three-degree diffraction zone is modelled for building boundaries both horizontally and vertically in Chapter 3. Thus, in that

model, from the perspective of a GNSS receiver, buildings are three degrees lower and narrower than their actual height and width. If the line-of-sight (LOS) falls within the diffraction region, the signal is predicted to be diffracted. Otherwise, it is predicted to be invisible.

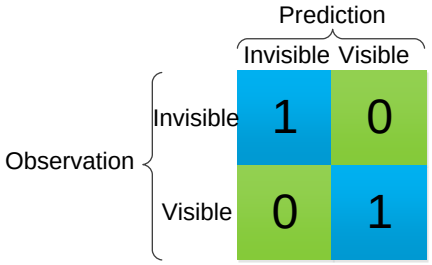

Figure 4.8.: A 2 by 2 scoring scheme SS_{22}

After each satellite is scored, each candidate position can then be scored via, for example, summing up the scores of each satellite. The candidate positions with higher scores indicate better matches, which conveys important information in the next step. An example function that sums up the scores from each satellite is shown in

$$f_{pos}(p) = \sum_{i=1}^{m} f_{sat}(s, p, SS) \tag{4.2}$$

where $f_{pos}(p)$ is the position score for grid point p; $f_{sat}(s, p)$ is the score of satellite s at grid point p; m is the number of satellites above the mask elevation angle; SS is the scoring scheme which defines a score based on predicted and observed satellite visibility.

By the end of this step, each grid position should have a score to represent the degree to which it matches the observed satellite visibility, and thus how likely that each candidate position is close to the true location. A shadow matching score map is thus obtained. An example of this map is shown in Figure 4.9, which shows data collected at location R1 (refer to Figure 4.12), to be described in more detail in Section 4.4.1.

This scoring scheme can been improved to acknowledge error caused by diffraction and reflection effects. Besides diffraction modelling described in Chapter 3, Chapter 5 further introduces how to smartly use signal to noise ratio (SNR) to properly model and compensate these error. Generally, a weak signal is regarded likely to be reflected or diffracted, thus it is given a lower weight compared to a strong signal, but an optimized weighting scheme should be used, as investigated in Chapter 5.

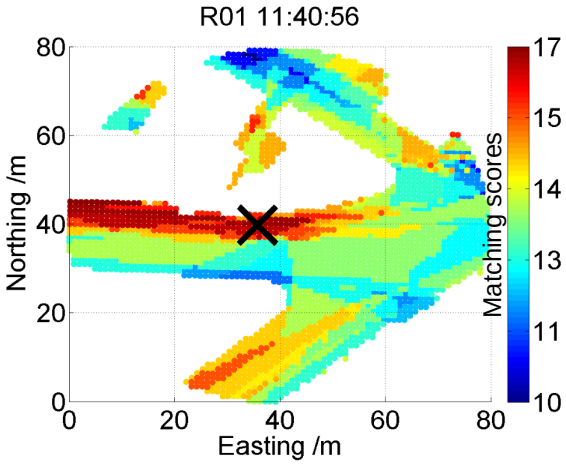

Figure 4.9.: A example of a shadow matching scoring map that shows a range of matching scores at a grid of locations. The true location is marked by a black cross.

4.3.7. Step 6: positioning using scores at candidate positions

The last step of the shadow-matching algorithm is to generate a positioning solution using scores from each candidate position. Shadow matching is essentially a pattern-matching positioning method, which is discussed in general terms in Groves (2013). As the process of Wi-Fi fingerprinting is similar to this process in shadow matching, the algorithms used in Wi-Fi fingerprinting may be used in shadow matching. Possible algorithms include, but are not limited to, k-weighted nearest neighbours (adopted in this chapter), a Kalman filter (adopted in Wang (2014*b*)) and a particle filter (adopted in Chapter 6).

To give an example, a method similar to k-nearest neighbours is described below

that estimates the location by averaging the grid positions with the highest scores. With the scoring scheme SS_{22}, scores take integer values. Therefore, several grid points typically share the highest score. The grid points with the highest score are regarded as nearest neighbors in terms of their score distance (i.e. difference in their scores). Since they share the same highest score, the score distance is 0. These points can thus be considered nearest to each other from this perspective. An average of their locations is deemed as the positioning solution. Mathematically, this means the location estimate is determined using equations 4.3 and 4.4 for the northing and easting projected coordinate components, N_a and E_a respectively:

$$N_a = \frac{\sum_{i=1}^{l} N_i}{l} \tag{4.3}$$

$$E_a = \frac{\sum_{i=1}^{l} E_i}{l} \tag{4.4}$$

where N_i and E_i are, respectively, the northing and easting coordinates of the i^{th} high-scoring candidate positions. Note that l varies from epoch to epoch depending on how many candidate positions share the highest score.

4.4. Assessments using geodetic and smartphone GNSS receivers

The satellite visibility determination method described in Chapter 3 is examined using survey-grade (geodetic) receivers. However, smartphone-grade GNSS receivers are more feasible in most potential applications of the shadow matching technique, due to its smaller size, cheaper cost and lower power consumption. Thus, in this section, both geodetic and smartphone GNSS receivers are used to access the performance of the shadow matching algorithm that is described in this Section 4.3. Comparisons are conducted between these two categories of receivers, in terms of cross-street and along-street positioning accuracy. This section first describes the experimental settings and configurations. The shadow-matching positioning perfor-

mance using geodetic GNSS receivers is then assessed and compared with that using smartphone GNSS receivers.

4.4.1. Experimental settings and shadow matching configurations

Experimental data was collected in the Aldgate area of central London using a geodetic GNSS receiver (Leica Viva GS15) and a consumer-grade GNSS receiver on a smartphone (Samsung Galaxy S3) running a bespoke Android data logging application developed by the author. A screen shot can be found in Figure 4.10. The SNR measurements, satellite azimuths and elevations, and the conventional GNSS position solution are all included in the National Marine Electronics Association (NMEA) message from the phone's GNSS chip. Data from the Leica Viva receivers are outputted as Leica's proprietary data, which can be transformed to standard RINEX observation files using TEQC, a toolkit for GNSS data pre-processing (Estey and Meertens, 1999), which includes time tags, pseudo-range and SNR measurements.

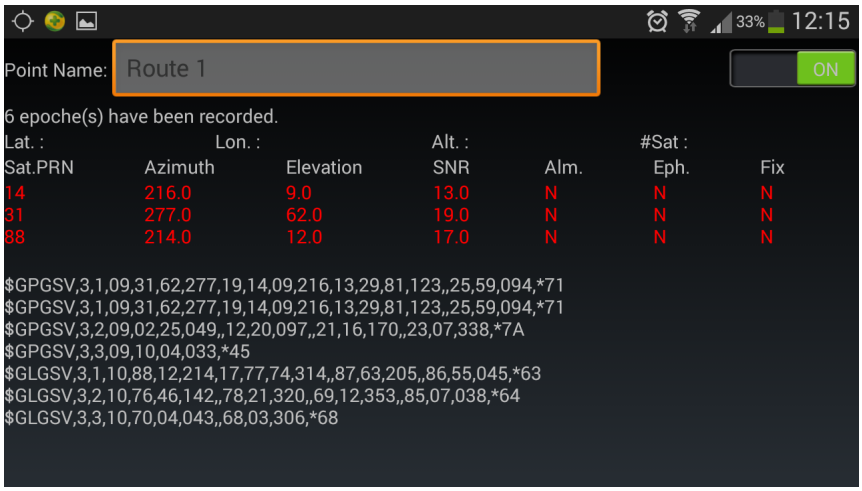

Figure 4.10.: A screen shot of the developed Android app which is used to record GNSS data for shadow matching (including satellite PRN, signal-to-noise ratio, azimuth, elevation and conventional GNSS positioning solution).

A 3D city model of the Aldgate area, provided by ZMapping Ltd, was used to generate the building boundary data used for the subsequent analysis. The model used in this study is a mixed level of details (LoD) 1 and LoD 2 model, with decimetre-level accuracy, transformed into the Virtual Reality Modelling Language (VRML) format. Here the convention on LoD used in CityGML is used, which is discussed in Section 3.1.

Figure 4.11 visualises the 3D model used in this study. The truth reference was determined using a tape to measure the distance to a distinctive feature, such as a building wall or the kerb between the road and footpath and then locating that feature on the 3D city models. This process is accurate to decimetre level, which is sufficient for this study since the aimed positioning accuracy is at meters level. Other methods in surveying may also provide the truth model. For example, static GNSS occupation of the test points may provide position with high accuracy (cm-dm). However, this method is not considered feasible because in the deep urban environments, severe multipath and NLOS reception significantly reduces the number of 'clean' GNSS signals and thus degrades positioning accuracy. An alternative is to set up GNSS stations in an open environment, from where total stations used to traverse this area. However, there isn't such open environment close to this area in central London. Thus, a truth model is obtained using the 3D city models.

Twenty experimental locations with various road layouts were selected in the area covered by the city model. Figure 4.12 is an aerial view of the experimental area, showing each site. Pairs of sites (prefixed by R and G) are located on opposite sides of the street, which enables the testing of shadow matching's ability to determine the correct side of the street. All sites were located on the footpath, close to a traffic lane.

The implementation of shadow matching is based on the description in Section 4.3. In the offline phase, a 1 meter by 1 meter grid has been generated, and the building boundaries determined at each grid point. In the online phase, position initialization is performed using conventional GNSS positioning results because this study

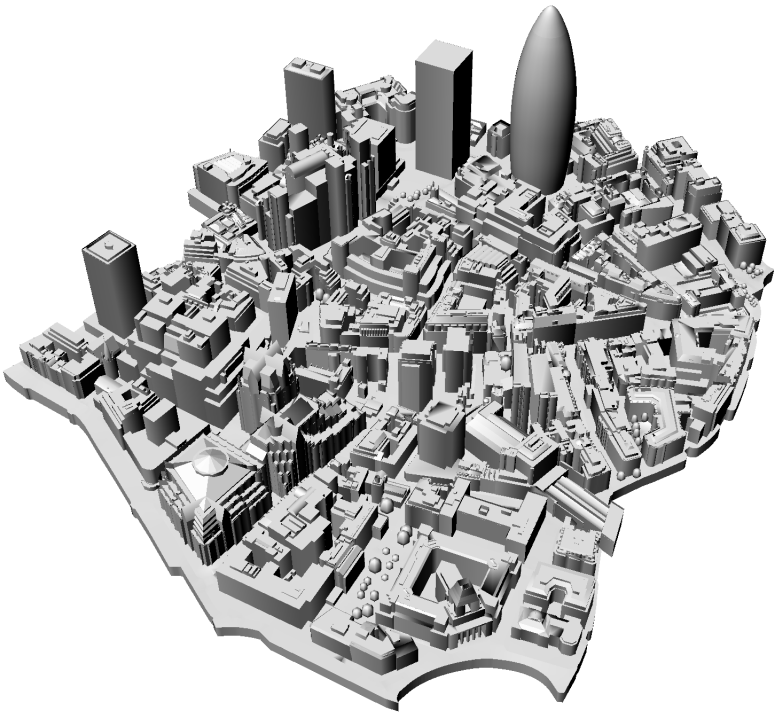

Figure 4.11.: The 3D model of London used in the experiments

focuses on comparing the different types of receivers. Instead, position initialization is based on the true position, acquired from the 3D city model. This is because the performance of shadow matching algorithm using different receivers are being compared, rather than the whole positioning system. Whereas different positioning algorithms/methods used by different receivers in the shadow matching positioning initialization can result in very different initial positions. Thus, in order to prevent initialization errors from contaminating the following scoring step, the search area for each site is centred at the true position. This area is within a radius of 20 metres of the true position, within which candidate positions are generated. Indoor points are eliminated by checking the point's visibility of sky. The scoring process uses a basic S_{22} scoring scheme (see Figure 4.8). The modified k-nearest neighbours algorithm is used to determine the positioning solution of shadow-matching algorithm,

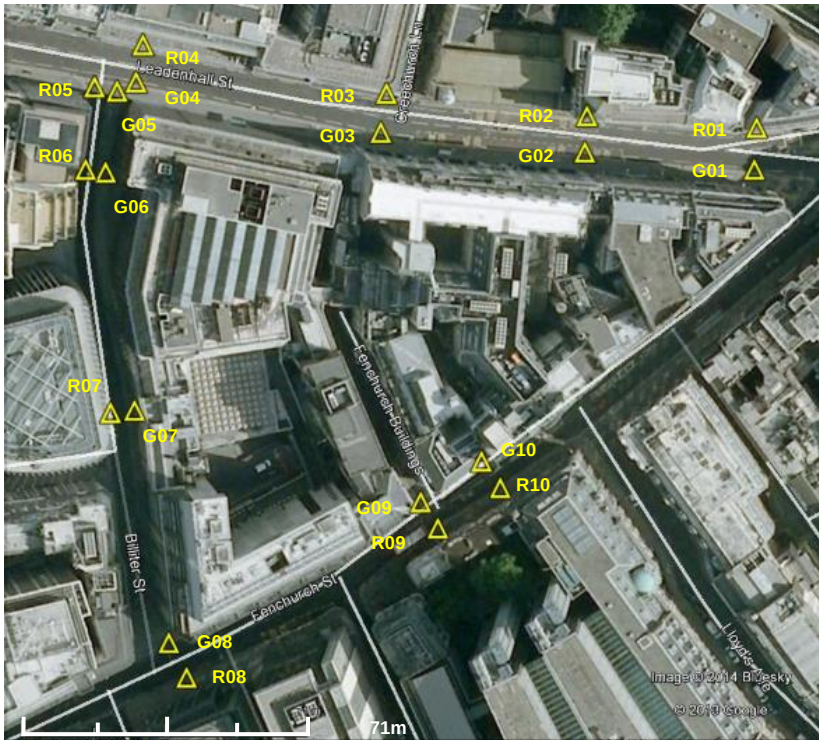

Figure 4.12.: An aerial view of the experimental area (satellite image from Google Earth)

as described in Subsection 4.3.7.

4.4.2. Experimental results and analysis

From the experimental results, conventional GNSS positioning is typically found performing relatively poorly in the across street direction, and better along the street. Figure 4.13 shows a typical example of the conventional GNSS positioning solution (at point G003) using weighted least square (WLS) with a Leica Viva GNSS receiver. It demonstrates that the cross street position from the conventional GNSS solution can vary by ~35 meters. This lower accuracy performance of conventional GNSS in cross-street direction is suggested by simulated GNSS performance in Subsection 3.4.3 using 3D city models. The same issue is also shown by the mathematical modelling in Groves (2011). The lower accuracy of conventional GNSS in cross-street direction demonstrates the demand for a technique like

shadow matching to improve cross-street positioning accuracy. More detailed analysis on conventional GNSS positioning using smartphone receivers and its comparison with shadow matching solutions are given in Subsection 5.4.2 and 6.5.2.

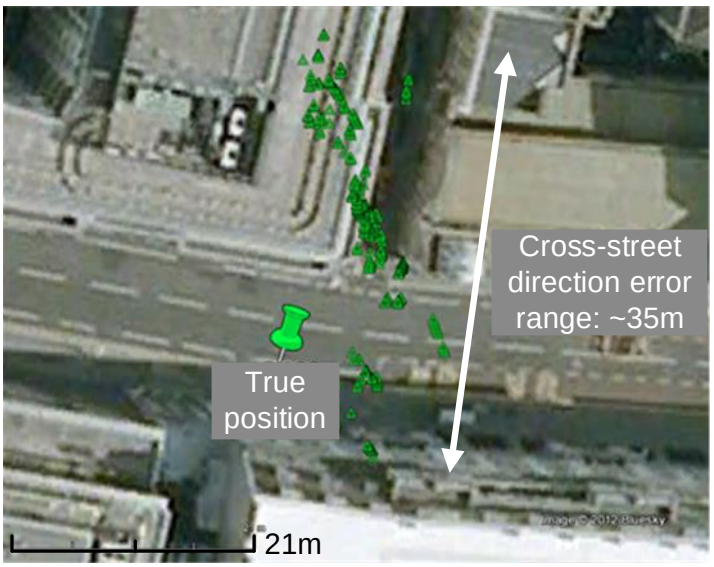

Figure 4.13.: Typical conventional GNSS positioning results showing lower accuracy in the across-street direction and higher accuracy in the along-street direction

To assess the performance of the shadow-matching algorithms using different grade of GNSS receivers, the north and east position errors were transformed to along-street and cross-street position errors. Figure 4.14 shows the mean absolute deviation (MAD) value of the cross-street position error at each site, using geodetic and smartphone GNSS receivers, marked in the figure as (a) and (b), respectively. The MAD is calculated using

$$MAD = \frac{1}{n}\sum_{i=1}^{n} abs(x_i) \tag{4.5}$$

where MAD is the mean abusolute deviation of cross-street positioning error, x_i is the cross-street positioning error at the i^{th} epoch, and n is the number of epochs.

Figure 4.14 shows that, the cross-street accuracy is typically better than the along-

street accuracy, for both geodetic and smartphone shadow matching solutions. Since cross-street direction is where conventional GNSS is less accurate, this direction is focused on in the analysis. It can be seen that, at most sites, the geodetic shadow-matching cross-street accuracy is better than 5m, whereas for smartphone shadow-matching solutions, there are 6 sites where its position error is bigger than 5m. This indicates that geodetic shadow-matching solutions outperforms smartphone shadow-matching solutions in the cross-street direction. However, there are a few cases where geodetic shadow-matching solutions are poorer than smartphone shadow matching e.g. G07, which might be caused by the fact that the data was collected at different times, so sometimes, the satellite configuration was more favorable with the smartphone data. This also suggests that the statistical results (to be presented) may be more sensible than the direct point-by-point comparison.

Figure 4.15 further shows the overall shadow matching positioning performance by averaging the MAD over all sites. It clearly shows the trend that geodetic shadow-matching solutions outperform smartphone shadow matching solutions on average.

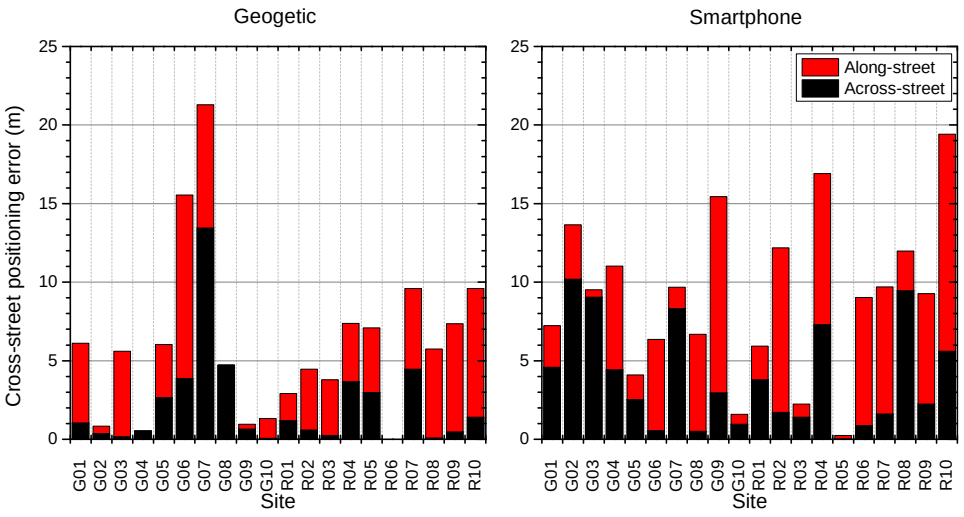

Figure 4.14.: Mean absolute deviation of shadow matching cross-street positioning error using geodetic and smartphone GNSS receivers

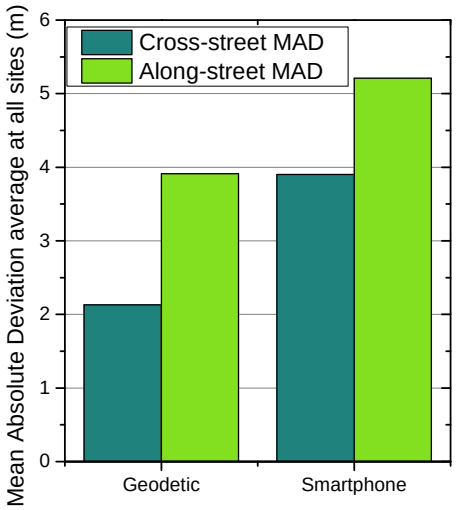

Figure 4.15.: Mean absolute deviation of shadow matching cross-street positioning error using geodetic and smartphone GNSS receivers averaged over all sites

More analysis was conducted to calculate the proportion of results for which the cross-street positioning error was within certain limits. This may be thought of as the success rate for achieving certain performance specifications. For example, a typical street is around 10m wide, so a positioning accuracy within 5m is considered good enough to determine the correct side of the street, while 2m is sufficient to distinguish the footpath from a traffic lane. Figure 4.16 shows the success rate averaged across all sites. The overall success rate for determining the correct side of a street was 81.0% using geodetic receivers, compared to 62.6% using smartphones. The success rate for distinguishing the footpath from a traffic lane was 59.5% for geodetic receivers and 35.2% for smartphones.

Judged based on both mean absolute deviation and proportion of results for which the cross-street positioning error was within certain limits, it is safe to draw the conclusion that shadow matching algorithms using geodetic receivers outperforms when smartphones are used. It should be noted that a basic version of shadow matching algorithms, among many possible alternatives, is used. Compared with geodetic receivers, smartphone GNSS receivers typically track more signals, and as

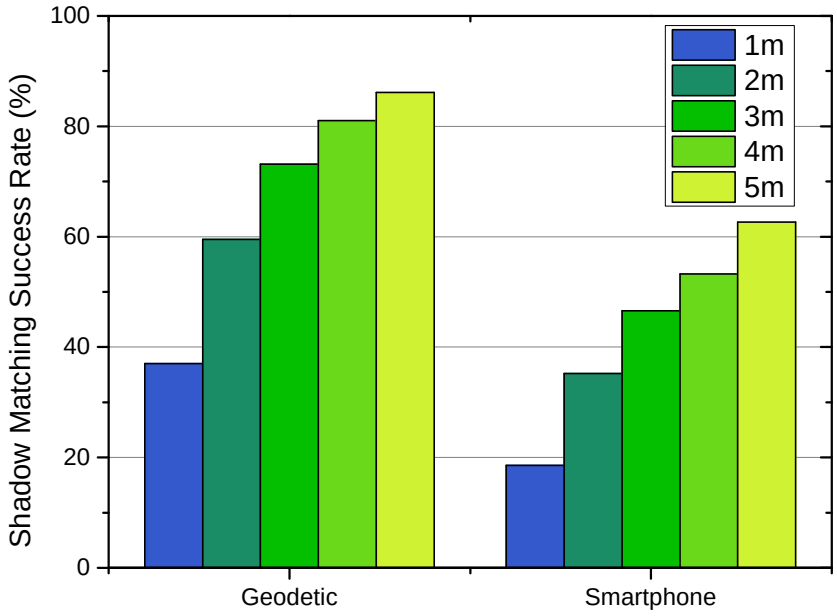

Figure 4.16.: Proportion of cross-street position errors within certain ranges (success rate) across all sites using geodetic and smartphone GNSS receivers

a trade off, it suffers from lots of NLOS being tracked. As more NLOS reception on smartphones confuses the shadow-matching algorithm, further research should be conducted to model NLOS reception and optimize the shadow matching algorithm to account for this effect. Details of this research are described in Chapter 5.

4.5. Chapter summary

In this chapter, the development history of the shadow matching technique is reviewed, with different design options described and compared. A two-phase six-step shadow-matching algorithm is proposed. The algorithm is implemented and tested using both geodetic and smartphone GNSS data. Real-world GNSS data has been collected at 20 different locations in the same urban area, both on a geodetic GNSS receiver and a smartphone app developed in this work. A comprehensive statistical performance analysis using different grade of GNSS receivers is presented. The

results show that the geodetic shadow-matching solutions achieve an average cross-street accuracy to 2.13m, outperforming shadow matching using smartphones, which exhibits 3.90m average cross-street positioning error. The success rate for determining the correct side of a street is 81.0%, better than 62.6% using smartphones; while the success rate for distinguishing the footpath from a traffic lane is 59.5%, also better than that using a smartphone, which achieves 35.2%. As shadow matching has a cross-street accuracy of a few meters, it is highly complementary to conventional GNSS positioning methods.

This chapter presents results from a very basic shadow-matching algorithm. Chapter 5 and 6 investigate the performance that can be achieved using more advanced algorithms.

Chapter 5.

Probability-based Shadow Matching Using Bayesian Techniques

This chapter focuses on the optimization of the satellite visibility scoring (step 4, illustrated in Figure 4.3) in the shadow matching algorithm described in Chapter 4. The importance of distinguishing direct line of sight (LOS) / non-line-of-sight (NLOS) in shadow matching algorithms, especially on smartphones, is introduced in Section 5.1. Two rounds of optimization are investigated. In the first round, signal visibility and diffraction in the scoring schemes are modelled by empirically setting thresholds of signal-to-noise ratio (SNR). To improve this modelling, the smartphone GNSS signals should be better understood, thus a LOS/NLOS signal analysis with respect to SNR and elevations is presented in Section 5.2. This analysis inspires the second round of optimization, using Bayesian techniques, which leads to a probability-based shadow-matching algorithm, as presented in Section 5.3. A comprehensive performance assessment is conducted to compare the probability-based shadow-matching algorithm, basic shadow-matching algorithm and conventional GNSS positioning, with static smartphone GNSS measurements at 20 locations. This chapter is partially based on Wang et al. (2013*a*), and another paper under review at Journal of Navigation (Wang et al., 2014).

5.1. Importance of LOS/NLOS determination in shadow matching

The generic shadow-matching algorithm introduced in Chapter 4 does not specifically account for possible performance challenges in urban environments. More specifically, challenges may come from phenomena including diffraction and NLOS reception that the user devices are vulnerable to in urban areas. The buildings, especially with glass, metal or wet surfaces, are particular strong reflectors that cause signal reflection in urban environments (Groves, 2013).

The signal reflection problem becomes more severe for smartphone GNSS positioning. Many potential applications of shadow matching use smartphone-grade GNSS user equipments (Groves, Wang and Ziebart, 2012). Although smartphone GNSS receivers cost much less than geodetic GNSS receivers, they can be subject to features including more severe signal tracking noise, multipath reception, and stronger non-line of sight (NLOS) reception due to the low gain and linear polarization of smartphone-grade GNSS antennae. These features impose difficulty when distinguishing right-hand circularly polarized (RHCP) direct-LOS signals from the generally left-hand circularly polarized (LHCP) NLOS/multipath signals using the SNR (Groves et al., 2010). The higher sensitivity of smartphone GNSS receivers is designed to increase positioning service availability, but as a trade off, they track the weak signals, most of which would be NLOS.

The generic shadow matching algorithm, as described in Chapter 4, is demonstrated to have worse performance when using smartphone GNSS, compared with geodetic GNSS receivers. This is because, essentially, the principle of shadow matching assumes that where a prediction is matched with an observation, the location is likely to be user's true location. If observed NLOS signals are not properly modelled, when an NLOS signal is observed at a location, it will confuse the shadow matching algorithm, which may falsely score lower at the true location, or higher at incorrect locations.

One approach to solve the NLOS problem is to focus on using sophisticated mathematical model to predict NLOS reception using 3D models, as demonstrated Suzuki

and Kubo (2012). The reality is that NLOS cannot be perfectly modelled in prediction due to the fact that there are too many factors to consider in practice, e.g. a good NLOS model requires knowing the physical materials of each part of the building surface, which is not routinely available for 3D building models, and signal blocking caused by user bodies and passing objects (vehicles and pedestrians). More importantly, prediction needs to match with observation to score correctly in the shadow matching algorithm. Thus, judging whether an observation is LOS or NLOS is very important.

In summary, shadow matching algorithms for GNSS positioning in urban canyons should be optimized to account for NLOS signal reception, especially for smartphones. In this chapter, techniques are developed to help classify the received signal strength as LOS or NLOS based on their SNR.

5.2. LOS/NLOS analysis in respect to SNR and elevation

The existing scoring scheme SS_{22} is shown in Figure 4.8. Only direct line-of-sight (LOS) signals are considered using this scoring scheme, whereas the shadow matching user equipment can also observe diffracted and reflected signals. This mismatch can degrade shadow-matching performance, as discussed in the Section 5.1.

A modified method to improve the basic scoring scheme has been proposed and tested in Wang et al. (2013*a*). This method is proved be able improve performance of shadow matching using geodetic GNSS receivers to a certain extent (refer to Wang et al. (2013*a*) for more details).

Although the modified shadow matching scoring schemes account for occurrence of weak signals and follow the common sense that a strong signal is more likely to be a LOS signal, fundamentally, the score assumes that there is a clear SNR boundary between direct LOS signal and NLOS and diffraction signals when, in reality, the boundary is fuzzy, particular with a smartphone. Thus, a more realistic model might be expected to give better results.

Determining a realistic model requires good understanding of the characteristics

of smartphone GNSS reception. This section aims at exploring the characteristics of smartphone GNSS receivers, with the expectation of discovering clues to improve the scoring schemes. In other words, the better smartphone GNSS characters are understood, the more chance that a better scoring scheme (to be presented in Section 5.3) can be designed.

5.2.1. Collection large experimental data sets

To understand the characteristics of smartphone GNSS, a large set of experimental data should be collected. Experimental data was collected in the Aldgate area of central London using Samsung Galaxy S3 Smartphones running a bespoke Android data logging application. Since the same experimental data as in Chapter 3 and 4 are used, please refer to Subsection 4.4.1 for more details about the static experiments. An aerial view of the experimental area (satellite image from Google Earth) can be found in Figure 4.12. Figure 4.11 visualises the 3D model used in this study.

It should be noted that the experimenters stood at each of the selected 20 locations, for two rounds of 6 minutes each. The time between the two rounds of data collection was 4 hours, allowing the satellite constellation to change significantly. Thus, it is considered that the two rounds of data are independent of each other. The second round of data is used for analysis in this section; whereas the first round of data is used for testing the new shadow matching algorithm. Satellite visibility information for both GPS and GLONASS (comprising time tag, satellite azimuth, elevation and SNR) were recorded at 1Hz for post-processing using shadow matching. Thus, a total of 24000 epochs, i.e. seconds, of smartphone GPS and GLONASS data were collected at the 20 locations. The number of data sets is considered a large data set of static smartphone GNSS data.

5.2.2. SNR and elevation analysis

Normally, a signal with a higher SNR is more likely to be direct LOS than NLOS. For example, signals reflected from non-shiny buildings are typically weaker than direct signals from satellite. However, glass buildings, wet walls and surrounding vehicles

can cause strongly reflected signals (Groves, 2013). Thus, some NLOS signals can be stronger than some direct LOS signals, with a smartphone antenna. With a better antenna (e.g. geodetic), LOS signal would have to be attenuated by people, foliage etc. to be weaker than the straight NLOS signals. On the other hand, weak LOS (no buildings directly block the line-of-sight) signals can also be received as a result of user body masking or signal attenuation caused by trees and surrounding pedestrians.

As discussed in Section 5.1, the characteristics of smartphone antennae make it more difficult to distinguish LOS from NLOS signals using SNR measurements. In this section, the SNR distributions of the direct LOS and NLOS signals are analysed separately. The 3D city model is used to determine which of the received signals are direct LOS and which are NLOS using the visibility prediction method described in Chapter 3 and knowledge of the true user position. Signals predicted to be visible are assumed to be direct LOS. Diffracted signals are counted in the NLOS category for this study. The results of this analysis can be used to improve the shadow-matching algorithm, as described in Section 5.3.

Figure 5.1 shows histograms for each of the test sites showing the normalized distributions of the measured SNR of the direct LOS and NLOS signals. Figure 5.2 shows the LOS and NLOS SNR distributions averaged across all of the experimental sites. Both direct LOS signals, shown in red, and NLOS signals, shown in blue, were received at every test site, verifying that smartphone GNSS receivers usually capture NLOS signals in urban areas. Comparing different sites, it can be seen that, at some (e.g., R02 and G10) a higher proportion of the signals received were direct LOS whereas at others (e.g., G07 and R09), more NLOS signals than LOS were received. Reasons for this may include the nature of the surrounding buildings and satellite geometry.

At every site, the LOS signals are likely to have higher SNRs than the NLOS signals. However, there is considerable overlap between them, particularly between 20 and 30 dB-Hz, confirming the expectation that both strong NLOS signals and weak LOS signals are commonly received by smartphones in dense urban environments.

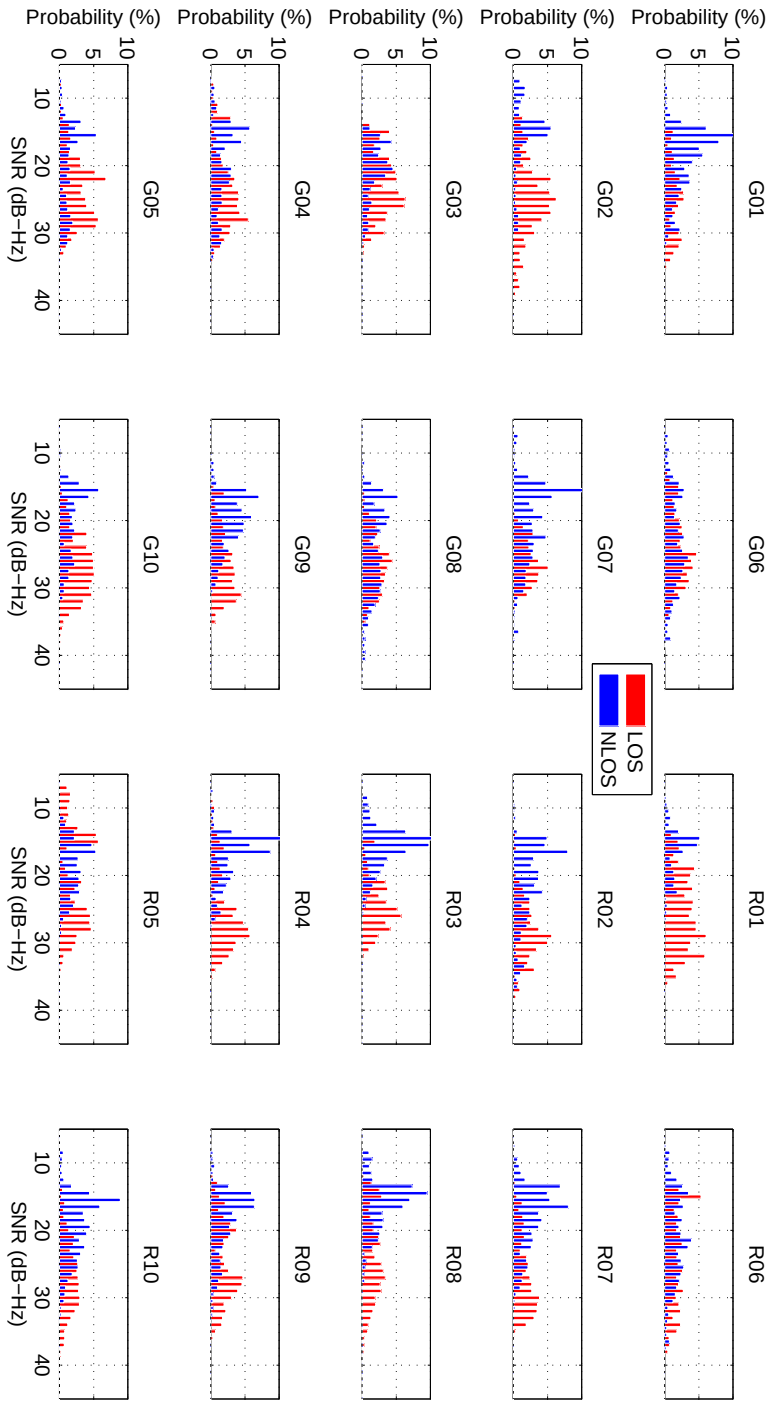

Figure 5.1.: Normalized SNR distributions of LOS and NLOS reception at each site

Thus, an absolute SNR boundary to distinguish LOS from NLOS signals cannot be defined. Instead, the data may be used to infer the probability that a signal received with a particular SNR is LOS. For example, it can be deduced from Figure 5.2 that the probability of a 24 dB-Hz signal being LOS is approximately 50%, whereas a 39 dB-Hz signal has a ~90% probability of being LOS.

Figure 5.3 shows the normalized measured SNR distributions for different satellite elevations averaged across all sites. The low elevation signals are more likely to be NLOS and the higher elevation signals are more likely to be LOS as they are less likely to be blocked by buildings. It can be seen that for elevations below 40°, the SNR drops as the elevation decreases, whereas above 40°, there is little relationship between SNR and elevation.

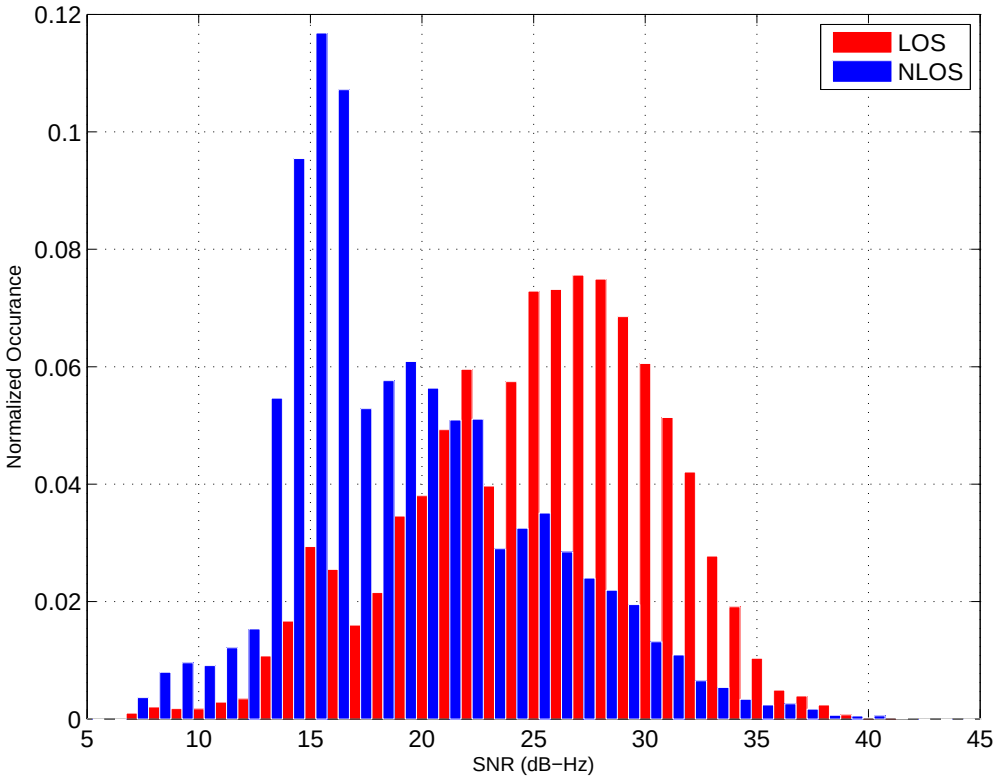

Figure 5.2.: Normalized SNR distributions of LOS and NLOS signals across all test sites

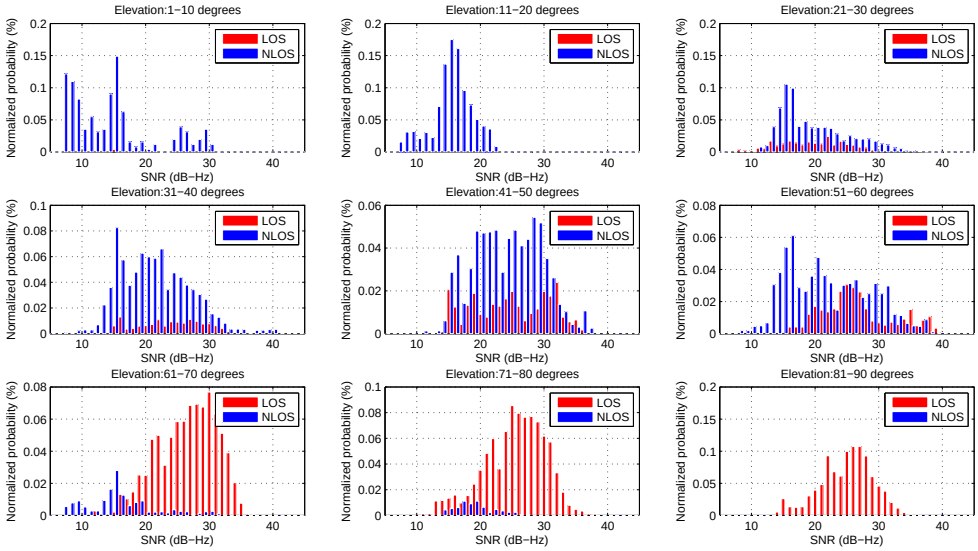

Figure 5.3.: Normalized SNR distributions of LOS and NLOS signals at different elevation angles

5.3. LOS/NLOS probability-based shadow matching

Given the smartphone GNSS characteristics as analyzed in Section 5.2, a Bayesian technique is proposed to improve the scoring scheme via sample statistics.

Given a known SNR from the smartphone GNSS receiver, the probability that a signal is a direct LOS can be calculated. In mathematical terms, this probability can be expressed as $p(LOS|SNR = s)$, where s may, for example, range between 5 to 45 dB-Hz for smartphone GNSS receivers. For each of the SNR values, there can be a correspondent conditional probability $p(LOS|SNR = s)$ that a signal is LOS. These conditional probabilities form a simple Bayesian network, where all of the probabilities can be stored in a "conditional probability table" (CPT) Nilsson (2009). The same principle applies to NLOS signals. Figure 5.4 illustrate an example network. Since a large number of GNSS visibility samples has been computed using the 3D city models in Section 5.2. It should be noted that each for two rounds of data collection is separated by 4 hours to allow the satellite constellation to change significantly. The CPTs can be estimated via 'sample statistics', to be further

discussed later.

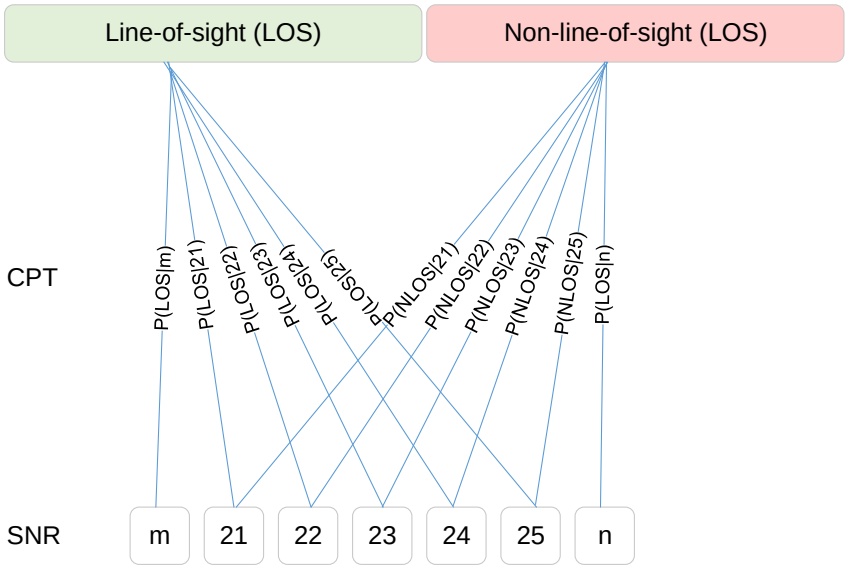

Figure 5.4.: Illustration of conditional probability table (CPT) computation. (m means SNR smaller than 21 dB-Hz and n means SNR larger than 25 dB-Hz)

As Figure 5.1 and Figure 5.2 show, there is considerable overlap between the SNR distributions of direct LOS and NLOS GNSS signals received by smartphones. Thus, it is not possible to set a definitive SNR threshold, above which a received signal may be assumed to be direct LOS. Consequently, the simple visibility-prediction scoring scheme with definitive SNR threshold cannot be expected to work well. Instead, a probabilistic approach via conducting sample statistics, can be adopted to estimate the probabilities and calculate the conditional probability table (CPT) (Nilsson, 2009). In this approach, the probability of a signal being direct LOS is estimated from the measured SNR and the satellite visibility prediction from the 3D city model scored accordingly. A set of all these conditoinal probabilities $p(LOS|SNR = s)$ forms the conditional probability table (CPT), which stores the knowledge acquired from the sample statistics. From Bayes theorem, the probability of an observed signal being direct LOS given a measured SNR of s is

$$p(LOS|SNR = s) = \frac{p(SNR = s|LOS)p(LOS)}{p(SNR = s)} \tag{5.1}$$

where $p(SNR = s|LOS)$ is the probability of an SNR of s being measured, given that the signal is direct LOS, $p(LOS)$ is the probability of the signal being direct LOS and $p(SNR = s)$ is the probability of the measured SNR being s. If l_i is the proportion of signals measured that are direct LOS and for which the measured SNR is i and n_i is the proportion of signals measured that are NLOS and for which the measured SNR is i, then

$$p(SNR = s|LOS) = \frac{l_s}{\sum_i l_i} \tag{5.2}$$

$$p(LOS) = \sum_i l_i \tag{5.3}$$

and

$$p(SNR = s) = l_s + n_s \tag{5.4}$$

where it is assumed that $\sum_i (l_s + n_s) = 1$. Therefore, substituting equations 5.2, 5.3 and 5.4 into equation 5.1,

$$p(LOS|SNR = s) = \frac{l_s}{l_s + n_s} \tag{5.5}$$

Sample statistics can be computed to find the SNR distributions of LOS and NLOS signals, l_s and n_s. When the amount of experimental data is large enough, sample statistics can be used to determine CPT, which can be used in shadow matching satellite visibility scoring. In this work, the two rounds of experimental data are divided into a training set and a test set. The second round data are used to train a CPT model, i.e. a $p(LOS|SNR = s)$ model, and the first round of experimental

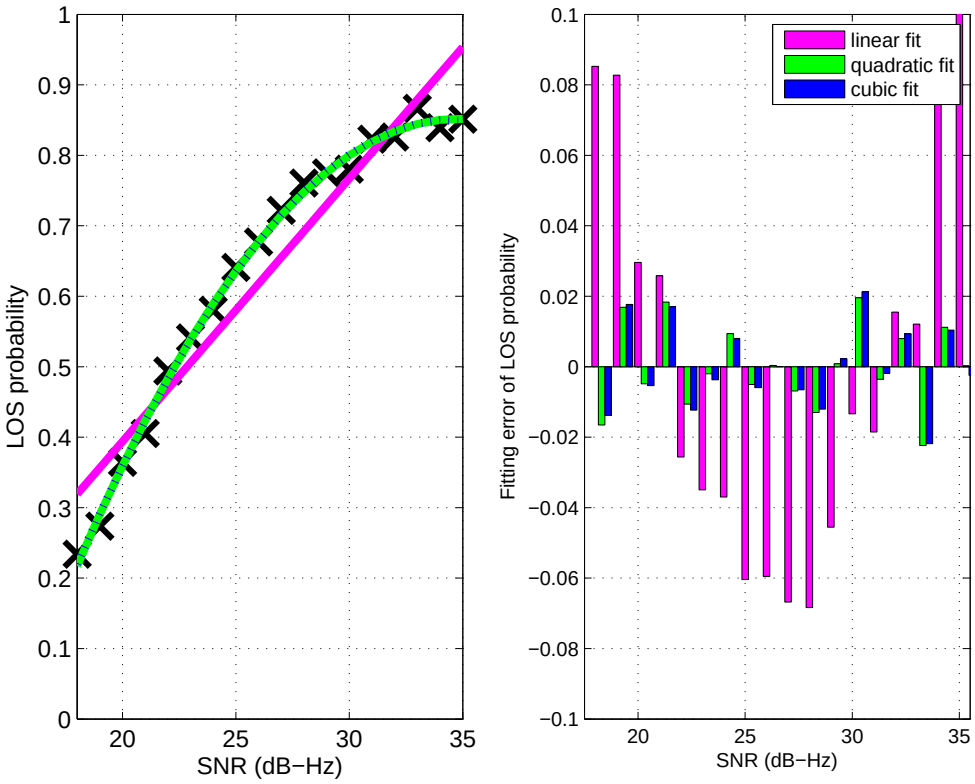

Figure 5.5.: Left: Probability of LOS, i.e. $p(LOS|SNR = s)$, when the SNR is between a upper bound and a lower bound, fitted as a linear function, a quadratic function, and a cubit function, shown in purple, green and blue, respectively. Right: The fitting error in terms of residuals shows good fitting with a quadratic function. A cubic function is not needed because it results in very similar residuals with a quadratic function.

data are used for testing purpose, as described in Section 5.4.

In a CPT model, it is assumed that when the SNR is higher than a specified upper bound, the p(LOS) is regarded as a constant probability close to (but not equal to) 1; when the SNR is lower than a specified lower bound, the p(LOS) is regarded as a constant probability close to (but not equal to) 0; when the SNR is in between the upper bound and lower bound, a polynomial fitted model can be used. An assumption is made that once the SNR is high enough, it is equally likely that the signal is a direct LOS signal. For example. For example, compared with a signal with SNR of 40 dB-Hz, another signal with SNR of 39 dB-Hz is regarded having the same probability that it is a direct LOS signal. This is because both 39 and 40 are very high SNR values. The same assumption is made for signals with

low SNRs. Another design is made to avoid extreme probabilities like 0 and 1. This design helps the CPT model to cope with a very strong reflection or a very weak direct LOS, by not giving them full confidence and thus allowing errors to occur.

Figure 5.5 (left) shows $p(LOS|SNR = s)$ for SNR between 17 (lower bound) and 35 (upper bound), marked by black crosses. It shows that $p(LOS|SNR = s)$ increases when the SNR increases. This can be expected, since a higher SNR implies a higher probability that a signal is LOS. The important question is, quantitatively, how does the $p(LOS|SNR = s)$ increase with the SNR. To model this relationship, a least squares method is used with three polynomial fittings, a linear fitting, a quadratic fitting, and a cubit fitting. Figure 5.5 (right) shows the fitting error using these three methods. It can be seen that linear fitting results in a larger error of at most 10% for each SNR with periodic residuals, whereas quadratic fitting offers, in most cases, better than 2% errors. Thus, a linear fitting is under-fitting and should not be chosen. Using a higher order of polynomial fitting, i.e. cubic fitting, it provides very similar fitting errors. Thus, it can be regarded that the quadratic fitting already model the overall shape of $p(LOS|SNR = s)$ very well, and a cubic fitting is thus not needed. Thus, in this work, a quadratic fitting is adopted. Combining the quadratic fitting with the aforementioned assumptions when the SNR is higher than the upper bound and lower than the lower bound, a complete CPT model of $p(LOS|SNR = s)$ can be obtained:

$$p(LOS|SNR = s) = \begin{cases} p_{o-min} & s < s_{min} \\ a_2 s^2 + a_1 s + a_0 & s_{min} \leqslant s \leqslant s_{max} \\ p_{o-max} & s > s_{max} \end{cases} \tag{5.6}$$

where p_{o-min} and p_{o-max} are, respectively, the minimum and maximum probabilities of the observed signal being LOS; s_{min} and s_{max} are, respectively, the minimum and maximum SNRs at which the quadratic function applies; and a_0, a_1, and a_2 are the coefficients of that function. For the results presented in Section 5.4, the parameters were: $p_{o-min} = 0.2$, $p_{o-max} = 0.9$, $s_{min} = 17$, $s_{max} = 35$, $a_0 = -1.86887109$, $a_1 = 0.1563262666$, *and* $a_2 = -0.002245615412$. The p_{o-min} and p_{o-max} are determined from the quadratic part of the CPT model by assigning the

value of $p(LOS|SNR = 17)$ and $p(LOS|SNR = 35)$, respectively. The values of a_0 a_1 *and* a_2 are determined from the sample statistics using the second round of experimental data as described earlier. The value of s_{min} and s_{max} are set from experience.

It should be noted that this model is trained using a Galaxy Samsung S3 smartphone, using another model of smartphone may or may not need adjustments to the parameters, which needs further research. However, it can be expected that the general shape of p(LOS) should remain similar.

Once $p(LOS|SNR = s)$ is obtained, the probability that the predicted and measured satellite visibility match, p_m, can be computed:

$$p_m = 1 - p(LOS|SNR = s) - p(LOS|BB) + 2p(LOS|SNR = s)p(LOS|BB) \quad (5.7)$$

where $p(LOS|BB)$ is the probability predicted from the building boundary that a LOS signal is receivable. $p(LOS|BB)$ is set to 0.9 if the satellite is predicted to be visible, and to 0.2 otherwise. These values allow for diffraction and 3D model errors. The overall matching probability is obtained by multiplying the individual-satellite matching probabilities. However, it is more convenient to add the individual-satellite scores. Therefore, a log-likelihood-based score between 0 and 1 is calculated from p_m using

$$f_{sat} = \frac{log(p_m) - log(p_{m-min})}{log(p_{m-max}) - log(p_{m-min})} \quad (5.8)$$

where $p_{m-min} = 0.26$ and $p_{m-max} = 0.82$ can be set as the minimum and maximum possible values of the matching probability, p_m.

5.4. Performance assessment using smartphone GPS and GLONASS

Static shadow-matching performance was assessed using smartphone grade GNSS chip with both GPS and GLONASS data streams collected at 20 sites, each for two

rounds, separated by 4 hours to allow the satellite constellation to change significantly, as described in Section 5.2. The second round of this data is used to train the CPT model, as described in Subsecion 5.2.1; whereas the first round of data is used for testing purposes in this section. The shadow-matching algorithm described in Chapter 4 was used with the visibility scoring scheme described in Section 5.3. This section first discusses a selection of satellite visibility scoring maps produced by the probability-based shadow-matching algorithm. The cross-street positioning performance is then assessed and compared with basic shadow matching and conventional GNSS positioning.

5.4.1. Satellite visibility scoring

A 1-metre grid spacing is used to convey building boundary information in this work. As described in Chapter 7, a 3-metre grid spacing is also tested showing that positioning is about 6% more accurate with a 1-metre grid spacing than with a 3-metre spacing. A 40-metre radius circle, centred at the conventional GNSS positioning solution from the smartphone GNSS chip, defines the boundary of the shadow-matching search area, within which each grid position is scored. The 40 metre radius value is empirically determined, since it is observed that conventional GNSS positioning error is normally within 40 metres from the true position. Setting a larger number for this parameter will increase the confidence that the true position is within the search region; however, it also impose heavier computation load. Clearly, there is a trade-off between computation load and positioning accuracy. 40 metre radius search region is a compromise used in this research.

Figure 5.6 shows examples of the shadow-matching scoring maps obtained at four of the experimental locations. The coloured dots represent the grid positions, excluding indoor locations. The highest scoring grid points are marked in dark red and the lowest scoring grid points are marked in dark blue. The true position is marked by a black cross. It can be seen that in most cases, the highest scoring points are in the correct street and on the correct side, as shown in the top left and top right subplots for R01 and G09. However, high-scoring points can also appear on other streets, as shown in the bottom right subplot, and in the spaces behind

buildings. In a few cases, the highest scores do not appear in the expected area as the bottom left subplot shows. This is typically caused by strong NLOS reception via highly reflective glass and metal buildings. A long-term solution to this problem is to predict NLOS reception using the 3D city model.

Figure 5.6 clearly shows that shadow matching is much more sensitive in the cross-street direction than in the along-street direction, in line with expectations. This complements conventional GNSS positioning which is generally more precise in the along-street direction in urban areas due to the signal geometry. Thus, combining the cross-street shadow-matching solution with the along-street conventional GNSS solution will generally give the best overall position solution (Groves, Ziyi, Wang and Ziebart, 2012). In this section, performance analysis focuses on the cross-street component of the position solution.

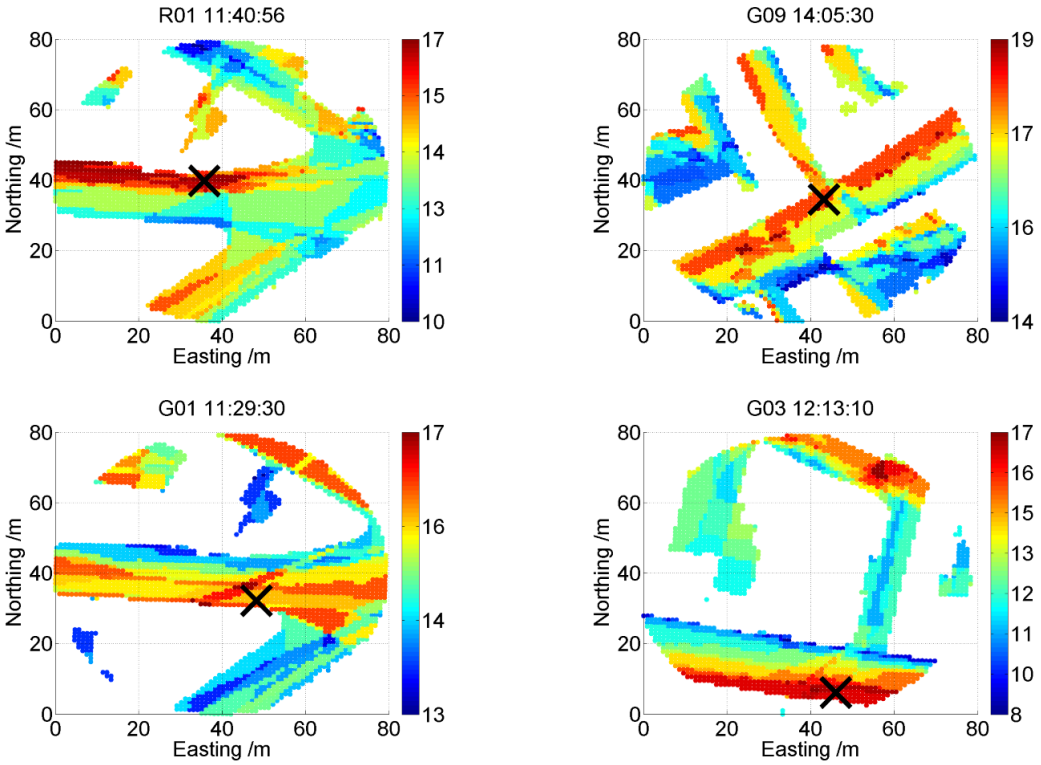

Figure 5.6.: Example shadow-matching scoring maps at one epoch from different sites

5.4.2. Performance comparison

To assess the performance of the optimized shadow matching algorithm against the basic shadow matching algorithm and the conventional GNSS positioning solution, the north and east position errors were transformed to along-street and cross-street position errors. Figure 5.7 shows the absolute value of the cross-street position error at each site from the first round of data. The conventional GNSS navigation solution from the smartphone GNSS chip is compared with shadow-matching using both the probability-based scoring scheme described in Section 5.3 and the basic S_{22} scheme shown in Figure 4.8. Figure 5.8 shows the corresponding mean absolute deviation (MAD) of each cross-street position error, using equation 4.5. Note that the results at each site are highly correlated because each observation period was 6 minutes, during which the constellation geometry changed slowly.

Figures 5.7 and 5.8 show that, in most cases, shadow matching outperforms conventional GNSS positioning and the new probability-based shadow-matching algorithm outperforms the basic algorithm. At some sites, such as G09, the shadow-matching accuracy is better than 2m at most epochs. However, there are a few cases where shadow matching is poorer than conventional GNSS positioning, e.g. G07. A common cause of poor shadow-matching performance is reception of a significant number of strong reflected signals, which can confuse the shadow-matching algorithm. Further analysis was conducted to calculate the proportion of results for which the cross-street positioning error was within certain limits. This may be thought of as the success rate for achieving certain performance specifications. For example, a typical street is around 10m wide, so a positioning accuracy within 5m is considered good enough to determine the correct side of the street, while 2m is sufficient to distinguish the footpath from a traffic lane. Figure 5.9 shows the success rate at each site, while Figure 5.10 shows the success rate across all sites. The overall success rate for determining the correct side of a street was 54.03%

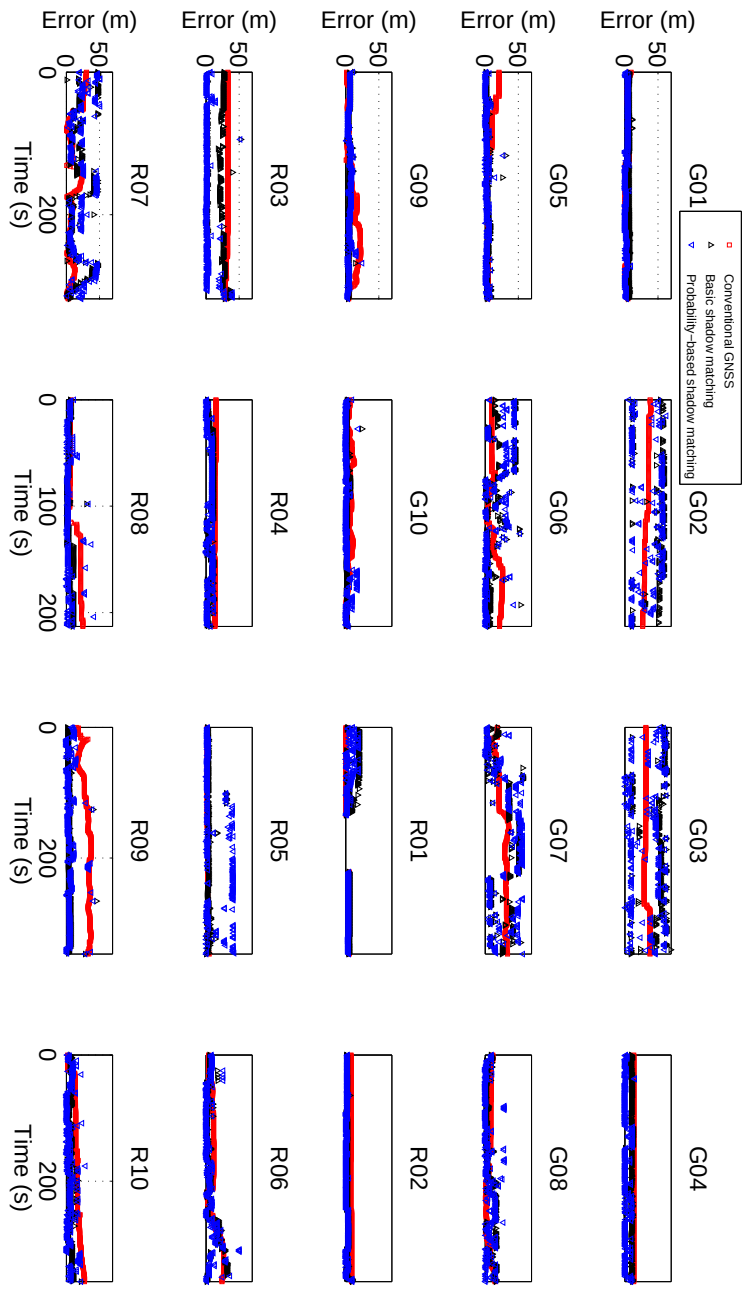

Figure 5.7.: Absolute cross-street positioning error using conventional GNSS, basic shadow matching (using S_{22} scoring scheme) and probability-based shadow matching

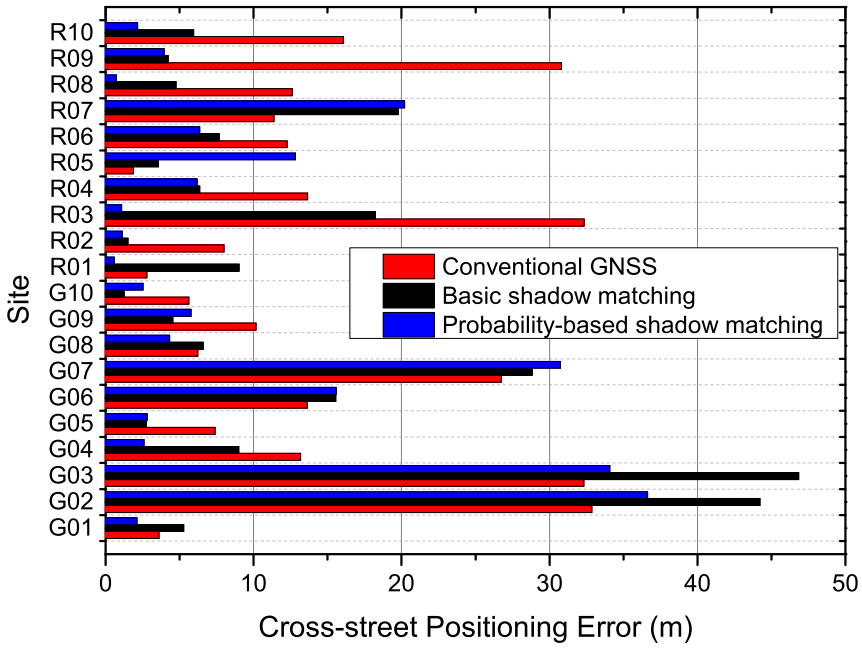

Figure 5.8.: Mean absolute deviation over all epochs of the cross-street position error using conventional GNSS, basic shadow matching and probability-based shadow matching.

using probability-based shadow matching, compared to 45.43% using basic shadow matching, and 24.77% using conventional GNSS positioning. The success rate for distinguishing the footpath from a traffic lane was 28.17% for probability-based shadow matching, 20.73% for basic shadow matching, and 9.52% for conventional GNSS positioning.

5.5. Chapter summary

Signal visibility and diffraction in the scoring schemes are firstly modelled by empirically setting thresholds of signal-to-noise ratio (SNR). To improve this modelling, separate signal-to-noise ratio distributions of direct LOS and NLOS GNSS signals received in a dense urban area have been measured using an Android smartphone and a 3D city model. Using these distributions, a function has been derived giving the probability that a received signal is direct LOS based on the measured SNR. Using

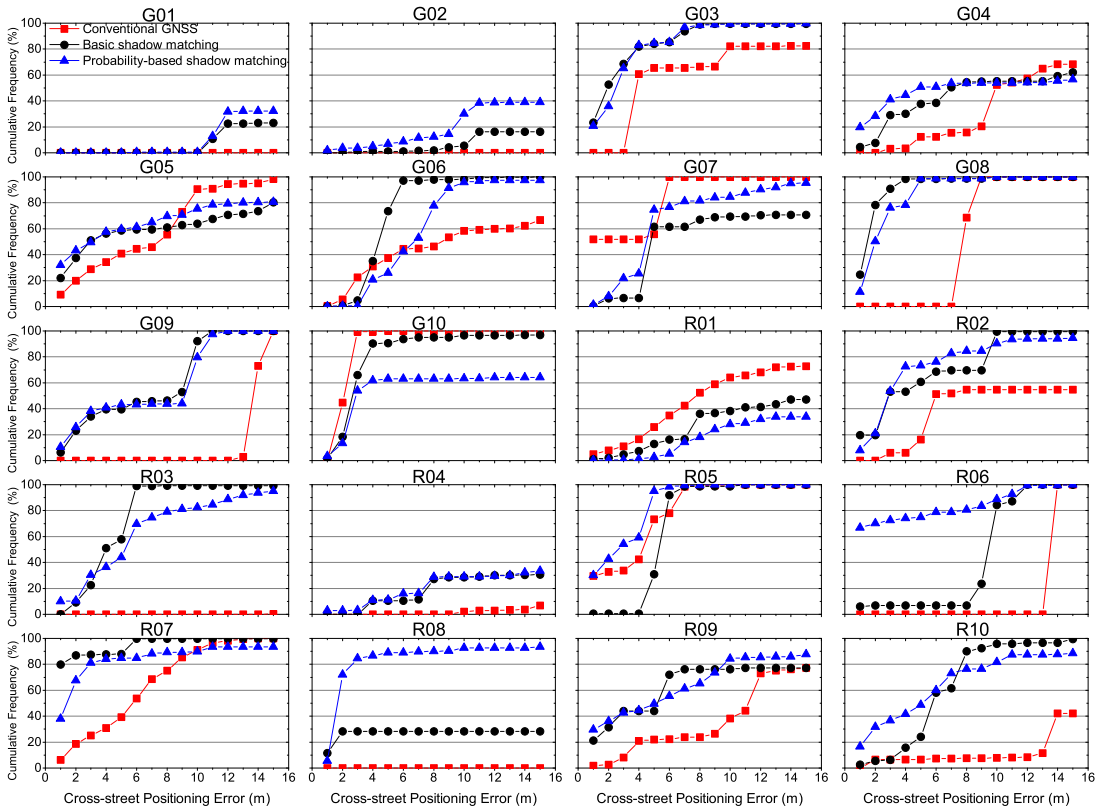

Figure 5.9.: Proportion of cross-street position errors within certain ranges at each site using conventional GNSS, basic shadow matching and probability-based shadow matching

this function, another optimization in shadow-matching's satellite visibility scoring scheme has been conducted for use with smartphone GNSS measurements. In this new probability-based shadow matching algorithm, a sample statistics technique is used to estimate the conditional probability table (CPT) in a simple Bayesian network.

Using GPS and GLONASS data recorded at 20 locations within central London, the first comprehensive performance assessment of smartphone GNSS shadow matching has been conducted. The results show that the probability shadow-matching algorithm proposed in this chapter significantly outperforms conventional GNSS positioning in the cross-street direction, and is statistically better than the basic shadow matching algorithm with S_{22} scoring scheme. The success rate for obtaining a cross-street position accuracy within 5m, enabling the correct side of a street to be determined, was 54.03% using probability-based shadow matching,

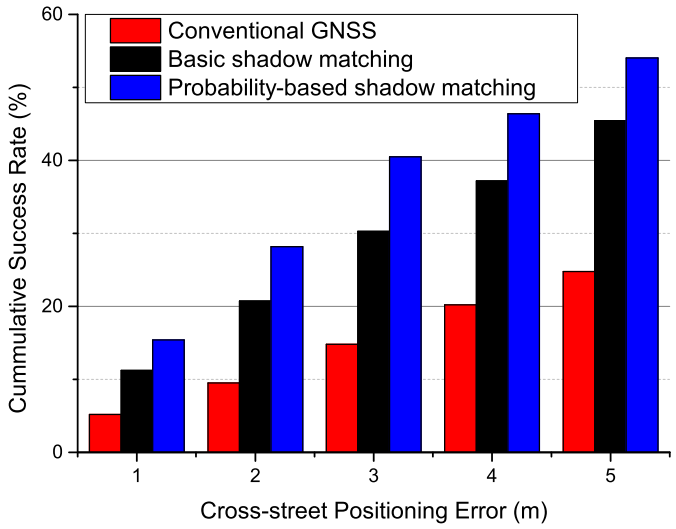

Figure 5.10.: Proportion of cross-street position errors within certain ranges across all sites using conventional GNSS, basic shadow matching and probability-based shadow matching.

compared to 45.43% using basic shadow matching, and 24.77% for the conventional GNSS position.

The research in this chapter assumes GNSS data from each epoch can only be used individually. Further research to improve shadow matching, particularly to handle kinematic applications, where knowledge of multiple epochs can be combined, will be introduced in Chapter 6.

Chapter 6.

Kinematic Shadow Matching

In this chapter, for the first time, and in parallel to Isaacs et al. (2014), kinematic shadow-matching positioning is investigated. Section 6.1 introduces the background and motivation of kinematic shadow matching. A new kinematic shadow-matching algorithm is presented in Section 6.2. In this algorithm, pros and cons of the key component options, namely position estimation schemes, are discussed in Section 6.3. Detailed algorithm descriptions of the selected scheme, a particle filter, are then given in Section 6.4. A comprehensive assessment of real-world experiments is presented in Section 6.5, with different criteria applied to compare the performance between the conventional GNSS navigation solution, the single-epoch shadow-matching system solution, and the kinematic shadow-matching system solutions. Finally, Section 6.6, summarize the research work in this chapter. This chapter is partially based on work presented in paper published in ION GNSS+ 2014 (Wang, 2014*b*), with further algorithm improvements and experiments conducted.

6.1. Motivation

The motivation for investigating kinematic shadow matching algorithms comes from the fact that navigation is typically kinematic, but previous research has focused on developing static shadow-matching positioning algorithms. A single-epoch shadow-matching algorithm, as presented in Chapter 4 and 5, is valid for static positioning, but not optimized for kinematic cases. This is because in single-epoch shadow

matching, GNSS data in each epoch is individually processed, without taking advantage of any knowledge from previous epochs. Although Suzuki and Kubo (2012) investigated multi-epoch positioning, the aim was to improve precision of static positioning using information from multiple epochs. Although Yozevitch et al. (2014, 2012) targeted for kinematic applications, only a single-epoch shadow matching algorithm was used.

Given that the update rate of a mobile GNSS device is normally 1 Hz, pedestrians and vehicles are not likely to move so fast that the environment changes dramatically between consecutive epochs. The single-epoch or static shadow-matching techniques are thus ignoring important information that exists in kinematic scenarios. In summary, the existing shadow matching techniques are not optimized for kinematic positioning. Therefore, this chapter discusses different estimation scheme options that can optimize shadow-matching positioning for kinematic cases, selects and implements the most appropriate scheme to optimize kinematic shadow-matching positioning.

6.2. Design of a kinematic shadow-matching algorithm

There can be different architectures of a kinematic shadow-matching system. Figure 4.2 gives the design options in terms of the overall system architecture. Rather than scoping at the system level, this section focuses on the algorithm-level design of a kinematic shadow-matching algorithm.

Kinematic shadow-matching algorithms can be designed by extending the generic single-epoch shadow-matching algorithm presented in Chapter 4. The flowchart of a single-epoch shadow-matching algorithm is illustrated in Figure 4.3. When moving to the kinematic positioning scenarios, the most important step to change is step 6, where a position estimation scheme is performed. In the single-epoch shadow-matching algorithm, a method that does not take advantage of information from previous epochs, e.g. a k-nearest neighbour (K-NN) algorithm, is used. Whereas in a kinematic shadow-matching algorithm, this step should be replaced by an ap-

propriate estimation scheme. An estimation scheme can, for instance, be a Kalman filter, a grid filter, or a particle filter. The trade-offs of using each of them are discussed in Section 6.3. The algorithm flowchart of the kinematic shadow-matching algorithm is illustrated in Figure 6.1.

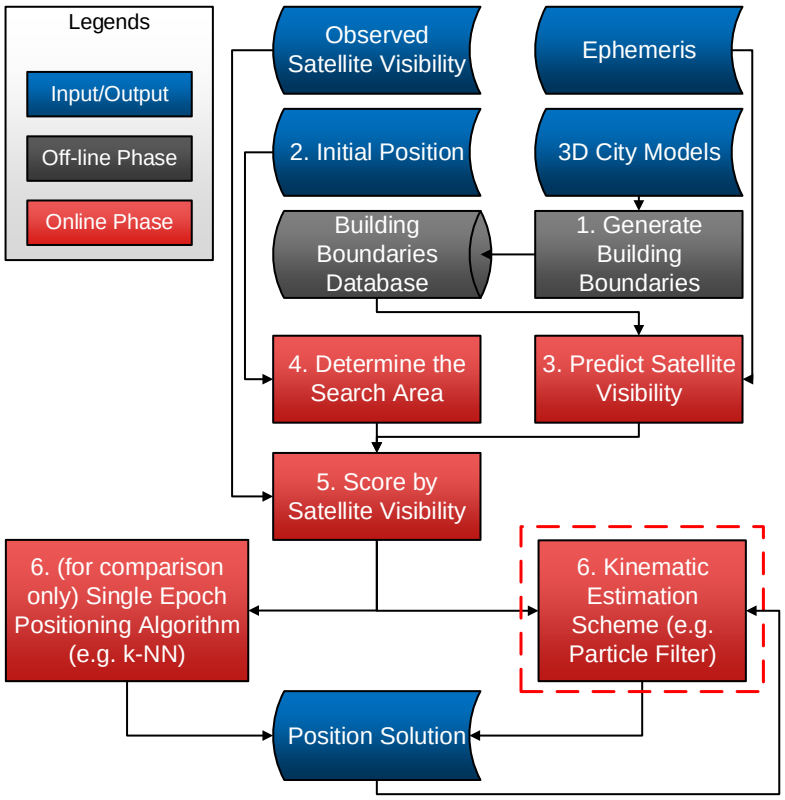

Figure 6.1.: Flowchart of kinematic shadow matching (the modified step 6 is surrounded by a red frame)

6.3. Bayesian methods - Kalman, grid-based, or particle filters

Bayesian estimation methods are widely applied in positioning engines. Combining noisy measurements observed over time using the Bayes theorem should typically be more accurate than using a single noisy measurement. Among the Bayesian methods that combine multiple measurements, three Bayesian techniques are considered

for implementation in kinematic shadow-matching over multiple epochs, namely Kalman filters, grid-based filters and particle filters.

The Kalman filter is a state estimation algorithm invented by R. E. Kalman (Kalman, 1960; Brown and Hwang, 1996; Groves, 2013). It is often used to estimate real-time states in positioning algorithms. A Kalman filter is considered to have the potential to help solve the kinematic shadow-matching positioning problem for two reasons. Firstly, Kalman filters are commonly used in the navigation community to integrate consecutive measurements or data from different sensors, and are proven to be efficient and effective (Groves, 2013). Conversely, it is frequently observed that in the shadow-matching algorithm, the candidate positions (those positions where GNSS measurements best match predictions) tend to form an approximation of an ellipse, as illustrated in Figure 6.2 (a), in which a shadow matching scoring map that shows an unambiguous highest-scoring area, marked in red. The data was collected at 11:40:56 on 26th, October 2012, using a Samsung Galaxy S3 smartphone. The true locations of the site is marked by a cross in the figure. The ellipses are used to highlight the best matching area. Thus, a Kalman filter should be able to represent this. In the author's work (Wang, 2014*b*), a Kalman filter designed for kinematic shadow-matching positioning, consists of 10 steps in three phases: initialization, state system propagation and measurement updating. However, Kalman filters are not focused on in this thesis because of their expected and proven defects.

A Kalman filter may not be the optimal solution for kinematic shadow matching. The standard Kalman filter is a linear Gaussian estimation algorithm. Although extended Kalman filters (EKF) and unscented Kalman filters (UKF) can adapt the Kalman filter to nonlinear systems (Gelb, 1974; Julier and Uhlmann, 2004), a shadow matching system is not only nonlinear, but also multimodally distributed, i.e. there could be ambiguity from the existence of multiple matching areas. This is illustrated in Figure 6.2 (b), where there are two best matching areas in the shadow matching scoring map. Thus the position solution is ambiguous. In this situation, a single-hypothesis model Kalman filter is not an adequate representation of the multiple hypothesis models; whereas grid-based or particle filters are adequate. The

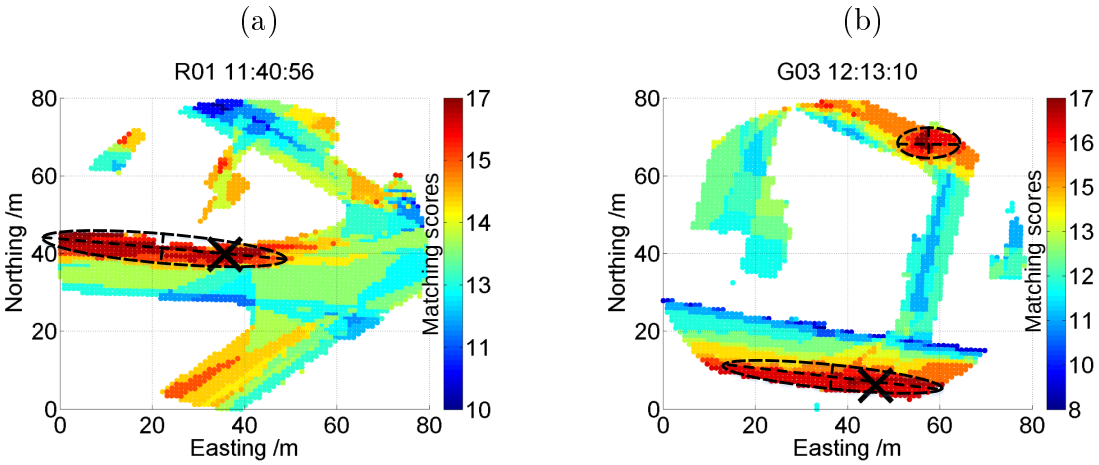

Figure 6.2.: Two shadow matching scoring maps that show highest-score (best matching) area can be unambiguous (a) or ambiguous (b), which means using a Kalman filter can be feasible but not all the time

data was collected at 12:13:10 on the same day.

A multiple-hypothesis Kalman filter (Reid, 1979) may account for this situation, but it is sometimes difficult to determine how many hypotheses models are needed. For example, it can be seen in Figure 6.2 (a) that apart from there being major matching areas, there are also several minor suboptimal matching areas. The benefit of using Kalman filters, though, would be that less computation power is needed, certainly compared with particle filters.

Besides the Kalman filter, a grid-based filter may also help solve the problem. A grid-based filter uses a discrete grid to represent posterior probability density function of any distribution (PDF), therefore it does not have to assume Gaussian distribution of measurement noise, nor only estimate linear combinations of system states. The idea of using a grid-based filter is inspired from the fact that shadow matching is based on a grid of points, where the building boundary information is available. If this grid is used in the grid-based filter, at least theoretically, it maximize the use of knowledge from the building boundaries. However, in the kinematic cases, the grid-based filter has a limitation on its resolution - it can not represent continuous probability states, whereas a natural property of kinematic movement is continuity. To complement this drawback, a dense grid may be used to reduce the error introduced by the discrete representation issue; however, the

grid density has to be properly determined based on the desired or best available accuracy. It sometime becomes difficult/tricky to determine the density of grid since the accuracy is also unknown. A denser grid also imposes higher processing load.

In addition to the Kalman filter and the grid-based filter, a particle filter algorithm is also considered in this work to improve kinematic shadow-matching positioning. Particle filtering is originally named bootstrap filtering (Gordon et al., 1993). The general concept is to use a set of Monte Carlo (randomly chosen) weighted samples (particles) to represent the posterior probability density function (PDF) (Thrun et al., 2005). Unlike the Kalman filter, particle filters are nonlinear non-Gaussian Bayesian estimation techniques (Gordon et al., 1993; Gustafsson et al., 2002). Furthermore, a particle filter can naturally handle multimodal distribution that a Kalman filter cannot. In fact, each particle can be regarded as a hypothesis model. Last but not the least, rather than fixing particle resolution in a grid filter, particle filters can adjust itself to have higher density of particles in the high probability region.

In summary, particle filters have a strong potential to better solve the kinematic shadow-matching problem. Although a Kalman filter may be more efficient to run, the restricted measurement model can not represent the natural properties of shadow matching resulting from its inherit ambiguity - it is non-linear and non-Gaussian. In addition to the non-linear and non-Gaussian nature of a particle filter, more importantly, it can estimate multiple hypothesis distributions. The robustness using a particle filter is thus better when compared with a Kalman filter (Wang, 2014*b*). Compared with a grid-based filter, particle filters are better in kinematic shadow matching, with the ability to adjust itself in spatial resolution. Thus, a particle filter is used in this work for kinematic shadow-matching positioning.

6.4. Particle filter design

An architectural overview of the particle filter is shown in Figure 6.3. There are four phases, comprising initialization, system updating, measurement updating and resampling, in 10 steps. These are detailed in the following descriptions.

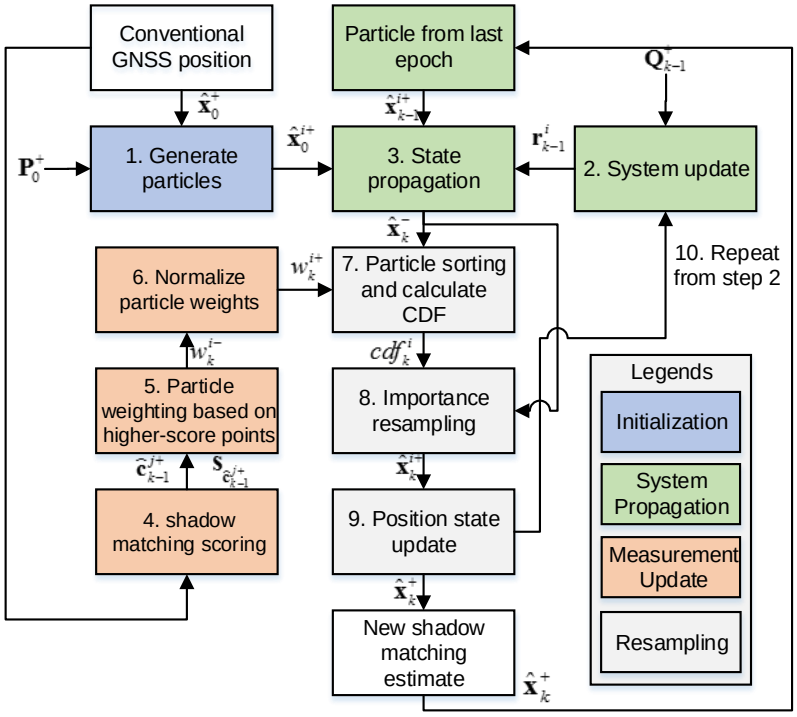

Figure 6.3.: The particle filter architecture for kinematic shadow-matching positioning

6.4.1. Initialization phase

Step 1: Initialization: Generate random particles $[\hat{\boldsymbol{x}}_0^{1+}, ..., \hat{\boldsymbol{x}}_0^{n+}]$ in a Gaussian distribution, based on the initial conventional GNSS positioning solution $\begin{pmatrix} n_0^g \\ e_0^g \end{pmatrix}^+$. A particle is a representation of posterior density function (PDF) of the state variables, i.e. the horizontal position.

$$\hat{\boldsymbol{x}}_0^+ = \begin{pmatrix} n_0^g \\ e_0^g \end{pmatrix}^+ \tag{6.1}$$

$$\mathbf{P}_0^+ = \begin{pmatrix} \sigma_{0,n}^2 & \sigma_{0,ne} \\ \sigma_{0,ne} & \sigma_{0,e}^2 \end{pmatrix} \tag{6.2}$$

$$[\hat{\boldsymbol{x}}_0^{1+}, ..., \hat{\boldsymbol{x}}_0^{n+}] \sim N(\hat{\boldsymbol{x}}_0^+, \mathbf{P}_0^+) \tag{6.3}$$

where in the Gaussian distribution, the initial mean position $\hat{\boldsymbol{x}}_0^+$ is denoted as $\begin{pmatrix} n_0^g \\ e_0^g \end{pmatrix}^+$, n_0^g is the northing component and e_0^g is the easting component of the initial GNSS position, and the error covariance matrix $\mathbf{P}_0^+$ is denoted as $\begin{pmatrix} \sigma_{0,n}^2 & \sigma_{0,ne} \\ \sigma_{0,ne} & \sigma_{0,e}^2 \end{pmatrix}$, the $\sigma_{0,n}^2$ and $\sigma_{0,e}^2$ are the variances of the northing and easting components of initial position error, respectively; and $\sigma_{0,ne}$ is the covariance between northing and easting components. In this work, $\sigma_{0,n}^2$ and $\sigma_{0,e}^2$ are set to be 20^2m^2, and $\sigma_{0,ne}$ is set to be 0. This means in each direction, it is assumed that 68.27% of particles lie within 20 metre deviation of the centre, which in the initialization phase is defined as the conventional GNSS position. Since the GNSS receiver does not provide information needed to calculate the correlation between northing and easting components, it is also assumed that there is no correlation between the two components. N represents the normal distribution, i.e. Gaussian distribution.

6.4.2. System update phase

Step 2: Generate random noise to account for user motion.

In order to take user motion into consideration, random noises $[\boldsymbol{r}_{k-1}^1, ..., \boldsymbol{r}_{k-1}^n]$ for each particle $\hat{\boldsymbol{x}}_{k-1}^{i+} \in [\hat{\boldsymbol{x}}_{k-1}^{1+}, ..., \hat{\boldsymbol{x}}_{k-1}^{n+}]$ are generated, obeying a Gaussian distribution $\boldsymbol{N}[\mathbf{0}, \mathbf{Q}_{k-1,r}]$, where $\mathbf{Q}_{k-1,r}$ is the covariance matrix of the system noise.

$$r_{k-1}^i = \begin{pmatrix} n_{k-1}^i \\ e_{k-1}^i \end{pmatrix} \tag{6.4}$$

$$\mathbf{Q}_{k-1,r} = \begin{pmatrix} \sigma^2_{k-1,r,n} & \sigma_{k-1,r,ne} \\ \sigma_{k-1,r,ne} & \sigma^2_{k-1,r,e} \end{pmatrix} \tag{6.5}$$

$$[\boldsymbol{r}^1_{k-1}, ..., \boldsymbol{r}^n_{k-1}] \sim \boldsymbol{N}\left[\mathbf{0}, \mathrm{Q}_{k-1,r}\right] \tag{6.6}$$

where $\sigma^2_{k-1,r,n}$ and $\sigma^2_{k-1,r,e}$ are the northing and easting components of the system noise variance, and $\sigma_{k-1,r,ne}$ is the error covariance between easting and northing components. In this work, since no IMU or magnetometer is used to provide the user's moving direction or speed, it is assumed that a user's movement follows a Gaussian distribution in which $\sigma^2_{k-1,r,n}$ and $\sigma^2_{k-1,r,e}$ is $2^2 m^2$ (a normal walking speed), and there is no correlation between the two components, thus $\sigma_{k-1,r,ne}$ is set to be 0. The system update rate is the same as the measurement update rate, i.e. once per second; this setting means it is assumed that user may walk with a speed of roughly 2 m/s.

Step 3: The user motion that is modelled as random noises $[\boldsymbol{r}^1_{k-1}, ..., \boldsymbol{r}^n_{k-1}]$ is then added to the particles $[\hat{\boldsymbol{x}}^{1+}_{k-1}, ..., \hat{\boldsymbol{x}}^{n+}_{k-1}]$ to update their states.

$$[\hat{\boldsymbol{x}}^{1+}_{k}, ..., \hat{\boldsymbol{x}}^{n+}_{k}] = [\hat{\boldsymbol{x}}^{1+}_{k-1}, ..., \hat{\boldsymbol{x}}^{n+}_{k-1}] + [\hat{\boldsymbol{r}}^{1+}_{k-1}, ..., \hat{\boldsymbol{r}}^{n+}_{k-1}] \tag{6.7}$$

6.4.3. Measurement update phase

Step 4: For the k-th epoch, perform the steps 1 to 4 in the GNSS shadow matching algorithm described in Figure 6.1, which is initialized at the last particle-filter positioning solution $\hat{\boldsymbol{x}}^{+}_{k-1}$. Scores that use the optimized scoring scheme described in Section 5.3 are acquired at a grid of positions within the search region of the shadow matching algorithm, noted as $[\hat{\boldsymbol{c}}^{1+}_{k-1}, ..., \hat{\boldsymbol{c}}^{m+}_{k-1}]$. Each of these grid positions is associated with a matching score, denoted as $s_{\hat{\boldsymbol{c}}^{j+}_{k-1}}$. points

Step 5: Compute the particle weights based on the shadow matching scoring outputs.

Before this step, the particles are assumed to have equal weights. A particle's new weight is evaluated based on its l-closest grid points in two sub-steps. In this study l is set to be 16, since it is assumed grid points within a roughly 2 meter range of the particle contribute to the weight. Figure 6.4 gives an example to illustrate that the two-meter range, and the concept that the more distance the grid point is to the particle, the lower weight it contributes to the overall weight of the particle (denoted as lighter in color).

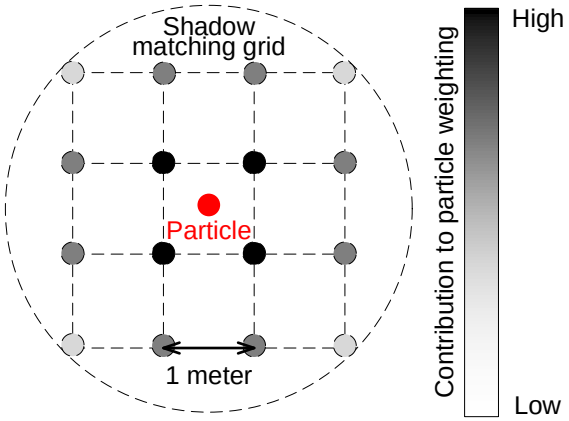

Figure 6.4.: Particle (marked in red) weighting based on shadow matching grid associated with matching scores (marked in different shades of black). The darker a grid position is means that its matching score has more contribution to the overall weighting of the particle.

The first sub-step is an initial weighting. For each particle $\boldsymbol{x}_k^{i-}(1 \leq i \leq n)$, its weight $w_k^{i-}(1 \leq i \leq n)$ is defined as a sum across intermediate results $w_k^{ij-}(1 \leq j \leq l)$, which is inversely proportional to the Euclidean distance d_k^{i-} between this particle $\boldsymbol{x}_k^{i-}$ and the grid position $\hat{\boldsymbol{c}}_{k-1}^{j+} \epsilon [\hat{\boldsymbol{c}}_{k-1}^{1+}, ..., \hat{\boldsymbol{c}}_{k-1}^{l+}]$, multiplied by the score of the j-th grid position $s_{\hat{\boldsymbol{c}}_{\boldsymbol{k-1}}^{\boldsymbol{j+}}}$. When the nearest candidate is within 1 meter to the current particle of interest, its distance is considered to be 1 meter.

$$w_k^{ij-} = \begin{cases} s_{\hat{\boldsymbol{c}}_{\boldsymbol{k-1}}^{\boldsymbol{j+}}}, & (d_k^{i-} < 1meter) \\ \frac{1}{d_k^{i-}} \times s_{\hat{\boldsymbol{c}}_{\boldsymbol{k-1}}^{\boldsymbol{j+}}}, & (d_k^{i-} > 1meter) \end{cases} \tag{6.8}$$

$$w_k^{i-} = \sum_{j=1}^{l} w_k^{ij-} \tag{6.9}$$

After this initial weighting, particles whose adjacent grid points have higher matching scores are weighted higher. However, particles with low weights should be eliminated, i.e. it is assumed that only particles that are with high weight should have contribution to the final weighting. Thus, in the second sub step, another operation is conducted to promote particles with weight of the top p percent of scores:

$$\widehat{w}_k^{i-} = \frac{w_k^{i-} - min(w_k^{i-}) - [max(w_k^{i-}) - min(w_k^{i-})] \times [1-p]}{[max(w_k^{i-}) - min(w_k^{i-})] \times p} \tag{6.10}$$

where $min(w_k^{i-})$ and $max(w_k^{i-})$ represent the minimum and maximum value of w_k^{i-}, respectively. In this work, p is set to be 5%, which means that the particles whose weight are within top 5 percent will contribute to resampling phase. Setting a larger number for p means the particle weights are less trusted. Consequently, more error can be tolerated; however, this way also increases the chance that unmatched areas contaminate the positioning solution. Setting a smaller number means only particles with very high level match can survive, thus may resulting in over trusting the highly matched particles. Thus, it is an empirical value to be set. After the second sub step, weight of these particles is still proportional to its initial weight.

Step 6: Normalize the weights of each particle, so that

$$\sum_{i=1}^{n} w_k^{i+} = 1 \ (0 \leq w_k^{i+} \leq 1) \tag{6.11}$$

$$w_k^{i+} = \frac{\widehat{w}_k^{i-}}{\sum_{i=1}^{n} \widehat{w}_k^{i-}} \tag{6.12}$$

6.4.4. Importance weight resampling

Resampling is needed to replace the particles with negligible weights, so that all the particles can still maintain its close representation of posterior density function (PDF) of the estimated position and thus accuracy can be maintained. At the same time, it saves computing resources by eliminating the particles with negligible weights (Groves, 2013).

Step 7: Incrementally sort the particles $[\hat{\boldsymbol{x}}_k^{1-}, ..., \hat{\boldsymbol{x}}_k^{n-}]$ according to their normalized weights w_k^{i+}, so that $\hat{\boldsymbol{x}}_k^{1-} < \hat{\boldsymbol{x}}_k^{2-} < ... < \hat{\boldsymbol{x}}_k^{n-}$, and compute the cumulative density function (CDF), noted as $[cdf_k^1, ..., cdf_k^n]$, using the following formula:

$$cdf_k^i = \sum_{h=1}^{i} w_k^{h+} \tag{6.13}$$

Step 8: Generate n random variables in a uniform distribution.

$$[u, ..., u_k^n] \sim U(0, 1) \tag{6.14}$$

For each $u_k^i \in [u_k^1, ..., u_k^n]$, find the corresponding particle by choosing the first particle in $[\hat{\boldsymbol{x}}_k^{1-}, ..., \hat{\boldsymbol{x}}_k^{n-}]$ for which its cdf_k^i is bigger than u_k^i ; as a result, a new set of particles $[\hat{\boldsymbol{x}}_k^{1+}, ..., \hat{\boldsymbol{x}}_k^{n+}]$ is generated.

Step 9: The average position of these new particles is deemed the positioning solution:

$$\hat{\boldsymbol{x}}_k^{+} = \frac{1}{n} \sum_{i=1}^{n} \hat{\boldsymbol{x}}_k^{i+} \tag{6.15}$$

Repeat 2 – 9.

6.5. Experiments and results analysis

To evaluate the performance of the proposed new algorithms, kinematic experiments were conducted in central London using smartphones. In this section, the 3D city model and the experimental routes are first outlined, with the configuration of the shadow-matching algorithm then described. Finally, positioning results of conventional GNSS positioning, single-epoch shadow matching, and particle filter shadow matching are compared.

6.5.1. Experimental configurations

A 3D city model of the Aldgate area of central London, supplied by ZMapping Ltd, was used. Refer to Chapter 3 for details. Figure 6.5 shows part of the city model used in this work, with experimental area marked.

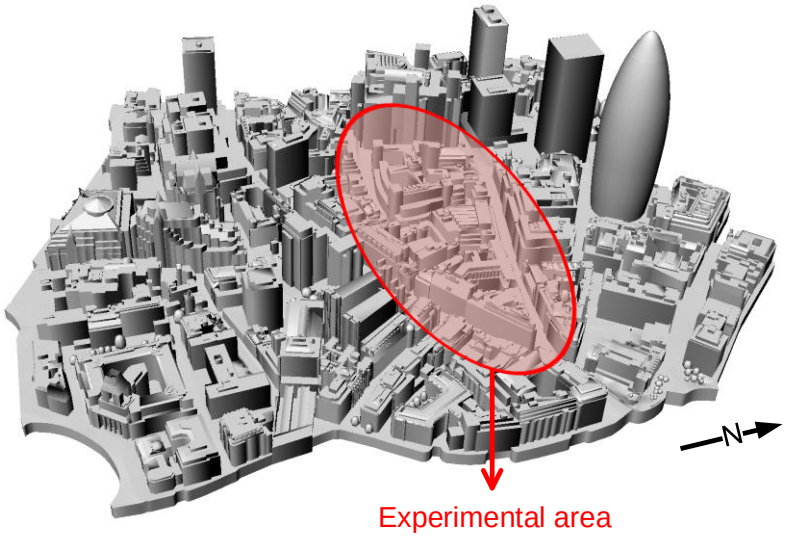

Figure 6.5.: The 3D city model used in shadow matching experiments. The area marked in red is where the three routes of experiments were conducted.

The experimental area is a built-up area, where three experimental routes were selected on Fenchurch Street and Leadenhall Street. Figure 6.6 shows photos taken at the street, showing the urban environments. Two of the routes, numbered route

1 and 3, were located on the northern side of Leadenhall Street and southern side of Fenchurch Street, respectively. Another specially designed route that covers both southern side of Leadenhall Street and northern side of Fenchurch Street is selected, to test the algorithm against the scenario when a traffic turn over exists. These routes allow system performance comparison between users at different sides of street. This design is because that if the proposed algorithm can determine the user's position no matter which side the user is at, it is more probable that the algorithm is not producing the correct answer by chance.

The directions of the two streets (Leadenhall Street and Fenchurch Street) are east-west and northeast-southwest, respectively. Due to the lack of updated 3D model data coverage available to the author, there are not available streets with north-south direction for experiments. The 3D model data used in this research was produced earlier than the year 2005, thus it is out of date for approximately 10 years compared with the date of this research. Numerous buildings have been demolished or built in the overall area, as a normal practice in central London. Thus, the experimental sites have to be carefully selected where the 3D models can still approximately reflect real world environments. This issue implies that updated 3D models are the per-requisite for shadow matching techniques, which potentially can be a drawback of applying the shadow matching technique.

Yet a lack of an exact north-south direction street does not affect this research significantly, since it is not as important and interesting as streets of east-west direction in the testing purpose of this study. This is because the north-south component of GNSS positioning accuracy is typically worse than that of the east-west component, especially in mid-latitude areas, e.g. United Kingdom (Meng et al., 2004). This is due to the global distribution of GNSS satellites, e.g. for United Kingdom, a larger portion of satellites operates on the southern hemisphere of the sky. Buildings on a east-west direction street block some of these satellites, at north-south direction, resulting in a worse positioning performance at this direction. Thus, an east-west direction street is expected to need shadow matching more significantly, and thus is more important and interesting to be tested.

All routes were selected on the footpath close to the traffic lanes. Figure 6.7 shows

an aerial view of the experimental routes in a satellite image from Google Earth. The truth model in this experiment is set using the 3D city model by identifying the same unique positions from the 3D city model and the real world. A pedestrian walked in steady speed from the start to the end of each route.

Figure 6.6.: Urban environments on route 1 (left), and route 2 (right)

Using the GNSS data-recording app adapted from earlier work (screenshot shown in Figure 4.10), a Samsung Galaxy S3 smartphone was used to record GNSS data on Route 1 and 3, and a Google Nexus 5 phone was used to record data on Route 2, both with a frequency at 1Hz. Both GPS and GLONASS observations were recorded, including satellite visibility information and positioning results from the smartphone GNSS chip. 500 particles are used in the particle filter. Other numbers of particles (1000 and 2000) have been tested and have shown similar results, thus it is assumed that 500 particles are enough to represent the PDF.

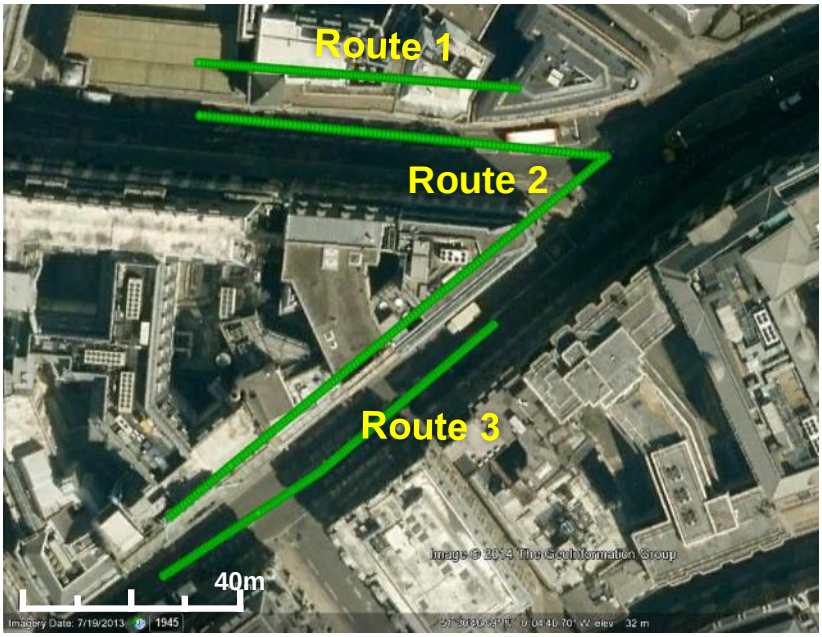

Figure 6.7.: The 3 experimental routes illustrated in a satellite image, noting that there is a distortion of the airborne image. In real world, the routes are set on the curves between pavements and vehicle lanes

6.5.2. Positioning performance assessment

In this section, the overall performance of the single-epoch and particle filter shadow-matching positioning systems are assessed and compared with the conventional GNSS solution from the smartphones.

To compare the performance of shadow matching against the conventional GNSS positioning solution, the position errors are transformed from local coordinates (northing and easting) to the along-street and across-street directions. As mentioned in Section 2.3, the cross-street direction is the main concern in this study, because the sensitivity in this direction matters to many applications of interest, including determining the correct side of the street for pedestrian navigation, and lane identification for vehicle navigation and intelligent transportation systems. Figure 6.8 (left) shows the positioning results (against time) of the conventional GNSS navigation solution from the smartphone GNSS chip, compared with the two shadow matching algorithms: single-epoch shadow matching and particle filter shadow matching,

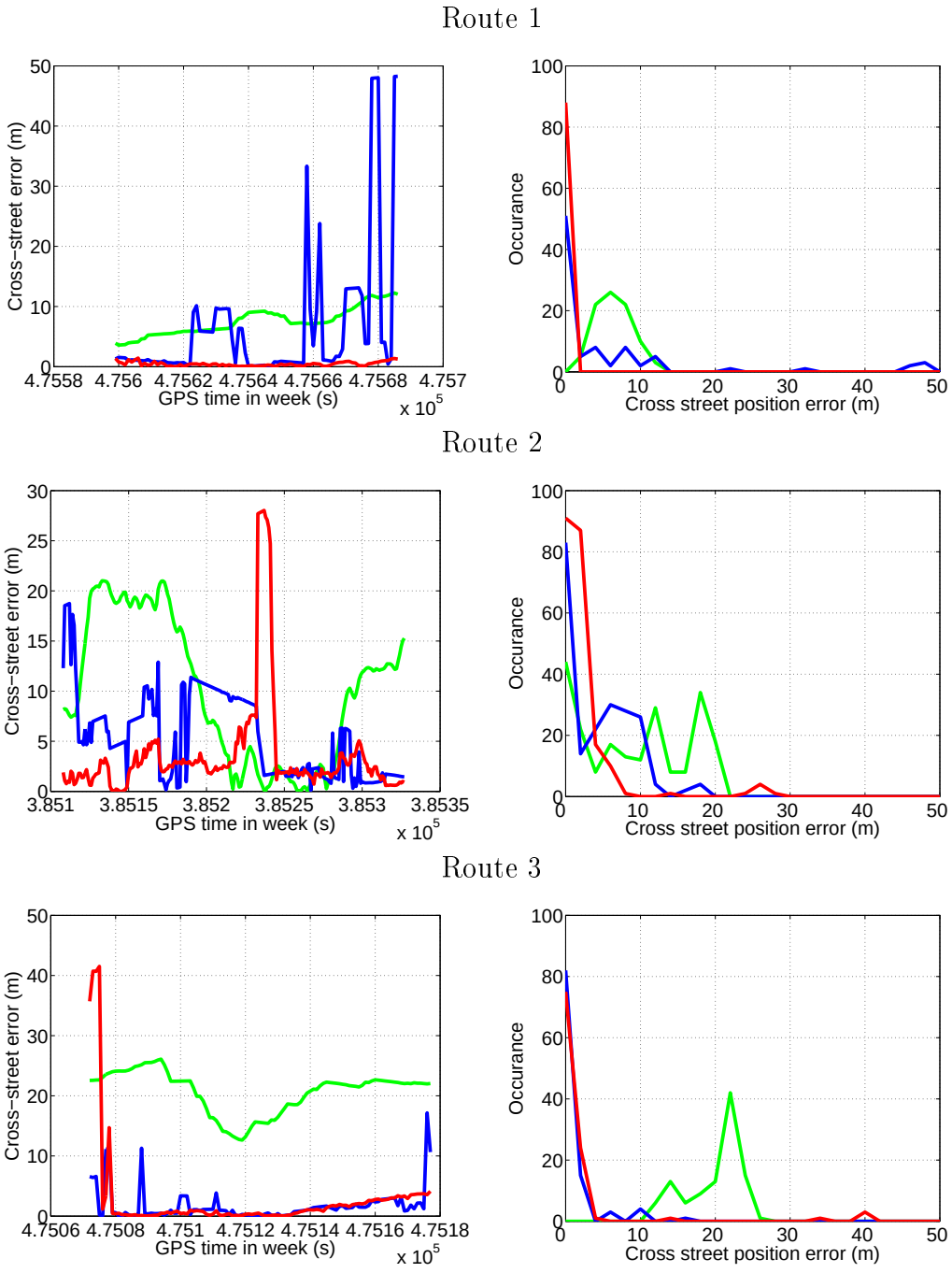

Figure 6.8.: Positioning error in time series (left) and histogram (right) of conventional GNSS (green), single-epoch shadow matching (blue), and particle filter shadow matching (red), in cross-street direction

expressed as absolute errors in the cross-street direction. The right graphs in the same figure show the histogram of the error distribution shown to the left.

There are a few interesting points that can be observed from this figure. Firstly, the overall characteristics of the shadow matching and conventional GNSS solutions are very different. The conventional GNSS solutions are smoother, as smoothing algorithms (e.g. a Kalman filter) are commonly used in navigation GNSS chipsets. However, the shadow matching solutions, no matter which version, tend to be closer to zero, which means their accuracy is better, though they vary more with time. Secondly, the particle filter shadow matching significantly outperforms both of the other methods, including the single epoch shadow matching. The Particle Filter shadow matching has a smoothing effect as well, which in many cases has fewer variations compared to the single-epoch shadow matching. For all the routes, the particle filter shadow matching positioning results show a clear peak at zero-error.

It is clearly demonstrated that the particle filter shadow matching solution has improved on the conventional positioning error, in the across-street direction, from typically 10 - 40 meters to within 2-3 meters (except the middle part of route 2) in all the routes. In route 2 and 3, the particle filter shadow matching is also better than conventional GNSS solutions and single epoch shadow matching in most epochs. In route 2, the epochs in the middle of the route when the particle filter positioning result has a larger error was when the experimenter was a making a turn. The turning in particle filter shadow matching is delayed compared with when the real event happened. This is the pay-off when using a filter, since when the turning actually happened, the particle filter may treat new measurements that suggests a turn to be errors. However, soon after more measurements suggesting the same turning, the filter then believes a turning has happened. This result suggest that when there is a turning, a particle filter shadow matching may need to be improved on checking it, but essentially, this is a trade off based on the level to trust abnormal measurements.

In order to evaluate the performance across all of the epochs, a statistical analysis was performed. Mean absolute deviation (MAD) was used as an indicator to evaluate the performance from a statistical perspective. MADs of cross-street position error

for conventional GNSS and shadow matching, single epoch shadow matching and particle filter shadow matching are compared in Figure 6.9. Bars in the left sub-figure show MADs for each route and the right sub-figure shows the mean MADs over all routes.

It is shown in Figure 6.9 that the across street positioning performance of particle filter shadow matching is significantly better than conventional GNSS positioning. The single epoch shadow-matching algorithm reduced the mean cross-street error, compared with conventional GNSS solutions, from 12.56m to 4.56m – by 61.2%, averaged over routes 1, 2, and 3. The particle filter shadow-matching algorithm reduced the mean cross-street error to 2.16m – by 81.6%, compared with conventional GNSS positioning solutions.

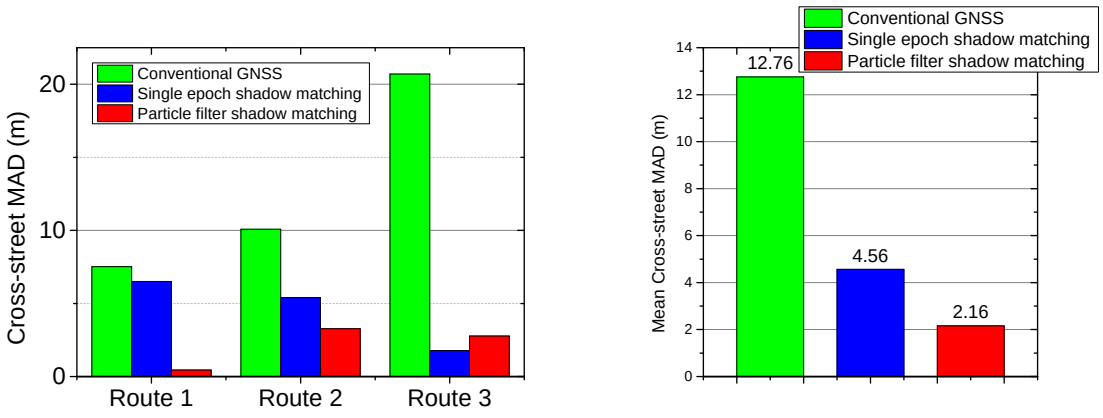

Figure 6.9.: Mean absolute deviation (MAD) of cross-street positioning errors using different methods

Further statistical comparisons were conducted to assess the positioning performance as a success rate of achieving a certain accuracy threshold in the cross-street direction, and the results are shown in Figure 6.10. As the street is around 10m wide, a positioning accuracy of less than 5m is considered good enough to distinguish sides of streets, while a positioning accuracy better than 2m is considered good enough to distinguish the footpath from a traffic lane, and traffic lanes from each other (lane identification).

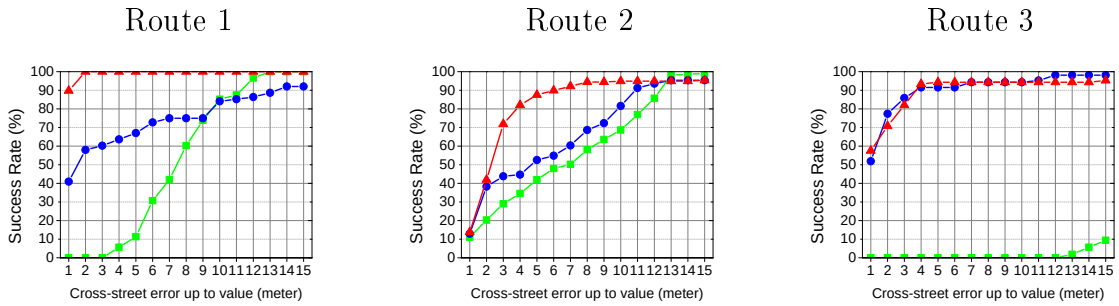

Figure 6.10.: Success rate comparison between different positioning methods in each route

It can be seen from Figure 6.10 that single epoch shadow matching is better than conventional GNSS. On average, particle filter shadow matching performs best as for determining the correct side of a street (5 meter error), its success rate in these results is 94.0%, while for single epoch shadow matching it is 70.4%, and for conventional GNSS it is a poor 17.8%. The success rate for distinguishing a footpath from a traffic lane (2 metre error) is 70.9% for particle filter shadow matching, while for single-epoch shadow matching it is 57.9%, and merely 6.8%, for conventional GNSS positioning.

6.6. Chapter summary

While single-epoch shadow matching works only for static applications, now, for the first time (parallel with Isaacs et al. (2014)), kinematic shadow matching is tackled. Since a Kalman filter has its limitations, including linear and Gaussian distribution assumptions; a particle filter, a non-linear non-Gaussian estimator, is designed. Compared with single-epoch shadow matching, the particle filter shadow matching optimize position estimation of moving objects (pedestrians or vehicles with GNSS enabled devices) using data from multiple epochs.

Real-world kinematic experiments were conducted in an urban area in London. An Android application was adpated to record the GNSS data stream on a smartphone. Three different routes, on two different streets, were tested by a pedestrian, providing a performance assessment of the new system. The second route also includes a direction change. Evaluation and comparison between three methods

(conventional GNSS, conventional single-epoch shadow matching, and particle filter shadow matching) was conducted. The particle filter is proven able to smooth the results compared with single-epoch shadow matching, as can be seen in Figure 6.8. Compared with conventional GNSS, the single-epoch shadow matching reduces the mean cross-street positioning error from 12.56m to 4.56m – by 61.2%, and further down to 2.16m using the particle filter shadow matching. The particle filter shadow matching improves the success rate of distinguishing the footpath from a traffic lane (2-meter-error) from 57.9% to 70.9%, compared with single-epoch shadow matching; and the success rate of distinguishing sides of streets (5-meter-error) from 70.4% to 94.0%.

In summary, the 3 experimental routes together prove that the proposed particle filter improves positioning accuracy significantly compared with single-epoch shadow matching, which was introduced in Chapter 5, and they both outperform positioning results of conventional GNSS. Thus, particle filter shadow matching has the potential to improve mobile device positioning in urban areas from street level to lane-level.

Chapter 7.

Adapting Shadow Matching for Mobile Applications

This chapter aims at answering the question - is shadow matching feasible in practice? Three perspectives of this question are tackled. The first perspective comes from whether the computation load of the shadow matching technique (as presented in Chapter 4) is small enough for real-time positioning on resource limited mobile platforms, e.g. smartphones. The low-computational power of mobile devices can be an obstacle to the practicality of a real-time shadow matching positioning system. To the author's knowledge, no work has been reported by other researchers to implement a shadow matching algorithm on mobile systems that can run in real time. In this research, the 3D models are pre-processed, thus the real-time computational load is smaller than for algorithms that engage directly with the 3D models. For the first time, a smartphone-based real-time shadow matching positioning system is proposed and implemented, aiming at real-time meters-level cross-street accuracy in urban canyons, as presented in Section 7.1 and 7.2. The positioning performance of the real-time positioning system is briefly assessed in Section 7.3. Furthermore, in the context that emerging GNSS constellations (e.g. Galileo and Beidou) will be available, at least planned, by 2020, the future of shadow matching should be predicted and supported by experimental results and reasonable assumptions. Thus the second perspective is to predict the future performance of shadow matching. Numerical predictions of shadow matching performance from this perspective are

described in Section 7.4. The final perspective considers potential issues that may raise from large-scale deployment, including availability of 3D models, data storage and transfer requirements, which are discussed in Section 7.5. Sections 7.1, 7.2, 7.3 and 7.5 are partially based on a paper presented in ION GNSS+ 2013 (Wang et al., 2013*c*); while section 7.4 is based on part of Wang et al. (2014).

7.1. A real-time shadow matching system

This section describes the design of a real-time shadow-matching positioning system. The overall architecture of the real-time positioning system is first described. Algorithm modifications, which are essential for real-time efficiency, are then presented.

7.1.1. Overall system architecture

There are different approaches to design a shadow-matching system. In a real-time shadow matching system, the approach in which a cloud server interacts with the smartphone user is preferred, with reasons give in Section 4.2. In this design, the smartphone first sends a positioning request with an initial position (e.g. GNSS or Wi-Fi positioning solution) to a server in the cloud. The server then gathers the building boundary data (as explained in Subsection 4.3.2) that enables shadow-matching positioning, according to the user's initial position and sends them back to the user. Finally, the smartphone performs the shadow-matching algorithm and determines a positioning solution. The overall architecture of the shadow-matching system is illustrated in Figure 7.1.

7.1.2. Algorithm optimization for better efficiency

The main strategy for improving real-time efficiency is that the building boundaries are pre-computed and stored on a server. The benefits of this strategy are discussed in general in Section 4.2. Here, the advantages that benefits a real-time positioning system is focused on. From the perspective of mobile devices, the system trades

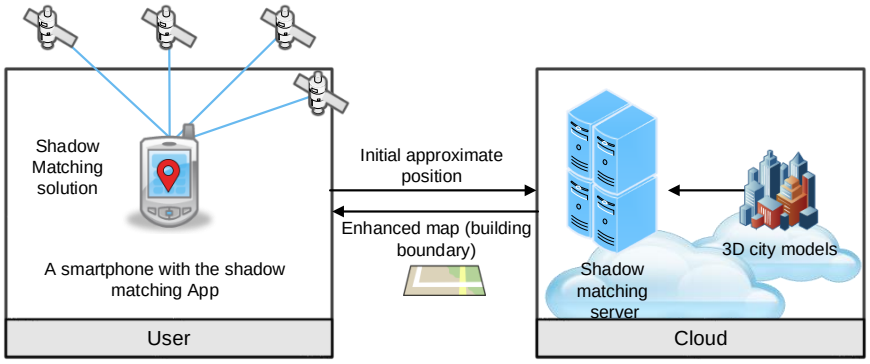

Figure 7.1.: Overall architecture design of a real-time shadow matching system

time and real-time computing power against a one-off processing requirement at the server side. Specifically, this is achieved by representing the 3D model in a specially designed form - building boundaries at each candidate position. The logic behind this strategy is that the vast amount of data in a 3D city model is not of direct interest to the real-time shadow-matching algorithm. The interest is where the edges of the buildings are located from a user's perspective. Thus, utilizing this knowledge, only the building boundaries at each candidate position are abstracted from the 3D model. This method saves real-time computational load because individual mobile devices do not need to compute the building boundaries on the fly. Instead, they can simply request building boundaries at a certain range of locations, or cache a desired region.

Using stored building boundaries, fewer than fifty comparison and addition operations are required to calculate an overall shadow matching score for one candidate position with two GNSS constellations. Therefore, shadow matching may be performed in real time on a mobile device with several hundred candidate positions, where necessary.

7.2. Application development on Android devices

An application (app) that runs on the Android operating system has been developed. This section briefly introduces the smartphone and the operating system involved

in this work, then describes the application development in more detail.

7.2.1. Smartphone and the Android operating system

The smartphone used in this work is a Samsung Galaxy S3 smartphone. It receives signals both GPS and GLONASS satellites. The smartphone runs on the Android operating system, a Linux-based operating system primarily for mobile devices. It is the most common smartphone operating system. According to the figures released from analyst firm International Data Corporation (IDC), Android smartphone shipments accounted for 75% of all smartphones shipped worldwide in the third quarter 2012 (IDC, 2012).

While Android and iOS are probably the two most popular smartphone operations systems, iOS does not provide an interface for individual satellite signal reception information, thus it is not used.

7.2.2. App design and development

The app has been developed in the Java programming language using Eclipse, a popular software development environment (SDE) for Android application development (Google, 2014*b*). The app was built on standard Android platform 4.0.3, using the Android application programming interface (API) to retrieve information from the GNSS chip. In this implementation, the building boundary data was computed on a server, and then stored on the SD card of the smartphone, rather than on a remote server.

The Android operation system listens to the real-time GNSS messages from the GNSS chip, interprets GNSS information from them, and provides the information to app developers through the Android API. The information is also accessible in National Marine Electronics Association (NMEA) format from an Android API function GpsStatus.NmeaListener. The public interface GpsStatus.Listener outputs, in real-time, the information provided by the GNSS chip, and contains a number of attributes. The useful attributes for this application include the azimuth, elevation and SNR of GPS and GLONASS satellites in view. The latest location determined

by the GNSS chip is output by the public interface LocationListener. This data feeds into the shadow matching positioning engine, together with the building boundary data stored on an SD card. The new positioning engine then computes the user's position by defining a search region centered at the conventional GNSS solution. Finally, the positioning results are displayed on maps using the Google Maps API. The flowchart of the app is illustrated in Figure 7.2.

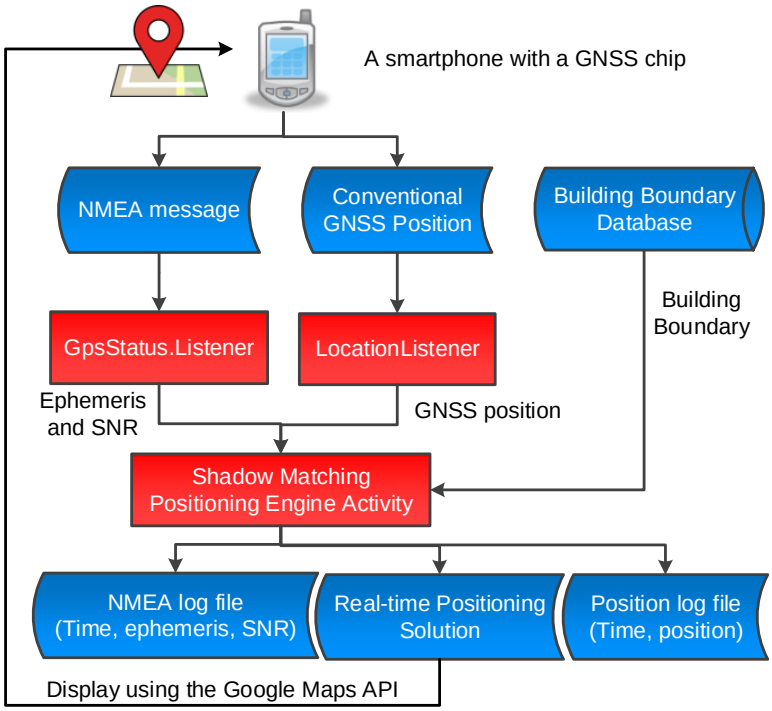

Figure 7.2.: The flowchart of the real-time application running on Android devices

7.3. Real-time experiments

To evaluate the performance of a real-time shadow matching system on smartphones, experiments were conducted in central London. The fundamental aim of this section is to demonstrate that an mobile application with the proposed shadow matching architecture can run in real-time on a smartphone. Additionally, this section also

discusses whether a compromise on accuracy is necessary to maintain the real-time processing efficiency.

Subsection 7.3.1 outlines the 3D city model and the test sites, and describes the configuration of the shadow-matching system, which uses a basic S_{22} scoring scheme with a grid of 3 meter spacing. A typical example of the real-time experiments is described in subsection 7.3.2. Recorded GNSS data is then processed using an identical algorithm to that in the real-time system. Subsection 7.3.3 shows the scoring maps, which are important intermediate results of the shadow-matching system. The positioning results compared between the new system and conventional GNSS positioning are given in Subsection 7.3.4.

7.3.1. Experimental settings

The 3D city model of the Aldgate area of central London, supplied by ZMapping Ltd, was used. It is the same 3D model used through out the thesis. Refer to Section 3.2 for more detail. The model has a high level of detail and decimetre-level accuracy. Figure 4.11 shows the city model.

Four experimental locations with different road conditions were selected on Fenchurch Street, a built-up urban area. shows photos taken at the street, showing the urban environments. Two of the sites, named RT1 and RT2, were located at a 'T' junction between Fenchurch Street and Fenchurch Buildings Road. The other two sites, named RT3 and RT4, were selected between junctions on Fenchurch Street. In addition, RT1 and RT3 are located on opposite side of the street, enabling the new system to also be tested for its ability to distinguish the correct side of the street. The same layout applies to RT2 and RT4. All sites were selected on the footpath close to the traffic lanes. Figure 7.4 shows an aerial view of the city model and a orthophoto, illustrating the locations of the four experimental sites. The truth model is set using the 3D city model, as explained in Subsection 4.4.1. The slight offset of about 3m between the city model and the orthophoto is caused by the geometric distortions of the orthophotos.

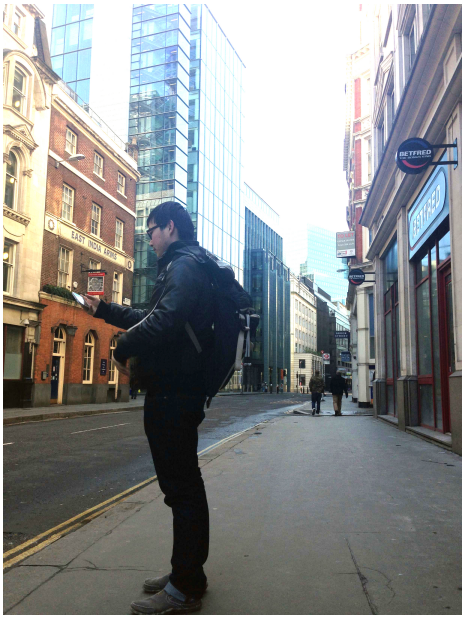

Figure 7.3.: Photos taken at the experimental sites, showing the urban environments in experiments

Before the experiment, in the offline phase of this work, a grid with 3-meter spacing was generated. Indoor points were then eliminated and building boundaries were determined at outdoor points. The building boundaries were stored in a specially defined format in a database, and pre-loaded on the smartphone used in this experiment. A basic S_{22} scoring scheme is used in the shadow matching positioning algorithm.

Real-time shadow-matching positioning was performed on a Samsung Galaxy S3 smartphone with a 5-second interval for real-time position display in Google Maps. The experimenter stood at each location for 6 minutes. Both GPS and GLONASS observations were used. Real-time satellite visibility information and positioning results were recorded at a 1-second interval for later analysis.

7.3.2. Real-time experiments

A real-time shadow-matching positioning experiment was conducted. The typical processing time for the system was found to be 1-2 seconds with a Samsung Galaxy S3 smartphone, measured using another smartphone. The smartphone used in this experiment, Galaxy S3, was a model released in 2012 with a Quad-core 1.4 GHz

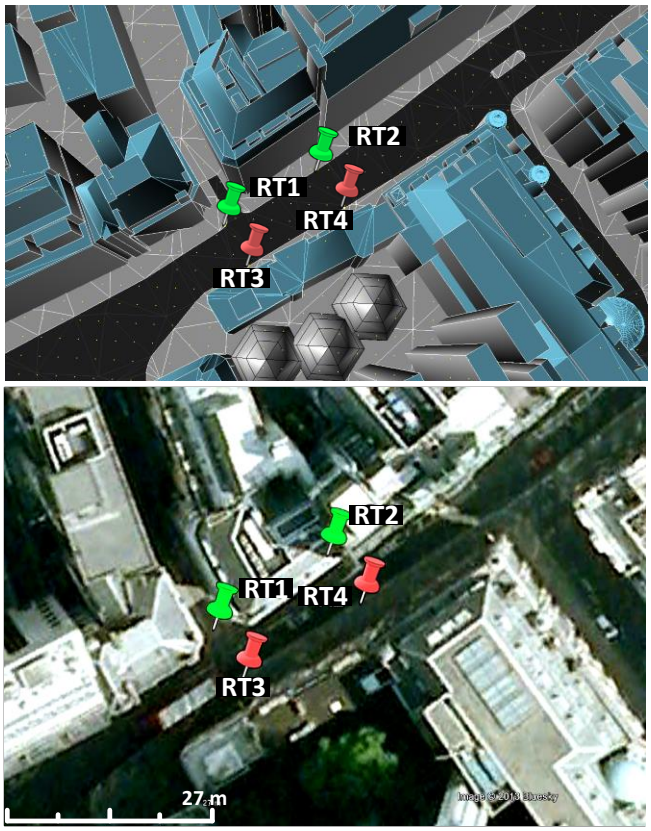

Figure 7.4.: An aerial view of the experimental site on Fenchurch Street: 3D city model (above) and orthophotos. (below)

Cortex-A9 processor and a 1 GB RAM. If a more recent model of smartphones is used, e.g. Samsung Note 4, which doubles CPU speed and triples memory space (Quad-core 2.7 GHz Krait 450 (SM-N910S) processor and 3GB ROM), an even faster performance can be expected. It also should be noted that no multi-core optimization was conducted, i.e. only one CPU core was used in the experiment. Taking the potential improved CPU, memory and multi-core techniques into consideration, the demonstration shows that the basic shadow matching algorithm, presented in Chapter 4, is fully workable on a smart device, e.g. a smartphone. A video demo of the experiment can be found on Youtube (Wang, 2014*a*).

In real-time, a 40-meter radius candidate circle, centred at the conventional GNSS positioning solution provided by smartphone GNSS chip, is used to generate candidate positions defining the search region for the shadow-matching technique. The

pre-calculated candidate grid of building boundaries (i.e. the off-line phase database) is loaded at this stage.

Figure 7.5 shows a photo taken in the real-time experiment using the developed shadow-matching application (app) at site RT2. As the application is a prototype of the real-time shadow-matching system, both the conventional GNSS solution of the smartphone GNSS chip and the positioning solution of the new system are displayed to the experimenter for a real-time comparison. The blue points are the conventional GNSS solutions, while the red points represent the solutions of the shadow matching system. For illustration purposes, the true position is marked by a white cross, and the cross-street and along-street direction is also marked. It is shown in Figure 7.5 that the conventional solutions are on the wrong side of the street, and distributed sparsely in the cross-street direction in comparison with the solutions of the shadow matching system. However, the conventional GNSS positioning solution in the along-street direction is correct. The shadow-matching real-time solutions are distributed more consistently in the across-street direction, on the correct side of the street. The characteristics of real-time shadow matching is the same with post-processed shadow matching in term of providing high positioning accuracy in the across-street direction, which is determined by the nature of shadow matching - the measurements of building's shadows are dominantly in the cross-street direction.

This is in line with the expected benefits of the new system which gives better across-street accuracy, and provides evidence suggesting that, in the long term, combining the cross-street position component of a shadow matching positioning system with the along-street component of a conventional GNSS position will provide a better overall positioning solution.

7.3.3. Analysis of shadow matching scoring results

At each observation epoch, a comparison is made between the predicted and observed satellite visibility, and the score scheme is applied accordingly. To illustrate the distribution of scores at the grid points, Figure 7.6 shows examples of the score maps at each experimental location. The coloured dots represent the candidate

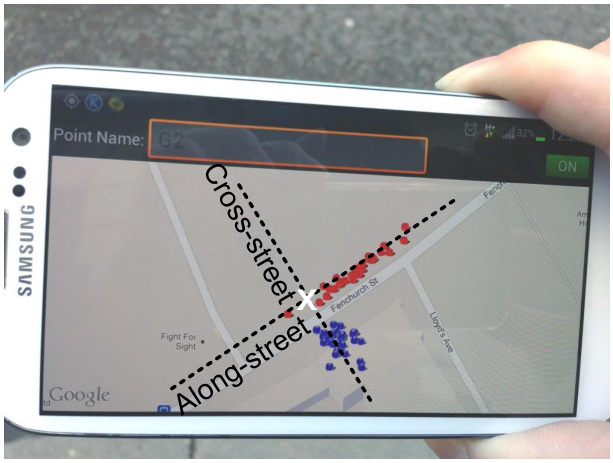

Figure 7.5.: A photo of the real-time experiment using the developed shadow-matching application on a smartphone at site RT2, showing that shadow matching (marked in red) offers higher accuracy in cross-street direction, and conventional GNSS (marked in blue) provides higher accuracy in the along-street direction.

positions. The scale represents the score obtained for the candidate position in the shadow-matching algorithm, with higher scores representing a higher confidence level that the user is at this location. The true location of the experimental site is shown by a black cross in each colour map.

In Figure 7.6, it is clearly demonstrated that the scoring shadow-matching algorithm is sensitive to changes in the cross-street direction, but less sensitive in the along-street direction. This is in line with expectations, and complements conventional GNSS positioning which is generally more precise in the along-street direction in urban areas due to the signal geometry. Combining the cross-street shadow-matching solution with the along-street conventional GNSS is an approach to intelligent urban positioning (IUP) Groves, Ziyi, Wang and Ziebart (2012). Refer to Figure 7.5 for an real-time example illustrating this feature.

There are some spaces between buildings that fall within the search area, but the highest scoring points are predominantly in the correct street. It can also be inferred from Figure 7.6 that in most cases, the highest score areas (dark red) appear on the correct side of the street. However, the high scores do not always appear at

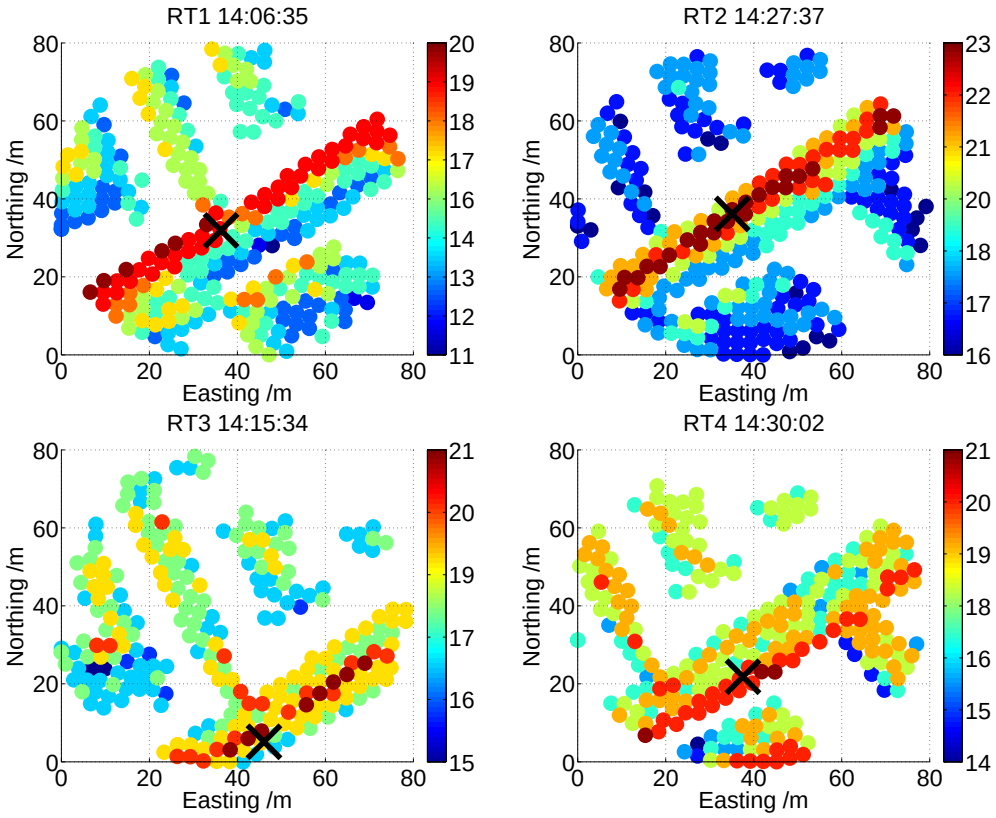

Figure 7.6.: Shadow-matching scoring map at one epoch for four experimental sites

the expected area. This multiple matching area phenomena can be handled using a particle filter, as described in Chapter 6. In order to further analyze the consistency of positioning performance of the implemented positioning system over the whole period of the experiment, more analysis is presented in the Subection 7.3.4.

7.3.4. Performance comparison with conventional GNSS

In this section, the overall performance of the real-time shadow-matching positioning system is assessed and compared with the conventional GNSS solution from the GNSS chip in the Samsung Galaxy S3 smartphone, both in real-time. The performance in the cross-street direction is the main concern.

A 3m grid spacing of the building boundaries is used in the real-time shadow matching algorithm. The grid spacing may influence the shadow matching positioning accuracy. For comparison purpose, a post-processing shadow matching algorithm using a 1m grid spacing is also conducted.

To assess the performance of real-time shadow matching against the conventional GNSS positioning solution, the position errors are transformed from local coordinates (Northing and Easting) to the along-street and across-street directions. Figure 7.7 shows the positioning results of the conventional GNSS navigation solution from the smartphone GNSS chip, compared with the shadow-matching positioning results, expressed as errors in the across-street direction. It shows that, in most cases, the shadow matching solution outperforms the conventional GNSS positioning solution. The shadow matching solution has improved the conventional positioning error from typically 10 - 40 meters to within 5 meters in the most epochs. In the case of RT2, the shadow-matching solution accuracy is better than 2m in most epochs.

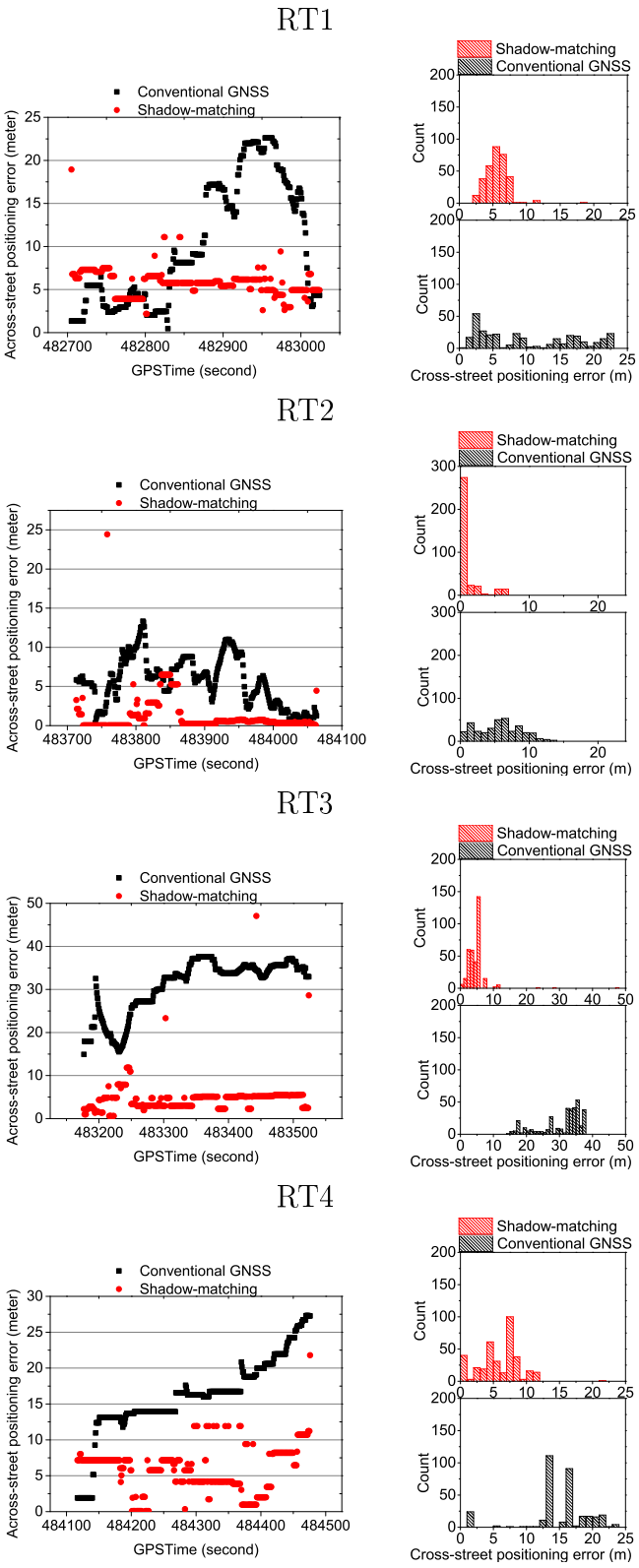

Figure 7.7.: Comparison of cross-street positioning error between conventional GNSS solution provided by the smartphone and the shadow-matching solution, both based on real-time data

On the right side of each sub-figure in Figure 7.7, the position error distribution is compared between the shadow-matching solution and the conventional solution. It is shown that shadow matching improves the positioning accuracy, reducing the average error to less than 5 meters on average in each case.

In order to evaluate the performance across all of the epochs, a statistical analysis was performed. An indicator, mean absolute derivation (MAD), as described in formula 4.5, was used to evaluate the performance from this perspective. In order to show the improvements of shadow matching over conventional GNSS positioning, the MADs at each site are compared in Figure 7.8. The bar shows the mean across-street positioning error using the conventional and shadow-matching algorithm, respectively. It should be noted that the statistics cover a 6-minute observation period, during which the constellation geometry changed slowly, so the results are highly correlated, temporally, allowing consistency of the system to be evaluated. It is shown in Figure 7.8 that the across street positioning performance of shadow matching is significantly better than conventional GNSS positioning solution. The shadow-matching positioning algorithm reduced the average cross-street error by 36.9%, 77.6%, 90.8% and 71.3% for RT1, RT2, RT3, and RT4 respectively. The new positioning system reduces the cross-street positioning error from 14.81 m of the conventional solution to 3.33 m of the new system, averaged over all four experimental sites. This is a 77.5% reduction of cross-street positioning errors on average. The RMS difference shows that the consistency of the shadow-matching solution also outperforms the conventional solution.

Further statistical comparisons have been conducted to assess the positioning performance as a success rate over 6 minutes, and the results are shown in Figure 7.9. As the street is around 10m wide, a positioning accuracy of less than 5m is considered good enough to determine the correct side of the street, while a positioning accuracy better than 2m is considered good enough to distinguish the footpath from a traffic lane. Averaged over the four experimental sites, the success rate using shadow matching for determining the correct side of a street is 54.4%, significantly improved from the success rate of 20.9% for the conventional solution. The success rate of

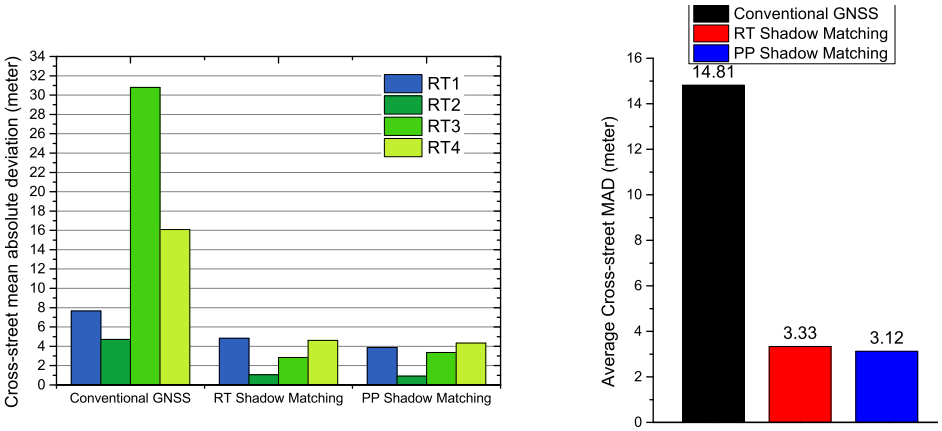

Figure 7.8.: Left: Comparison of the cross-street mean absolute deviation over all epochs between the conventional GNSS positioning solution, the real-time (RT) and post-processing (PP) shadow-matching solution, noting that the RT shadow matching uses a 3 meter spacing scoring grid, while the PP shadow matching uses a 1 meter spacing scoring grid; Right: the averaged cross-street positioning error from 4 experimental sites

distinguishing the footpath from a traffic lane is 25.6% for shadow matching, also considerably increased from 7.7%, for the conventional GNSS positioning.

Figure 7.10 shows the positioning results of the new system compared with the conventional GNSS solution in Google Earth. The blue dots represent the locations of the conventional GNSS solution, recorded in real-time. The purple dots denote the positioning solutions provided by the new system. The tags represent the true location of the site in each case. It can be seen that typically, the new system gives solutions more consistent with each other in cross-street direction. The solutions also have better accuracy in the cross-street direction, compared to the conventional solution. However, the conventional solution is more accurate in the along-street direction, in line with expectations.

The shadow matching positioning system is a suitable complementation to conventional GNSS positioning. As shadow matching improves the cross-street positioning significantly, it shows a high potential to be combined with conventional GNSS and other possible techniques for better overall performance.

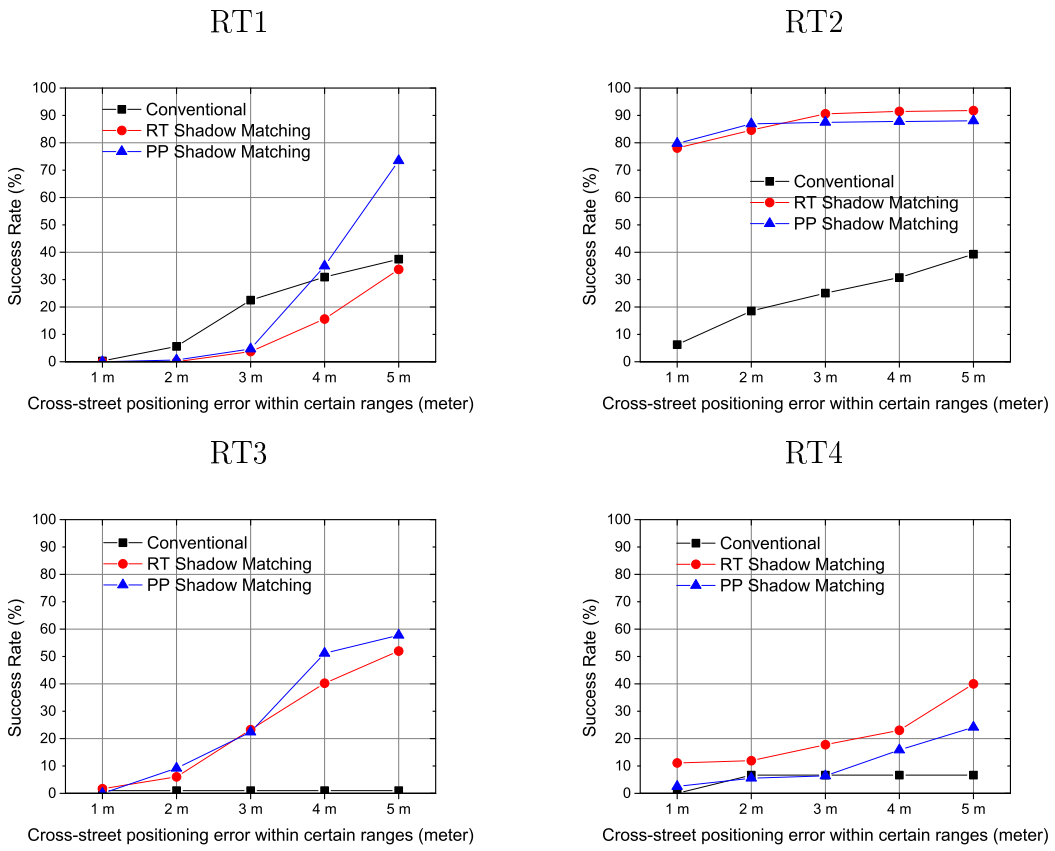

Figure 7.9.: Success rate of cross-street positioning error within certain ranges, compared between the conventional GNSS solution, the real-time (RT) and post-processing (PP) shadow-matching solution

It should be noted that selection of a suitable grid spacing of building boundaries influences the performance and speed of the shadow matching system. The current implementation of the real-time shadow-matching system utilizes a grid of building boundaries with 3-meter spacing. It already shows a significant performance improvement in comparison with conventional GNSS positioning. A grid with 2-meter spacing, 1-meter spacing or even denser spacing can potentially be applied. In this work, a 1-meter spacing was also tested. This version of shadow matching, described here as a post-processing shadow matching, provides an improved performance of 6% in terms of a reduction of the mean error averaged over the four sites, as can be seen in Figure 7.8. From the positioning success rate of each site, as shown in Figure 7.9, it can be seen that the performance of the real-time and post-processing shadow matching differs site by site and are similar to each other. However, using the grid with a 1-meter spacing requires roughly 9 times more computational time

Figure 7.10.: The positioning solution shown in Google Earth orthophoto view (The blue dots represent the locations of the conventional GNSS solution. The purple dots denote the positioning solutions provided by the new system. The tags represent the true location of the site in each case. Image © 2013 Bluesky)

in comparison with using a grid with 3-meter spacing. Clearly, there is a trade-off between the accuracy of the shadow-matching system and the running time. The reason a grid with 3-meter spacing is finally used in the real-time system is that it gives the best compromise between performance and speed. Variable grid spacing is also possible, e.g. start with 3m and then go to 1m around the matching area.

7.4. Performance prediction of four-constellation shadow matching

Shadow matching has been assessed for its performance with the current GNSS constellations in Chapter 5. However, GNSS constellations are developing with time, so it is important to question how shadow matching will perform in the future. Shadow matching uses multiple satellites to localize the user's position. Thus, using more satellites might be expected to produce a more accurate position solution.

To predict how shadow matching will perform in the future when Galileo and BDS, are fully operational, a four-constellation scenario was simulated by combining GPS and GLONASS data from two separate visits to each experimental site. More details of the experimental settings are described in Chapter 5. The interval between visits was about four hours, allowing the satellite constellation geometry to change significantly. The probability-based shadow matching algorithm is used in this assessment, as described in Chapter 5.

Figure 7.11 shows the MADs for each site and averaged across all sites of the cross-street positioning errors of two- and four-constellation shadow matching, together with conventional GNSS positioning (from the first observation period only). At some sites, shadow matching performed better with four constellations, while at others, it performed better with two constellations. Looking at the average across all of the sites, the two-constellation implementation performed slightly better.

Figure 7.12 shows the success rate for achieving cross-street positioning errors within certain bounds. Using four constellations slightly increased the probability of achieving a cross-street position solution within 1, 2 or 3m, but reduced the likelihood of achieving a position within 4 or 5m. A possible explanation is that in environments where the current shadow-matching algorithm works well, additional satellites provide additional information that is used to refine the position solution. However, in environments unfavourable to shadow matching, such as those with lots of highly reflective buildings, using more satellites results in more strong NLOS signals that confuse the shadow-matching algorithm.

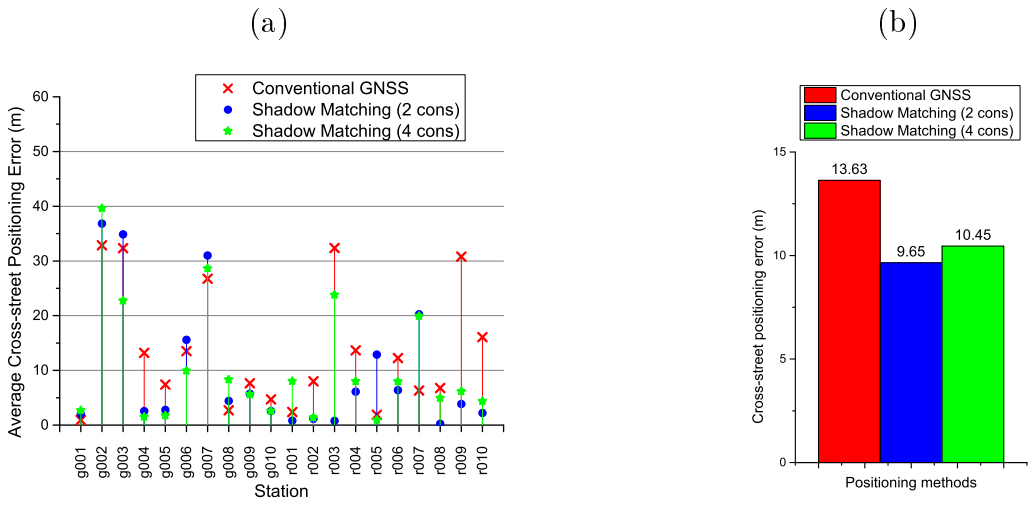

Figure 7.11.: The MAD of the cross-street positioning error of 2- and 4-constellation shadow matching and 2-constellation conventional GNSS for each site (a) and averaged across all sites (b)

Overall, these results show that the number of available satellites is not the main factor limiting shadow-matching performance. Improvements to the algorithms will be needed to increase shadow matching's reliability.

7.5. Large-scale implementation of shadow matching

7.5.1. Availability of 3D city models and satellite information

The shadow-matching system relies on knowing building's locations (from 3D, 2.5D city models, or high resolution digital surface models), therefore, the availability of the models is of importance. Fortunately, there are an increasing number of 3D city models available through the internet. A few commercial examples include Google Maps 3D by Google Inc. (Google, 2014*a*), iOS 3D Maps by Apple Inc. (Apple, 2014), Bing Maps 3D by Microsoft Corporation (Microsoft, 2014), Nokia Here Maps 3D (Nokia, 2014) and Edushi 3D Maps (available for China) (Edushi, 2014). In addition to the commercial 3D maps, some free and cheap 3D maps are provided by some organisations, including Open Street Maps 3D (OSM-3D) (OpenStreetMap,

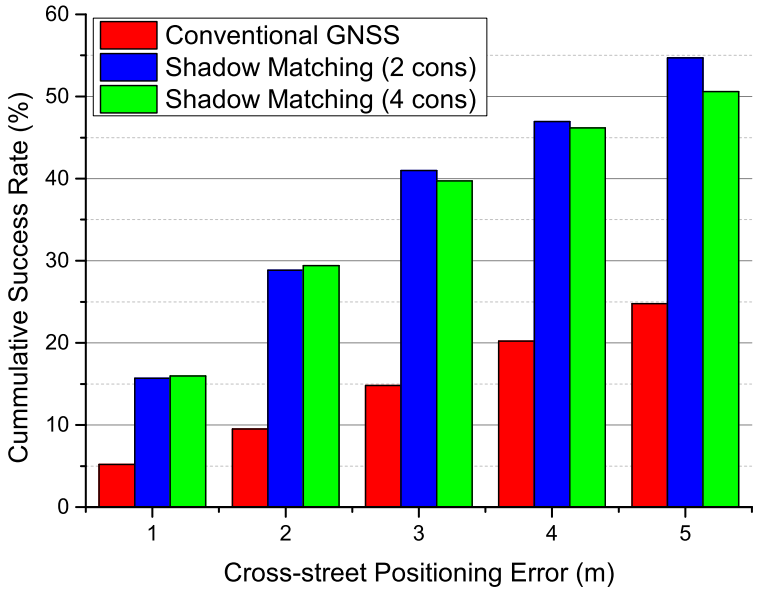

Figure 7.12.: The cumulative success rate of cross-street positioning error with certain meters of bound, comparing conventional GNSS and shadow matching with 2 and 4 constellations

2014).

The satellite tracking information required by the shadow matching system in real-time has also been available to use. The shadow-matching system only requires information on whether the satellites are tracked or not, instead of pseudo-range or carrier phase measurements. The required information is provided on a regular basis in NMEA sentences (NMEA, 2014), as a uniform interface standard, by many consumer-grade GNSS receivers, and by mobile devices with an Android operating system. With the signal-to-noise ratio (SNR) message also regularly available through NMEA sentences, shadow matching can provide more reliable performance, as demonstrated in Chapter 5, using probability-based SNR modelling techniques.

7.5.2. Data storage and transfer requirements

Shadow matching requires the knowledge of the building boundaries to work. Thus, the building boundaries database should be transferred to the user device on the fly or pre-downloaded (Groves, Wang and Ziebart, 2012). Building boundaries with

a 1-degree resolution in azimuth require about 300 bytes of storage per grid point, without compression.

As mentioned in Groves, Wang and Ziebart (2012); Wang et al. (2013*c*), with a 3 by 3 meter grid, a 1km long 20m wide street would contain 2222 grid points, which would require 651 kB of data storage. If the similarities between adjacent azimuths are exploited for compressing data, substantial data compression should be possible; perhaps up to a factor of ten. A 4 GB flash drive could store 6292 – 62920 km of road network. The Great London metropolitan area contains about 15,000 km of road.

However, the built-up areas that require shadow matching for better positioning may be 10% of the total. Thus, it may be practical to preload the building boundaries onto a smartphone. An alternative method is to transfer the data over the mobile network as required. On a 100-meter long 20-meter wide street, only 222 grid points are needed for shadow matching, which requires 141 kB of data. Transferring this would take less than two seconds using the 3G mobile phone network with a normal data plan. Thus, in practice, it is feasible to implement shadow-matching system on a smartphone, a PND, or other consumer-grade navigation device.

7.6. Chapter summary

This chapter adapts shadow matching for mobile applications and assesses its feasibility in practice. A smartphone-based shadow-matching system, assisted by knowledge derived from 3D models of the buildings, has been designed. The new system is optimized to improve computational efficiency to account for the low processing power and limited storage on smartphones. The design of the real-time shadow-matching system and the optimizations has then been implemented, with details explained. A shadow-matching application (app) for the Android operating system has been developed.

Furthermore, with the previous shadow-matching algorithms tested mainly on personal computers, for the first time, a demonstration is performed on a smartphone with a real-time GNSS data stream. The computational efficiency of the system is

thus verified, showing its potential for larger scale deployment. The experiment was conducted at four locations. Analysis was conducted to evaluate the performance of the system. The experimental results show that the proposed real-time system outperforms the conventional GNSS positioning solution. Instead of using a 1 meter grid spacing as in the post-processing shadow matching system (refer to Chapter 4), a 3 by 3 meter grid is used in the real-time system, providing a balance taking a trade-off between efficiency and accuracy.

In addition, the performance of four-constellation GNSS shadow matching was predicted using GPS and GLONASS data collected at two different times at the same sites. The additional satellites slightly improve shadow-matching performance under benign conditions, but not in more challenging environments.

Finally, the implementation of shadow matching on a larger scale has been assessed, showing that both server-based and handset-based models are feasible in terms of processing load, dissemination of building boundary information and availability of 3D mapping.

It should be noted that the system does not require real-time rendering of 3D scenes or any additional hardware, making it power-efficient and cost-effective. An increasing number of smartphones have multi-core CPU, GPU, or both, enabling parallel processing techniques and hardware acceleration techniques to be exploited for improved efficiency of shadow matching.

Chapter 8.

Conclusions

This study brings the shadow matching principle from a simple mathematical model, though experimental proof of concept, system design and demonstration, algorithm redesign, comprehensive experimental tests, real-time demonstration and feasibility assessment, to a workable positioning solution. The conclusions of this research are presented in Section 8.1. Five topics that are related to shadow matching techniques have been investigated in this study, comprising evaluation of GNSS positioning in urban environments, shadow-matching system design, handling non-line-of-sight (NLOS) signals in shadow matching algorithm on smartphones, kinematic shadow matching algorithms, and feasibility assessment of shadow matching techniques. Specific research questions and detailed conclusions are described under each topic. References within the thesis are given where appropriate. Future research recommendations and potential applications of this research are discussed in Section 8.2.

8.1. Conclusions of this research

8.1.1. Evaluation of GNSS positioning in urban environments

Can conventional GPS and GLONASS (using single-frequency pseudo-range measurements) meet the positioning requirements in urban environments? More specifically, in urban environments, how is the positioning performance different for pedestrians and vehicles, at traffic junctions

and between junctions, and in the along-street and cross-street directions?

Positioning performance using GPS and GLONASS was found to be unreliable, based on the number of visible satellites and their geometry, in urban canyons. Performance was found better for vehicles than pedestrians, who are closer to the buildings; and was better at junctions than between junctions, where there are typically more surrounding buildings. Finally, positioning precision was found to be generally lower in the cross-street direction than in the along-street direction, because the buildings constrain the satellite signal geometry as illustrated in Figure 1.1. This finding motivated investigation into shadow matching techniques, which showed the potential to improve positioning performance in the cross-street direction.

To draw this conclusion mentioned above, a satellite visibility determination toolkit was developed for predicting GNSS performance in urban environments using 3D building models, as described in Chapter 3. The toolkit was verified at two test points with field trials. Comparison of satellite visibility between prediction and observation demonstrated that direct line-of-sight signals can be predicted using the 3D city model and the toolkit. However, due to the complexity of the environments, diffracted and reflected signals were also observed that the original model did not predict. As diffracted signals are potentially useful in positioning, the simulation has been modified to predict them. Verification with real observations shows that the implemented diffraction model successfully predicted most of the strong diffracted signals.

If GPS and GLONASS can not guarantee reliable positioning in urban canyons, does adding multiple constellations (Galileo and BDS) solve this problem? In other words, can GNSS alone solve the positioning problem in urban canyons?

Even with all four constellations, GNSS performance will still be unreliable at some urban locations in 2020. Performance using four fully-operational GNSS constellations was predicted to be much better than GPS and GLONASS only, but still unreliable at a few of the test locations. GNSS signal availability has been quanti-

tatively verified to double by the year 2020, based on the assumption that both the Galileo and BDS systems will be fully operational by then, as their published plans, though the currently delayed progress may suggest this point will also be delayed.

This conclusion was drawn by evaluating positioning performance using different combinations of GNSS, including GPS, GLONASS, Galileo and BDS, from simulation using a 3D model of London. Solution availability, RAIM availability and precision at different directions have been assessed for both pedestrian and vehicle routes within a urban environments.

Thus, based on the simulations, to ensure a reliable positioning service in urban canyons, conventional GNSS from smartphones should be augmented with other techniques. There are a number of methods, including combining GNSS with other signals, sensors and data sources in an integrated navigation system (refer to Chapter 2 for more details). Another solution is the scope of the thesis - GNSS shadow matching, which can potentially improve the across-street positioning accuracy by comparing the observed GNSS signal availability with that predicted using a 3D city model (refer to Chapter 4 for more details).

8.1.2. Shadow-matching system design

> *Following the principle of shadow matching, how to design a positioning system that uses knowledge of 3D city models, i.e. what are the different options in the overall design? What are the pros and cons of each of them?*

The overall principle of shadow matching is to match GNSS signal observations with predictions determined using 3D models. There are a variety of options designing a detailed algorithm that fulfills this principle.

In terms of what to calculate first, there can be zone-based or point-based shadow matching algorithms, as discussed in Section 4.2. A zone-based approach starts with calculating the satellite signal shadow cast by buildings, using 3D city models; whereas a point-based shadow matching algorithm can start with calculating building boundaries (as explained in Section 4.3) at each candidate point (user's

potential location) using 3D city models. A zone-based approach makes it straightforward to leverage GPU hardware acceleration (e.g. using OpenGL shaders) to speed up shadow computing; whereas a point-based approach allows separating the 3D model processing from positioning process, in this work, via an intermediate format, namely building boundaries. Thus a point-based approach has a reduced real-time computation load.

In terms of where to put the shadow matching computation load, there can be options including cloud computing, local processing or a combined approach, as illustrated in Figure 4.2. Completely allocating shadow matching processing to the cloud or on the mobile device was considered time consuming and energy inefficient. Whereas dividing the computation load between the two offers a good balance, though trade-offs have to be made between real-time accuracy and computation time, depending on available computation power provided by mobile devices.

8.1.3. Handling non-line-of-sight (NLOS) signals in shadow matching algorithm for urban environments

When signal reflection or diffraction occurs, how to handle the resulting mismatches between observation and predictions?

Two modelling options for the received signal strength were considered to improve shadow matching performance on smartphones as presented in Chapter 5. The first option uses empirically determined discrete thresholds to determine whether an observed satellite signal is direct LOS. Furthermore, a probability-based shadow matching was proposed, and proven to improve the positioning performance via improved NLOS handling. Separate signal-to-noise ratio (SNR) distributions of direct LOS and NLOS GNSS signals received in a dense urban area were measured using an Android smartphone and a 3D city model, using large data sets of measurements. SNR models that handle NLOS signals are derived from a Bayesian technique using sample statistics methods, based on the SNR distributions.

What is the optimum scoring scheme, given the constraints of the current visibility prediction algorithm, in a shadow matching algorithm for smart-

phones, and how to determine the parameters in this scheme? (given that real signals are not just direct or blocked, but reflected, diffracted, multipath-contaminated and attenuated by body shadowing and the effects of antennas with highly directional gain patterns?)

Using distributions of SNR learned from a large set of real-world GNSS data, a function has been derived giving the probability that a received signal is direct LOS based on the measured SNR, using the 3D city models. Using this derived function, an optimized shadow-matching's satellite visibility scoring scheme has been achieved for use with smartphone GNSS measurements. In this new probability-based shadow matching algorithm, a sample statistics technique is used to estimate the conditional probability table (CPT) from large amount of GNSS measurement data.

Based on comprehensive experimental data, what is the performance of shadow matching, compared with conventional GNSS positioning? What is the performance difference between a basic shadow-matching algorithm and a probability-based shadow matching?

Using GPS and GLONASS data recorded at 20 locations within central London, the first comprehensive performance assessment of smartphone GNSS shadow matching has been conducted. The results show that the probability shadow-matching algorithm proposed in Chapter 5 significantly outperforms conventional GNSS positioning in the cross-street direction, and are statistically better than the basic shadow matching algorithm with S_{22} scoring scheme in Chapter 4. The success rate for obtaining a cross-street position accuracy within 5m, enabling the correct side of a street to be determined, was 54.03% using probability-based shadow matching, compared to 45.43% using basic shadow matching, and 24.77% for the conventional GNSS position.

8.1.4. Kinematic shadow matching algorithms

For kinematic applications, how to combine shadow matching information from multiple epochs to get a better position solution (particularly if you have an ambiguous fix)?

For the first time (in parallel to Isaacs et al., 2014), kinematic shadow-matching positioning is investigated in Chapter 6. The key advantage a kinematic shadow matching algorithm should take is to make use of information from multiple epochs.

A Kalman filter, a grid filter, and a particle filter are compared in terms of their ability to describe non-linear and non-Gaussian distributed measurement errors, spacial resolution of posterior density function (PDF), and capability in handling ambiguous position fix. A Kalman filter is predicted and proven (Wang, 2014*a*) to have its limitations, including linear and Gaussian distribution assumptions. A particle filter, a non-linear non-Gaussian estimator, is preferred. Compared with single-epoch shadow matching, the particle filter shadow matching improves the position estimation of moving objects (pedestrians or vehicles with GNSS-enabled devices) using data from multiple epochs, without the constraints of linear and Gaussian distribution assumptions of the measurement model, and offers self-adapted spatial resolution of the PDF, as described in in Chapter 6.

> *How accurate positions can be obtained from kinematic shadow matching (compared with conventional GNSS and probability-based single-epoch shadow matching)?*

To answer this question, real-world kinematic experiments were conducted in an urban area in London. An Android application was adapted to record the GNSS data stream on a smartphone. Three different routes, on two different streets, were tested by a pedestrian, providing a performance assessment of the new system. The second route also includes a direction change. Evaluation and comparison between three methods (conventional GNSS from smartphones, probability-based single-epoch shadow matching in Chapter 5, and particle filter shadow matching in Chapter 6) was conducted. The particle filter is proven able to smooth the results compared with single-epoch shadow matching, as can be seen in Figure 6.8. Compared with conventional GNSS, single-epoch shadow matching reduces the mean absolute deviation (MAD) cross-street positioning from 12.56m to 4.56m – by 61.2%, and further down to 2.16m using the particle-filter shadow-matching algorithm. Particle-filter-based shadow matching improves the success rate error of distinguish-

ing the footpath from a traffic lane (2-meter-error) from 57.9% to 70.9%, compared with single-epoch shadow matching; and the success rate of distinguishing sides of streets (5-meter-error) from 70.4% to 94.0%.

In summary, the kinematic experiments together prove that the proposed particle filter (in Chapter 6) improves the positioning accuracy significantly compared with the single-epoch probability-based shadow matching algorithm, described in Chapter 5, and they both outperform positioning results of conventional GNSS.

8.1.5. Feasibility assessment of shadow matching techniques

Can the designed shadow matching algorithm run in real-time on a mobile device?

It is demonstrated that shadow matching algorithms can run in real-time on a smartphone. Smartphone-based shadow-matching system, assisted by knowledge derived from 3D models of the buildings, has been designed and implemented, as presented in Chapter 7. The new system is optimized to improve computational efficiency to account for the low processing power and limited storage capacity of smartphones. A shadow-matching real-time application (app) for Android operating system has been developed. The experimental results show that the real-time system outperforms the conventional GNSS positioning solution, reducing the cross-street positioning error by 69.2% on average.

Is there a trade-off that has to be made between high efficiency and high accuracy in shadow matching?

It is shown that a trade-off between efficiency and accuracy exists, in the shadow matching algorithms, as expected. Selection of a suitable grid spacing of building boundaries influences both the performance and speed of the shadow matching system. The current implementation of the real-time shadow-matching system, described in Chapter 7, uses a grid of building boundaries with 3-meter spacing. It already shows a significant performance improvement in comparison with conventional GNSS positioning. A grid with 2-meter spacing, 1-meter spacing or even denser spacing can potentially be applied. In this work, a 1-meter spacing was also

tested, providing an improved performance of 6% in terms of reduction of mean error averaged over the four sites, compared with the post-processing shadow matching using the algorithm described in Chapter 4. However, using the grid with 1-meter spacing requires roughly 9 times more computational time in comparison with using a grid with 3-meter spacing. Clearly, there is a trade-off between the accuracy of the shadow-matching system and the running time. The reason a grid with 3-meter spacing was finally used in the real-time system is that it gives the best compromise between performance and speed.

> *Is it feasible to store enhanced map data for shadow matching on user's devices, or transmit over the mobile network? How much data storage is required per unit area?*

It is feasible to implement shadow-matching system on a smartphone with enhanced map data either stored on devices or transfered over the mobile network. With a 3 by 3 meter grid for the real-time shadow matching scenario presented in Chapter 7, it is estimated that a 4 GB flash drive could store 6292 – 62920 km of road network, enough for the Great London metropolitan area, without any data compression. However, the built-up areas that require shadow matching for better positioning may be 10% of the total. Thus, it may be practical to preload the building boundaries onto a smartphone. It is also estimated that transferring the required data for shadow matching would take less than two seconds using the 3G mobile phone network with a normal data plan, as presented in Chapter 7.

> *How does the number of GNSS constellations impact shadow matching performance?*

The performance of four-constellation GNSS shadow matching was predicted and compared with using only GPS and GLONASS in Section 7.5. The additional satellites were found to slightly improve shadow-matching performance under benign conditions, but not in more challenging environments. More specifically, using four constellations slightly increased the probability of achieving a cross-street position solution within 1, 2 or 3m, but reduced the likelihood of achieving a position within 4 or 5m. Overall, results showed that the number of available satellites is not

the main factor limiting shadow-matching performance, as presented in Chapter 7. Improvements to the algorithms will be needed to increase shadow matching's reliability.

> *What is the shadow-matching performance difference between a smartphone versus a geodetic GNSS receiver?*

Smartphone-grade GNSS receivers are more feasible for most potential applications of the shadow matching technique, but have different characteristics with geodetic GNSS receivers offers, as discussed in Section 4.4 and Section 5.1. Analysis based on real-world GNSS data collected at 20 locations, both on a geodetic GNSS receiver and a smartphone app developed in this work, suggests that the geodetic shadow-matching solutions outperforms shadow matching using smartphones. The comparison were made with both solutions computed using the basic shadow matching algorithm described in Section 4.3.

8.2. Recommendations for future research and potential applications

8.2.1. Future research

Since Chapter 3 demonstrates that conventional GNSS has a lower accuracy in the cross-street direction than in the along-street direction, and from various experiments in this work, it is demonstrated that shadow matching provides better accuracy in the cross-street direction than in the along-street direction compared with conventional GNSS, it is suggested that, in the future, the cross-street component of shadow-matching should be combined with the along-street component of conventional GNSS. This idea was proposed in Groves, Ziyi, Wang and Ziebart (2012), now, this is confirmed by the work presented in this thesis (e.g. as shown in Figure 7.5). To ensure that the shadow-matching information is weighted correctly in a combined solution, a method to determine the uncertainty and reliability of the shadow-matching solution should be developed. The probability determination method developed in the weighting step of a particle filter, as presented in Chapter

6, or the method used to compute the error covariance matrix in the Kalman filter (Wang, 2014*a*), might be used for this purpose.

Reflected signals should be predicted in the satellite visibility prediction phase of shadow matching to identify NLOS signals. This is because, in shadow matching, basically, predictions should match with observations to contribute to a positioning solution. Thus, both predictions and observations should be properly understood. This thesis focuses more on understanding observations from the SNR measurements, leaving the understanding of predictions to be investigated in the future. Actually, there are two benefits of identifying reflected signals in the satellite visibility prediction phase. The first is that a better initial position can be achieved in the first step of the shadow-matching algorithm. Secondly, the knowledge of a predicted NLOS signal can further improve the scoring scheme in shadow-matching algorithm. Both these benefits can potentially improve the performance of shadow matching.

3D maps have different resolutions. Currently, research on shadow matching is conducted using a high-resolution 3D building model of London. However, for shadow matching on a bigger scale, detailed 3D building models may or may not be available everywhere; or 3D building models may not be needed with extremely high accuracy. An increase of the 3D building model resolution may not significantly improve the performance of shadow matching once the resolution has already reached a certain level. Normal 2D map is much more widely available and have benefits of low cost and low data storage. Employing 2D maps in shadow matching may exploit these advantages. Thus, the relationship between performance of shadow matching and level of detail of the city map is worth further investigation.

8.2.2. Applications

In this thesis, shadow matching has been demonstrated able to provide lane-level positioning, and possibly metres-level across-street accuracy. Metres-level across-street accuracy in urban areas benefits a number of existing LBS and creates new applications. For example, vehicle lane detection may be feasible with meters-level across-street accuracy. Although lane guidance systems are now common for in-car

navigation systems, a lane detection system may enable a lane guidance system to not only guide the correct lane but also alert when the present lane is incorrect. Similarly, intelligent transportation systems (ITS) may use this technique to direct individual vehicles for maximizing traffic flow, and for prioritizing emergency vehicles. In situations where crossing the road takes considerable effort for pedestrians, location-based advertising (LBA) systems could use this technique to target the most suitable customers on the same side of the street. Some augmented-reality games may enhance the experience of the players through more accurate positioning. Perhaps most importantly, step-by-step guidance for the visually impaired and for tourists can benefit from higher positioning accuracy in urban areas in order to work. Navigation in mountainous regions could also benefit from this system when a digital elevation model (DEM) is available.

For many applications, the modelling technique presented in Chapter 3 could also be used to predict the best route through a city at a given time, or the best time to perform GNSS positioning at a given location. This technique could also be applied to GNSS signals prediction in mountainous area by using a digital elevation model (DEM) instead of a city model.

Bibliography

Agrawal, Mohit (2009), 'Introduction to Location Based Services (LBS)'.
URL: *http://www.telecomcircle.com/2009/06/introduction-to-lbs/*

Alperin, Roger C (1987), 'Heron's area formula', *The College Mathematics Journal* **18**(2), 137–138.

Apple (2014), 'iOS 7 turn by turn navigation'.
URL: *https://www.apple.com/uk/ios/maps/*

Azaro, R, M Donelfi, M Benedetti, P Rocca and A Massa (2008), 'A GSM signals-based positioning technique for mobile applications', *Microwave and Optical Technology Letters* **50**(8), 2128–2130.
URL: *<Go to ISI>://000256780300044*

Barnes, Joel, Chris Rizos, Jinling Wang, David Small, Gavin Voigt and Nunzio Gambale (2003), Locata: a new positioning technology for high precision indoor and outdoor positioning, *in* 'Proceedings 2003 International Symposium on GPS\ GNSS', pp. 9–18.

Benford, Steve, Will Seager, Martin Flintham, Rob Anastasi, Duncan Rowland, Jan Humble, Danaë Stanton, John Bowers, Nick Tandavanitj, Matt Adams, Ju Farr, Amanda Oldroyd and Jon Sutton (2004), The Error of Our Ways: The Experience of Self-Reported Position in a Location-Based Game UbiComp 2004: Ubiquitous Computing, Vol. 3205, Springer Berlin / Heidelberg, pp. 70–87.
URL: *http://dx.doi.org/10.1007/978-3-540-30119-6_5*

Bensky, Alan (2008), *Wireless positioning technologies and applications*, Artech House.
URL: *http://books.google.co.uk/books?id=nEHbAAAAMAAJ*

Bernstein, D and A Kornhauser (1998), AN INTRODUCTION TO MAP MATCHING FOR PERSONAL NAVIGATION ASSISTANTS, Technical report.
URL: *citeulike-article-id:9343151*

Betaille, D, F Peyret, M Ortiz, S Miquel and L Fontenay (2013), 'A New Modeling Based on Urban Trenches to Improve GNSS Positioning Quality of Service in Cities', *Intelligent Transportation Systems Magazine, IEEE* **5**(3), 59–70.

Bingham, J K and M J Veth (2009), Vision-Aided, Cooperative Navigation for Multiple Unmanned Vehicles, *in* 'Proceedings of the 2009 International Technical Meeting of the Institute of Navigation - ITM 2009', Inst Navigation, Washington, pp. 804–813.
URL: *<Go to ISI>://000279863400079*

Boehm, J (2009), Terrestrial LiDAR in Urban Data Acquisition, *in* 'Photogrammetric Week 09', Wichmann Verlag: Heidelberg, pp. 169 – 178.

Bourdeau, A and M Sahmoudi (2012), 'Tight Integration of GNSS and a 3D City Model for Robust Positioning in Urban Canyons'.

Bradbury, J, M Ziebart, P A Cross, P Boulton and A Read (2007), 'Code Multipath Modelling in the Urban Environment Using Large Virtual Reality City Models: Determining the Local Environment', *The Journal of Navigation* **60**(01), 95–105.

Bradbury, Joe (2007), Prediction of Urban GNSS Availability and Signal Degradation Using Virtual Reality City Models, *in* 'Proceedings of the 20th International Technical Meeting of the Satellite Division of The Institute of Navigation (ION GNSS 2007)', Fort Worth, TX, pp. 2696–2706.

Bradbury, Joe (2008), The Integration of City Models and GNSS for the Simulation and Modelling of Multipath and Availability: Paving the Way for New Applications, PhD thesis.

Brenner, Claus (2005), 'Building reconstruction from images and laser scanning', *International Journal of Applied Earth Observation and Geoinformation* **6**(3-4), 187–198.
URL: *http://www.sciencedirect.com/science/article/pii/S030324340400087X*

Brimicombe, Allan (2010), *Location-Based Services and Geo-Information Engineering*, Wiley.

Broll, W, I Lindt, I Herbst, J Ohlenburg, A K Braun and R Wetzel (2008), 'Toward Next-Gen Mobile AR Games', *Computer Graphics and Applications, IEEE* **28**(4), 40–48.

Brown, Robert Grover and Patrick Y C Hwang (1996), *Introduction to Random Signals and Applied Kalman Filtering*, 3 edn, Wiley.

Butler, Ken (2002), Tactical Automated Security System Air Force expeditionary security, *in* 'Proceedings of SPIE 2002', pp. 283–290.

Campoy, P, J F Correa, I Mondragon, C Martinez, M Olivares, L Mejias and J Artieda (2009), 'Computer Vision Onboard UAVs for Civilian Tasks', *Journal of Intelligent & Robotic Systems* **54**(1-3), 105–135.
URL: *<Go to ISI>://000264484900008*

Chee-Yee, Chong and S P Kumar (2003), 'Sensor networks: evolution, opportunities, and challenges', *Proceedings of the IEEE* **91**(8), 1247–1256.

Cheng, Yu-Chung, Yatin Chawathe, Anthony LaMarca and John Krumm (2005), Accuracy Characterization for Metropolitan-scale Wi-Fi Localization, *in* 'Proceedings of the 3rd International Conference on Mobile Systems, Applications, and Services', MobiSys '05, ACM, New York, NY, USA, pp. 233–245.
URL: *http://doi.acm.org/10.1145/1067170.1067195*

China (2014), 'Compass (BeiDou) status'.
URL: *http://www.beidou.gov.cn/*

Cui, Youjing and Shuzhi Sam Ge (2003), 'Autonomous vehicle positioning with GPS in urban canyon environments', *Robotics and Automation, IEEE Transactions on* **19**(1), 15–25.

Davidson, Pavel, Jussi Collin and Jarmo Takala (2011), 'Application of particle filters to a map-matching algorithm', *Gyroscopy and Navigation* **2**(4), 285–292.

Dissanayake, G, S Sukkarieh, E Nebot and H Durrant-Whyte (2001), 'The aiding of a low-cost strapdown inertial measurement unit using vehicle model constraints for land vehicle applications'.

Dodson, A H, X Meng and G W Roberts (2001), Adaptive method for multipath mitigation and its application for structural defelection monitoring, *in* 'Proceedings of the International Symposium on Kinematic Systems in Geodesy, Geomatics and Navigation, Alberta, Canada, June 2001,'.

Dowman, Ian and Vaibhav Arora (2012), '3D data: Exploring new horizons', *Geospatial World* **August**, 7.

D'Roza, T and G Bilchev (2003), 'An Overview of Location-Based Services', *BT Technology Journal* **21**(1), 20–27.
URL: *http://dx.doi.org/10.1023/A:1022491825047*

Edushi (2014), 'Edushi 3D maps'.
URL: *http://beijing.edushi.com/*

Enkelmann, Wilfried (2001), 'Video-Based Driver Assistance–From Basic Functions to Applications', *International Journal of Computer Vision* **45**(3), 201–221.
URL: *http://dx.doi.org/10.1023/A:1013658100226*

Ercek, R, P De Doncker and F Grenez (2006), Statistical determination of the PR error due to NLOS-Multipath in Urban Canyons, *in* 'ION GNSS 2006', pp. 1771–1777.

Ercek, Rudy, Philippe De Doncker and Francis Grenez (2005), Study of Pseudo-Range Error Due to Non-Line-of-Sight-Multipath in Urban Canyons, *in* 'Proceed-

ings of the 18th International Technical Meeting of the Satellite Division of The Institute of Navigation (ION GNSS 2005)', Long Beach, CA, pp. 1083–1094.

Estey, Louis H and Charles M Meertens (1999), 'TEQC: the multi-purpose toolkit for GPS/GLONASS data', *GPS solutions* **3**(1), 42–49.

EU (2014), 'Galileo status'.
URL: *http://www.esa.int/esaNA/galileo.html*

Farley, G, M Chapman and Ion (2008), An Alternate Approach to GPS Denied Navigation based on Monocular SLAM Techniques, *in* 'Proceedings of the 2008 National Technical Meeting of the Institute of Navigation - NTM 2008', Inst Navigation, Washington, pp. 810–818.
URL: *<Go to ISI>://000279793700080*

Farrell, Jay A (2008), *Aided navigation: GPS with high rate sensors*, McGraw-Hill Professional.

Farret, J C, M C Dos Santos and L Sukeova (2010), 'INITIAL L2C MULTIPATH AND NOISE PERFORMANCE ANALYSIS FROM REAL DATA', *Boletim De Ciencias Geodesicas* **16**(1), 73–85.
URL: *<Go to ISI>://000276727100005*

Fisher, J., S. Simpson and T. Welsh (2002), An Urban Canyon Multipath Model for Galileo, *in* 'European Navigation Conference (ENC)'.
URL: *http://gbppr.dyndns.org/mil/radar/An_Urban_Canyon_Multipath_Model_for_Galile*

Francois, Peyret, Betaille David and Mougel Florian (2011), Non-Line-Of-Sight GNSS signal detection using an on-board 3D model of buildings, *in* '11th International Conference on ITS Telecommunications (ITST)', St. Petersburg, pp. 280—-286.

Gaisbauer, Christian and Andrew U Frank (2008), Wayfinding Model For Pedestrian Navigation, *in* '11th AGILE International Conference on Geographic Information Science 2008'.

Gelb, A. (1974), *Applied Optimal Estimation*, MIT Press, Cambridge, MA.

Georgy, Jacques, Tashfeen Karamat, Umar Iqbal and Aboelmagd Noureldin (2010), 'Enhanced MEMS-IMU/odometer/GPS integration using mixture particle filter', *GPS Solutions* pp. 1–14.
URL: *http://dx.doi.org/10.1007/s10291-010-0186-4*

GJU (2006), 'Galileo Open Service Signal In Space Interface Control Document (OS SIS ICD) Draft 0'.

Godha, S and M Cannon (2007), 'GPS/MEMS INS integrated system for navigation in urban areas', *GPS Solutions* **11**(3), 193–203.
URL: *http://dx.doi.org/10.1007/s10291-006-0050-8*

Google (2014*a*), 'Google 3D Warehouse'.
URL: *https://3dwarehouse.sketchup.com*

Google (2014*b*), 'Using Eclipse for Android platform development'.
URL: *https://source.android.com/source/using-eclipse.html*

Gordon, N.J., D. J. Salmond and A. F. M. Smith (1993), 'A Novel Approach to Nonlinear/Non-Gaussian Bayesian State Estimation', *Proc. IEE Radar Signal Process* **140**, 107–113.

Greenfeld, Joshua S (2002), Matching GPS observations to locations on a digital map, *in* 'Transportation Research Board 81st Annual Meeting', p. 12.

Gröger, G, T H Kolbe, A Czerwinski and C Nagel (2008), 'OpenGISÂ® City Geography Markup Language (CityGML) Encoding Standard, OGC standard'.

Groves, P D, Z Jiang, M Rudi and P Strode (2013), A Portfolio Approach to NLOS and Multipath Mitigation in Dense Urban Areas, *in* 'ION GNSS+ 2013', Nashville, Tennesse, pp. 3231 – 3247.

Groves, Paul (2013), 'Multipath vs. NLOS signals: How Does Non-Line-of-Sight Reception Differ From Multipath Interference?', *Inside GNSS* pp. 40–44.

Groves, Paul D (2011), 'Shadow Matching: A New GNSS Positioning Technique for Urban Canyons ', *The Journal of Navigation* **64**, 417–430.

Groves, Paul D (2013), *Principles of GNSS, Inertial, and Multisensor Integrated Navigation Systems*, Artech House, Boston, London.

Groves, Paul D, Graham W Pulford, Christopher J Mather, C Aaron Littlefield, David L J Nash and Mark R Carter (2007), Integrated pedestrian navigation using GNSS, MEMS IMU, Magnetometer and Baro-altimeter, *in* 'Proc. Royal Institute of Navigation conference, RIN NAV'07', London.

Groves, Paul D, Jiang Ziyi, Lei Wang and Marek K Ziebart (2012), 'Intelligent Urban Positioning using Multi-Constellation GNSS with 3D Mapping and NLOS Signal Detection'.
URL: *http://www.ion.org/publications/abstract.cfm?articleID=10262*

Groves, Paul D, Lei Wang and Marek K Ziebart (2012), 'Shadow matching: Improved GNSS accuracy in urban canyons', *GPS World* **23**(2), 14–18.

Groves, Paul D and Ziyi Jiang (2013), 'Height Aiding, C/N0 Weighting and Consistency Checking for GNSS NLOS and Multipath Mitigation in Urban Areas', *The Journal of Navigation* **66**.

Groves, Paul D, Ziyi Jiang, Ben Skelton, Paul Cross, Lawrence Lau, Yacine Adane and Izzet Kale (2010), Novel Multipath Mitigation Methods using a Dual-polarization Antenna, *in* 'Proceedings of the 23rd International Technical Meeting of The Satellite Division of the Institute of Navigation (ION GNSS 2010)', Portland, OR, pp. 140–151.

Guercke, R, C Brenner and M Sester (2009), 'Generalization of 3D City Models as a Service', *International Archives of the Photogrammetry, Remote Sensing and Spatial Information Sciences 38 (Part 2/W11) (on CD-ROM). .*
URL: *http://isprsserv.ifp.uni-stuttgart.de/proceedings/XXXVIII/2-W11/Guercke_Brenner_Sester.pdf*

Guolin, Sun, Chen Jie, Guo Wei and K J R Liu (2005), 'Signal processing techniques in network-aided positioning: a survey of state-of-the-art positioning designs', *Signal Processing Magazine, IEEE* **22**(4), 12–23.

Gustafsson, F and F Gunnarsson (2005), 'Mobile positioning using wireless networks: possibilities and fundamental limitations based on available wireless network measurements', *Signal Processing Magazine, IEEE* **22**(4), 41–53.

Gustafsson, F., N. Bergman, U. Forssell, J. Jansson, R. Karlsson and P.-J. Nordlund (2002), 'Particle Filters for Positioning, Navigation and Tracking', *IEEE Trans. on Signal Processing* **50**, 425–437.

Haala, Norbert and Jan Böhm (2003), 'A multi-sensor system for positioning in urban environments', *ISPRS Journal of Photogrammetry and Remote Sensing* **58**(1-2), 31–42.
URL: *http://www.sciencedirect.com/science/article/pii/S0924271603000157*

Hall, Timothy J., Mark A. Schwartz and Steven M. Hamer (1996), 'GPS-based traffic control preemption system'.
URL: *http://www.google.co.uk/patents/US5539398*

Hegarty, C J and E Chatre (2008), 'Evolution of the Global Navigation Satellite System (GNSS)', *Proceedings of the IEEE* **96**(12), 1902–1917.

Heimes, F and H H Nagel (2002), 'Towards Active Machine-Vision-Based Driver Assistance for Urban Areas', *International Journal of Computer Vision* **50**(1), 5–34.
URL: *http://dx.doi.org/10.1023/A:1020272819017*

Herrera, Juan C, Daniel B Work, Ryan Herring, Xuegang Ban, Quinn Jacobson and Alexandre M Bayen (2010), 'Evaluation of traffic data obtained via GPS-enabled mobile phones: The Mobile Century field experiment', *Transportation Research Part C: Emerging Technologies* **18**(4), 568–583.
URL: *http://www.sciencedirect.com/science/article/pii/S0968090X09001430*

Hofmann-Wellenhof, Bernhard, Herbert Lichtenegger and Elmar Wasle (2007), *GNSS - Global Navigation Satellite System: GPS, GLONASS, Galileo and more*, Springer.

IDC (2012), 'Android Marks Fourth Anniversary since Launch with 75.0% Market Share in Third Quarter, According to IDC'.
URL: *http://www.businesswire.com/news/home/20121101006891/en/Android-Marks-Fourth-Anniversary-Launch-75.0-Market*

ILA (2014), 'About In Location Alliance'.
URL: *http://inlocationalliance.org/*

Isaacs, Jason T, Andrew T Irish, Upamanyu Madhow and P Hespanha (2014), Bayesian Localization and Mapping Using GNSS SNR Measurements, *in* 'The Position Location and Navigation Symposium (PLANS)', Monterey, California.

Ito, S and N Kawaguchi (2005), 'Bayesian based location estimation system using wireless LAN'.

Ji, Shengyue, Wu Chen, Xiaoli Ding, Yongqi Chen, Chunmei Zhao and Congwei Hu (2010), 'Potential Benefits of GPS/GLONASS/GALILEO Integration in an Urban Canyon - Hong Kong', *The Journal of Navigation* **63**(04), 681–693.
URL: *http://dx.doi.org/10.1017/S0373463310000081*

Jiang, Ziyi, Paul Groves, W Y Ocheing, Shaojun Feng, C D Milner and P G Mattos (2011), Multi-Constellation GNSS Multipath Mitigation Using Consistency Checking, *in* 'ION GNSS 2011', Oregon Convention Center, Portland, Oregon.

Jones, Gary V., James C. Beck, Richard Keegan and Kevin Judge (1999), 'Automatic determination of traffic signal preemption using GPS, apparatus and method'.
URL: *http://www.google.co.uk/patents/US5926113*

Joshi, R R (2001), A new approach to map matching for in-vehicle navigation systems: the rotational variation metric, *in* 'Intelligent Transportation Systems, 2001. Proceedings. 2001 IEEE', pp. 33–38.

Julier, S J and J K Uhlmann (2004), Unscented filtering and nonlinear estimation, *in* 'Proceedings of the IEEE', Vol. 92, pp. 401–422.

Kalman, R E (1960), 'A New Approach to Linear Filtering and Prediction Problems', *ASME Transactions, Series D: Journal of Basic Engineering* **82**, 35–45.

Kim, H I, K D Park and H S Lee (2009), 'Development and validation of an integrated GNSS simulator using 3D spatial information', *Journal of the Korean Society of Surveying Geodesy Photogrammetry and Cartography* **27**(6), 659–667.
URL: *http://www.scopus.com/inward/record.url?eid=2-s2.0-78049439995&partnerID=40&md5=424d01c4bb3fa73232000ebf66a58f70*

Kleijer, F, D Odijk and E Verbree (2009), Prediction of GNSS availability and accuracy in urban environments - Case study Schiphol Airport. Chapter 23 of "Location Based Services and TeleCartography II", Springer-Verlag, Berlin Heidelberg, pp. 387–406.

Kolbe, Thomas H, Gerhard Gröger and Lutz Plümer (2005), CityGML: Interoperable access to 3D city models, *in* 'Geo-information for disaster management', Springer, pp. 883–899.

Krakiwsky, E J, C B Harris and R V C Wong (1988), A Kalman filter for integrating dead reckoning, map matching and GPS positioning, *in* 'Position Location and Navigation Symposium, 1988. Record. Navigation into the 21st Century. IEEE PLANS '88., IEEE', pp. 39–46.

Kwon, Jaimyoung, Transportation California. Dept. of, Berkeley Institute of Transportation Studies University of California, Transit Partners for Advanced and Highways (2007), *Evaluation of PeMS to improve the congestion monitoring system*, California PATH Program, Institute of Transportation Studies, University of California at Berkeley, Berkeley, Calif.

Kwon, Woong and Sukhan Lee (2002), 'Performance evaluation of decision making strategies for an embedded lane departure warning system.', *J. Field Robotics* **19**(10), 499–509.
URL: *http://dblp.uni-trier.de/db/journals/jfr/jfr19.html#KwonL02*

Ladd, Andrew M, Kostas E Bekris, Algis Rudys, Guillaume Marceau, Lydia E Kavraki and Dan S Wallach (2002), Robotics-based location sensing using wireless ethernet, *in* 'Proceedings of the 8th annual international conference on Mobile computing and networking', ACM, Atlanta, Georgia, USA, pp. 227–238.

Lee, Sang Hyuk, Soobin Lee, Heecheol Song and Hwang Soo Lee (2009), Wireless sensor network design for tactical military applications: remote large-scale environments, *in* 'Military Communications Conference, 2009. MILCOM 2009. IEEE', IEEE, pp. 1–7.

Lei, Z (2009), *Research on the GPS/Pseudolite Integration Positioning System*, World Acad Union-World Acad Press, Liverpool.
URL: *<Go to ISI>://000268886700053*

Lewis, F L (2004), Wireless Sensor Networks, *in* D. J.Cook and S. K.Das, eds, 'Smart Environments: Technologies, Protocols, and Applications', John Wiley.

Liu, Hui, H Darabi, P Banerjee and Jing Liu (2007), 'Survey of Wireless Indoor Positioning Techniques and Systems', *Systems, Man, and Cybernetics, Part C: Applications and Reviews, IEEE Transactions on* **37**(6), 1067–1080.

Luckey, Palmer (2014), 'Oculus Rift'.
URL: *http://en.wikipedia.org/wiki/Oculus_Rift*

Mao, Guoqiang, Baris Fidan and Brian Anderson (2007), 'Wireless sensor network localization techniques', *Computer Networks* **51**(10), 2529–2553.
URL: *http://www.sciencedirect.com/science/article/pii/S1389128606003227*

Mark Crossley (2012), 'A guide to coordinate systems in Great Britain'.
URL: *http://www.bnhs.co.uk/focuson/grabagridref/html/OSGB.pdf*

McCall, J C and M M Trivedi (2004), Visual context capture and analysis for driver attention monitoring, *in* 'Intelligent Transportation Systems, 2004. Proceedings. The 7th International IEEE Conference on', pp. 332–337.

McCall, J C and M M Trivedi (2006), 'Video-based lane estimation and tracking for driver assistance: Survey, system, and evaluation', *Ieee Transactions on Intelligent*

Transportation Systems **7**(1), 20–37.
URL: *<Go to ISI>://WOS:000237216300002*

Meguro, Jun-ichi, Taishi Murata, Jun-ichi Takiguchi, Yoshiharu Amano and Takumi Hashizume (2009), 'GPS multipath mitigation for urban area using omnidirectional infrared camera', *Trans. Intell. Transport. Sys.* **10**(1), 22–30.

Meiyappan, S., A. Raghupathy and G. Pattabiraman (2013), Positioning in GPS Challenged Locations - The NextNav Terrestrial Positioning Constellation, *in* 'Proceedings of the 26th International Technical Meeting of The Satellite Division of the Institute of Navigation (ION GNSS+ 2013)', Nashville, TN.

Meng, X, G W Roberts, A H Dodson, E Cosser, J Barnes and C Rizos (2004), 'Impact of GPS satellite and pseudolite geometry on structural deformation monitoring: analytical and empirical studies', *Journal of Geodesy* **77**(12), 809–822.
URL: *http://dx.doi.org/10.1007/s00190-003-0357-y*

Microsoft (2014), 'Explore 3D cities with the Bing Maps Preview app'.
URL: *http://www.bing.com/dev/en-us/maps-preview-app*

Miles, John, Martial Chevreuil, Fritz Busch, Lise Filion, Richard Harris and Valerie Briggs (2000), *PIARC ITS Handbook*, World Road Association (PIARC) Technical Committee on Network Operations.

Misra, Pratap and Per Enge (2010), *Global Positioning System: Signals, Measurements, and Performance Revised Second Edition*, Ganga-Jamuna Press (December 1, 2010).

Montillet, J-P., A. Taha, X. Meng and G. W. Robert (2007), 'Buried Assets: Testing GPS and GSM in Urban Canyons', *GPS World* **18**(3).

Montillet, J.-P., G. W. Roberts, C. Hancock, X. Meng, O. Ogundipe and J. Barnes (2009), 'Deploying a Locata network to enable precise positioning in urban canyons', *Journal of Geodesy* **83**(2), 91–103.
URL: *http://dx.doi.org/10.1007/s00190-008-0236-7*

Moore, I I James E, Seongkil Cho, Arup Basu and Daniel B Mezger (2001), 'Use of Los Angeles Freeway Service Patrol Vehicles as Probe Vehicles'.
URL: *http://www.escholarship.org/uc/item/8qf8430v*

Morrison, A, S Krishnan, A Anpalagan and Navigation Institute of (2006), Receiver Autonomous Mitigation of GPS Non Line-of-Sight Multipath Errors, *in* 'Proceedings of the 2006 National Technical Meeting of the Institute of Navigation - NTM 2006', Inst Navigation, Washington, pp. 141–148.
URL: *<Go to ISI>://000279767800008*

Mountain, David and Jonathan Raper (2001), 'Positioning techniques for location-based services (LBS): characteristics and limitations of proposed solutions', *Aslib Journal of Information Management* **53**, 404–412.

Nedic, S (2009), On GPS Signal Multipath Modeling in Dynamic Environments, *in* '2009 IEEE Aerospace Conference, Vols 1-7', IEEE, New York, pp. 1162–1172.
URL: *<Go to ISI>://000271964000113*

Nilsson, Nils J (2009), Chapter 28 Bayesian Networks, *in* 'The Quest for Artificial Intelligence', Cambridge University Press.
URL: *http://www.cambridge.org/us/academic/subjects/computer-science/artificial-intelligence-and-natural-language-processing/quest-artificial-intelligence?format=PB*

NMEA (2014), 'About the National Marine Electronics Association (NMEA): ORGANIZATIONAL PROFILE'.
URL: *http://www.nmea.org/content/about_the_nmea/about_the_nmea.asp*

Nokia (2014), 'Nokia Here maps for life'.
URL: *http://here.com/*

Novakovic, G, A Dapo and H Mahovic (2009), 'Development and Pseudolite Applications in Positioning and Navigation', *Geodetski List* **63**(3), 215–241.
URL: *<Go to ISI>://000271449600002*

Obst, M, S Bauer and G Wanielik (2012), 'Urban multipath detection and mitigation with dynamic 3D maps for reliable land vehicle localization'.

Ochieng, W Y, K F Sheridan, K Sauer, X Han, P A Cross, S Lannelongue, N Ammour and K Petit (2002), 'An Assessment of the RAIM Performance of a Combined Galileo/GPS Navigation System Using the Marginally Detectable Errors (MDE) Algorithm', *GPS Solutions* **5**(3), 42–51.
URL: *http://dx.doi.org/10.1007/PL00012898*

OpenStreetMap (2014), 'Open Street Maps'.
URL: *http://www.openstreetmap.org/*

Palmer, Duncan, Terry Moore, Chris Hill, Marcus Andreotti and David Park (2011), 'Radio Positioning using the Digital Audio Broadcasting (DAB) Signal', *The Journal of Navigation* **64**(01), 45–59.
URL: *href="http://dx.doi.org/10.1017/S037346331000041X*

Peyraud, Sébastien, David Bétaille, Stéphane Renault, Miguel Ortiz, Florian Mougel, Dominique Meizel and François Peyret (2013), 'About Non-Line-Of-Sight Satellite Detection and Exclusion in a 3D Map-Aided Localization Algorithm', *Sensors* **13**(1), 829–847.
URL: *http://www.mdpi.com/1424-8220/13/1/829 http://www.mdpi.com/1424-8220/13/1/829/pdf*

Purcell, Timothy J, Ian Buck, William R Mark and Pat Hanrahan (2002), 'Ray tracing on programmable graphics hardware', *ACM Transactions on Graphics* **21**(3).
URL: *http://portal.acm.org/citation.cfm?doid=566654.566640*

Quddus, Mohammed A., Washington Y. Ochieng, L. Zhao and Robert B. Noland (2003), 'A general map matching algorithm for transport telematics applications', *GPS Solutions* **7**(3), 157–167.
URL: *http://dx.doi.org/10.1007/s10291-003-0069-z*

Quddus, Mohammed A, Washington Y Ochieng and Robert B Noland (2007), 'Current map-matching algorithms for transport applications: State-of-the art and

future research directions', *Transportation Research Part C: Emerging Technologies* **15**(5), 312–328.
URL: *http://www.sciencedirect.com/science/article/pii/S0968090X07000265*

Quest-Geo-Solutions-Ltd (2004), 'Grid InQuest DLL User Manual (Version 6)'.

Rabinowitz, M and J J Spilker Jr. (2005), A new positioning system using television synchronization signals, *in* 'Broadcasting, IEEE Transactions on', Vol. 51, pp. 51–61.

Rashid, Omer, Paul Coulton and Reuben Edwards (2005), Implementing Location Based Information/Advertising for Existing Mobile Phone Users in Indoor/Urban Environments, *in* 'Proceedings of the International Conference on Mobile Business', IEEE Computer Society, pp. 377–383.

Rashid, Omer, Paul Coulton and Reuben Edwards (2008), 'Providing Location Based Information/Advertising for Existing Mobile Phone Users', *Personal Ubiquitous Comput.* **12**(1), 3–10.
URL: *http://dx.doi.org/10.1007/s00779-006-0121-4*

Ratti, C, R M Pulselli, S Williams and D Frenchman (2006), 'Mobile Landscapes: using location data from cell phones for urban analysis', *Environment and Planning B: Planning and Design* **33**(5), 727–748.
URL: *http://www.envplan.com/abstract.cgi?id=b32047*

Reid, D B (1979), 'An algorithm for tracking multiple targets', *Automatic Control, IEEE Transactions on* **24**(6), 843–854.

Rhinoceros (2014), 'Rhinoceros'.
URL: *http://www.rhino3d.com/*

Rizos, Chris and Chris R Drane (1998), *Positioning Systems in Intelligent Transportation Systems*, Artech House, Inc, Norwood, MA, USA.

Roberts, G W, X Meng, A H Dodson and E Cosser (2002), 'Multipath mitigation for bridge deformation monitoring', *Journal of Global Positioning Systems* **1**, 25–33.

Roos, Teemu, Petri Myllymäki, Henry Tirri, Pauli Misikangas and Juha Sievänen (2002), 'A Probabilistic Approach to WLAN User Location Estimation', *International Journal of Wireless Information Networks* **9**(3), 155–164.
URL: *http://dx.doi.org/10.1023/A:1016003126882*

RussianFederalSpaceAgency (2014), 'GLONASS status'.
URL: *http://www.glonass-center.ru/en/GLONASS/*

Saab, S S and Z M Kassas (2006), 'Power matching approach for GPS coverage extension', *Intelligent Transportation Systems, IEEE Transactions on* **7**(2), 156–166.

Sayed, A H, A Tarighat and N Khajehnouri (2005), 'Network-based wireless location: challenges faced in developing techniques for accurate wireless location information', *Signal Processing Magazine, IEEE* **22**(4), 24–40.

Schiller, Jochen and Agnès Voisard (2004), *Location-Based Services*, Elsevier.

Shoval, Noam (2008), 'Tracking technologies and urban analysis', *Cities* **25**(1), 21–28.
URL: *http://www.sciencedirect.com/science/article/pii/S0264275107000777*

Shreiner, Dave, Graham Sellers, John M Kessenich and Bill M Licea-Kane (2013), *OpenGL programming guide: The Official guide to learning OpenGL, version 4.3*, Addison-Wesley Professional.

Steed, Anthony (2004), Supporting Mobile Applications with Real-Time Visualisation of GPS Availability, *in* S.Brewster and M.Dunlop, eds, '6th International Symposium, MobileHCI', Vol. 3160, Springer Berlin Heidelberg, Glasgow, UK, chapter 40, pp. 373–377.
URL: *http://dx.doi.org/10.1007/978-3-540-28637-0_40*

Suh, Y and R Shibasaki (2007), 'Evaluation of satellite-based navigation services in complex urban environments using a three-dimensional GIS', *IEICE Transactions on Communications* **E90-B**(7), 1816–1825.

URL: *http://www.scopus.com/inward/record.url?eid=2-s2.0-48749110416&partnerID=40&md5=69ff1d945dead95c74334cd2760e6d6e*

Susca, S and Navigation Inst (2010), GNSS-independent Navigation Solution Using Integrated LiDAR Data, *in* 'Proceedings of the 2010 International Technical Meeting of the Institute of Navigation - ITM 2010', Inst Navigation, Washington, pp. 205–213.
URL: *<Go to ISI>://000280139100022*

Suzuki, T and N Kubo (2013), Correcting GNSS Multipath Errors Using a 3D Surface Model and Particle Filter, *in* 'ION GNSS 2013', Nashville, TN, pp. 1583–1595.

Suzuki, T. and N. Kubo (2014), N-LOS GNSS Signal Detection Using Fish-Eye Camera for Vehicle Navigation in Urban Environments, *in* 'ION GNSS+ 2014', Tampa, FL.

Suzuki, Taro and Nobuaki Kubo (2012), GNSS Positioning with Multipath Simulation using 3D Surface Model in Urban Canyon, *in* 'ION GNSS 2012', Nashville, TN.

Suzuki, Taro, Yoshiharu Amano and Takumi Hashizume (2011), High-accuracy GPS and GLONASS positioning by multipath mitigation using omnidirectional infrared camera, *in* 'ICRA 2011', pp. 311–316.

Syed, S. and M.E. Cannon (2004), Fuzzy Logic Based-Map Matching Algorithm for Vehicle Navigation System in Urban Canyons, *in* 'ION National Technical Meeting', San Diego, CA.

Syed, Z, P Aggarwal, Y Yang and N El-Sheimy (2008), 'Improved Vehicle Navigation Using Aiding with Tightly Coupled Integration'.

Syrjarinne, Jari and Lauri Wirola (2008), 'GNSS Solutions: accuracy, integrity, continuity and availability', *Inside GNSS* pp. 20–24.

Thrun, Sebastian, Dieter Fox and Wolfram Burgard (2005), *Probabilistic Robotics*, MIT Press.

Tiberius, Christian and Verbree, Edward (2004), GNSS positioning accuracy and availability within Location Based Services: The advantages of combined GPS-Galileo positioning, *in* 'NaviTec 2004', Noordwijk, Netherlands.

Trevisani, E and A Vitaletti (2004), Cell-ID location technique, limits and benefits: an experimental study, *in* 'Mobile Computing Systems and Applications, 2004. WMCSA 2004. Sixth IEEE Workshop on', pp. 51–60.

Urmson, Chris, Joshua Anhalt, Drew Bagnell, Christopher Baker, Robert Bittner, M N Clark, John Dolan, Dave Duggins, Tugrul Galatali, Chris Geyer, Michele Gittleman, Sam Harbaugh, Martial Hebert, Thomas M Howard, Sascha Kolski, Alonzo Kelly, Maxim Likhachev, Matt McNaughton, Nick Miller, Kevin Peterson, Brian Pilnick, Raj Rajkumar, Paul Rybski, Bryan Salesky, Young-Woo Seo, Sanjiv Singh, Jarrod Snider, Anthony Stentz, William Red Whittaker, Ziv Wolkowicki, Jason Ziglar, Hong Bae, Thomas Brown, Daniel Demitrish, Bakhtiar Litkouhi, Jim Nickolaou, Varsha Sadekar, Wende Zhang, Joshua Struble, Michael Taylor, Michael Darms and Dave Ferguson (2008), 'Autonomous driving in urban environments: Boss and the Urban Challenge', *Journal of Field Robotics* **25**(8), 425–466.
URL: *http://dx.doi.org/10.1002/rob.20255*

USA (2014), 'Official GPS status'.
URL: *http://www.gps.gov/systems/gps/performance/accuracy/*

VanDiggelen, Frank (2009), *A-GPS: Assisted GPS, GNSS, and SBAS*, 1 edition edn, Artech House.

Viandier, N, D F Nahimana, J Marais and E Duflos (2008), Gnss performance enhancement in urban environment based on pseudo-range error model, *in* 'Position, Location and Navigation Symposium, 2008 IEEE/ION', pp. 377–382.

Walker, Rodney and Kubik, Kurt (1996), Numerical Modelling of GPS Signal Propagation, *in* 'Proceedings of the 9th International Technical Meeting of the Satellite Division of The Institute of Navigation (ION GPS 1996)', Kansas City, MO, pp. 709—-717.

Wang, Jinling and Steve Hewitson (2006), 'GNSS receiver autonomous integrity monitoring (RAIM) performance analysis', *GPS Solutions* **10**(3), 155–170.

Wang, Lei (2014*a*), 'GNSS Shadow Matching real-time demo'.
URL: *http://youtu.be/jp12XQyCwQQ*

Wang, Lei (2014*b*), Kinematic GNSS Shadow Matching Using a Particle Filter, *in* 'ION GNSS+', Tampa.

Wang, Lei, Paul D Groves and Marek K Ziebart (2011), GNSS Shadow Matching Using A 3D Model of London, *in* 'European Navigation Conference', Grange Tower Bridge, London, United Kingdom.

Wang, Lei, Paul D Groves and Marek K Ziebart (2012*a*), GNSS Shadow Matching: Improving Urban Positioning Accuracy Using a 3D City Model with Optimized Visibility Prediction Scoring, *in* 'ION GNSS 2012', Nashville, Tennessee.

Wang, Lei, Paul D Groves and Marek K Ziebart (2013*a*), 'GNSS Shadow Matching: Improving Urban Positioning Accuracy Using a 3D City Model with Optimized Visibility Prediction Scoring', *NAVIGATION: Journal of The Institute of Navigation* **23**(3), 44–56.

Wang, Lei, Paul D Groves and Marek K Ziebart (2013*b*), Shadow Matching: Improving Smartphone GNSS Positioning in Urban Environments, *in* 'China Satellite Navigation Conference (CSNC) 2013 Proceedings', Vol. 245, Springer, chapter 57, pp. 613–621.
URL: *http://dx.doi.org/10.1007/978-3-642-37407-4_57*

Wang, Lei, Paul D Groves and Marek K Ziebart (2013*c*), Urban Positioning on a Smartphone: Real-time Shadow Matching Using GNSS and 3D City Models, *in* 'ION GNSS 2013'.

Wang, Lei, Paul D Groves and Marek K Ziebart (2014), 'Smartphone Shadow Matching for Better Cross-street GNSS Positioning in Urban Environments', *Accepted by Journal of Navigation* .

Wang, Lei, Paul D Groves and Marek Ziebart (2012*b*), 'Multi-constellation GNSS Performance Evaluation for Urban Canyons Using Large Virtual Reality City Models', *Journal of Navigationn* **65**(03), 459–476.
URL: *http://dx.doi.org/10.1017/S0373463312000082*

Webb, Toby A, Paul D Groves, Paul A Cross, Robert J Mason and Joseph H Harrison (2010), A new differential positioning method using modulation correlation of signals of opportunity, *in* 'Position Location and Navigation Symposium (PLANS), 2010 IEEE/ION', Indian Wells/Palm Springs, California, pp. 972–981.
URL: *10.1109/PLANS.2010.5507270*

White, Christopher E, David Bernstein and Alain L Kornhauser (2000), 'Some map matching algorithms for personal navigation assistants', *Transportation Research Part C: Emerging Technologies* **8**(1-6), 91–108.
URL: *http://www.sciencedirect.com/science/article/pii/S0968090X00000267*

Ygnace, Jean-Luc (2011), 'Travel time speed estimates on the french rhone corridor network using cellular phones as probes', *STRIP (System for Traffic Information and Positioning) Project* **201**.

Yim, Y B and Randall Cayford (2001), 'Investigation of vehicles as probes using global positioning system and cellular phone tracking: field operational test', *California Partners for Advanced Transit and Highways (PATH)* .

You, Yilun, Tat Jun Chin, Joo Hwee Lim, Jean-Pierre Chevallet, #233, line Coutrix and Laurence Nigay (2008), 'Deploying and evaluating a mixed reality mobile treasure hunt: Snap2Play'.

Yozevitch, B., B. Ben Moshe and H. Levy (2012), Breaking the 1 meter accuracy bound in commercial GNSS devices, *in* 'Electrical and Electronics Engineers in Israel (IEEEI), 2012 IEEE 27th Convention of', pp. 1–5.

Yozevitch, R, B BenMoshe and A Dvir (2014), 'GNSS Accuracy Improvement Using Rapid Shadow Transitions', *Intelligent Transportation Systems, IEEE Transactions on* **PP**(99), 1–10.

Zandbergen, Paul A (2009), 'Accuracy of iPhone Locations: A Comparison of Assisted GPS, WiFi and Cellular Positioning', *Transactions in GIS* **13**, 5–25.
URL: *http://dx.doi.org/10.1111/j.1467-9671.2009.01152.x*

Zhang, X G, Q Wang and D J Wan (2007), 'Map matching in road crossings of urban canyons based on road traverses and linear heading-change model', *Ieee Transactions on Instrumentation and Measurement* **56**(6), 2795–2803.
URL: *<Go to ISI>://000251745500083*

Zhou, C M, J Downey, D Stancil, T Mukherjee and Ieee (2009), A Compact Positioning and Velocity RF Sensor for Improved Inertial Navigation, *in* '2009 IEEE/Mtt-S International Microwave Symposium, Vols 1-3', IEEE MTT-S International Microwave Symposium, IEEE, New York, pp. 1421–1424.
URL: *<Go to ISI>://000273507400357*

Zito, R, G D'Este and M A P Taylor (1995), 'Global positioning systems in the time domain: How useful a tool for intelligent vehicle-highway systems?', *Transportation Research Part C: Emerging Technologies* **3**(4), 193–209.
URL: *http://www.sciencedirect.com/science/article/pii/0968090X95000065*

Appendix A.

Line and Triangle Intersection Determination Algorithm

Algorithms testing direct line-of-sight (LOS) visibility are mature in computer vision and are known as line segment-plane collision detection. Among those algorithms, one suitable for use in determining whether a satellite is blocked by buildings is described in this appendix.

A.1. Geometrical representation in satellite visibility determination

The satellite position and user position are denoted S and U in the model, respectively. The buildings in the city model are each represented by multiple triangles (triangle meshes). Consider a triangle ΔABC with vertices A, B and C. The intersection point of the segment US (line-of-sight vector) and the plane containing ΔABC is denoted I. The vector $\mathbf{r_{AB}}$denote the position of point B with respect to point A defining the line $\overline{AB}$. All other vectors are similarly defined. The normal vector to ΔABC is $\mathbf{n}$. The origin is O. This is illustrated in Figure A.1.

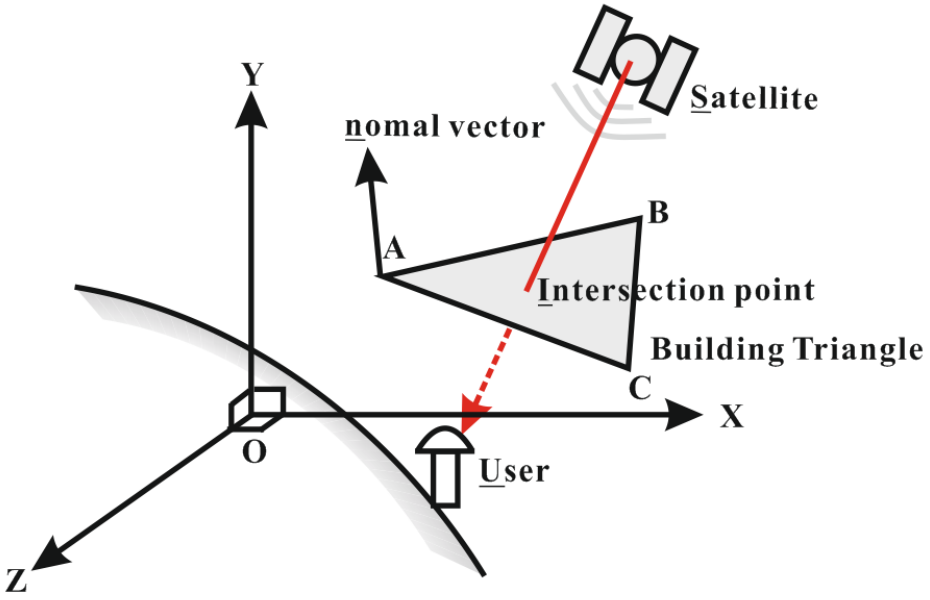

Figure A.1.: Intersection between user-satellite line of sight and a triangular component of a building model

A.2. Intersection algorithm

Ray and triangle intersection is a common operation in computer graphics. A three-step method is implemented comprising the following steps.

1) Determine whether there is an intersection of the plane containing ΔABC and the segment US.

2) Compute the point of intersection I where it exists.

3) Test whether the point of intersection I is inside or outside the boundary of ΔABC. The steps are now described in more detail. Equations A.1 and A.2 show vectors in the plane of ΔABC.

$$\mathbf{r_{AC}} = \mathbf{r_{OC}} - \mathbf{r_{OA}} \tag{A.1}$$

$$\mathbf{r_{AB}} = \mathbf{r_{OB}} - \mathbf{r_{OA}} \tag{A.2}$$

The normal vector to ΔABC:

$$\mathbf{n} = \mathbf{r_{AC}} \times \mathbf{r_{AB}} \tag{A.3}$$

As I lies on the line US, it is subject to the its parametric equation:

$$\mathbf{r_{OI}} = \mathbf{r_{OS}} + \mathbf{t}.(\mathbf{r_{OS}} - \mathbf{r_{OU}}) \tag{A.4}$$

The vector $\mathbf{r_{OI}}$, $\mathbf{r_{OS}}$ and $\mathbf{r_{OU}}$, respectively denote the points of I, S and U with respect to the origin O. t is a real number and $0 < t < 1$, since satellites have a longer distance to earth than users.

If $\mathbf{n}.(\mathbf{r_{OS}} - \mathbf{r_{OU}}) = 0$, then the user-satellite LOS vector is parallel with the plane, which means that there is no intersection between LOS. Otherwise, it intersect the plane of ΔABC.

The second step is to determine the position of the intersection point I. Because Ilies within the plane of ΔABC, $\mathbf{n}.(\mathbf{r_{OS}} - \mathbf{r_{OU}}) = 0$, therefore from (A.4),

$$[\mathbf{r_{OS}} + t.(\mathbf{r_{OU}} - \mathbf{r_{OS}}) - \mathbf{r_{OA}}].\mathbf{n} = 0 \tag{A.5}$$

Rearranging:

$$t = \frac{(\mathbf{r_{OA}} - \mathbf{r_{OS}}).\mathbf{n}}{(\mathbf{r_{OU}} - \mathbf{r_{OS}}).\mathbf{n}} \tag{A.6}$$

Substituting this into (A.4) gives the position of I.

The third step is to determine whether the point of intersection is within ΔABC. If it is, then the user-satellite LOS is blocked by ΔABC, which means that the building is blocking the GNSS signal. A method based on triangle area computation is used as described below.

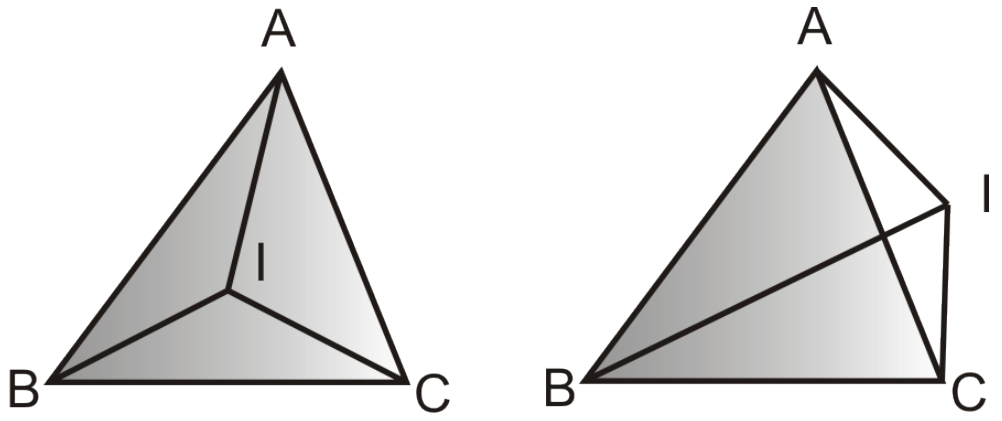

Figure A.2.: A point I lying within ΔABC (left) and outside ΔABC(right)

There are two scenarios to consider. One is where point of the intersection is within the triangle or on the boundary. The other where it is outside of the triangle. Let S denote the area of a triangle. If

$$S_{\Delta ABC} = S_{\Delta ABI} + S_{\Delta AIC} + S_{\Delta IBC} \tag{A.7}$$

Then I is inside ΔABC or on the boundary, as illustrated in Figure A.2 (left). While if

$$S_{\Delta ABC} < S_{\Delta ABI} + S_{\Delta AIC} + S_{\Delta IBC} \tag{A.8}$$

I is outside , as illustrated in Figure A.2 (right).

$$S_{\Delta ABI} + S_{\Delta AIC} + S_{\Delta IBC} = S_{\Delta ABC} + 2S_{\Delta AIC} > SS \tag{A.9}$$

The area of a triangle can be computed using Heron's formula (Alperin, 1987):

$$S_{\Delta ABC} = \sqrt{p \cdot (p-a) \cdot (p-b) \cdot (p-c)} \tag{A.10}$$

where

a is the length of side BC of ΔABC,

b is the length of side AC of ΔABC,

c is the length of side AB of ΔABC,

$p = \frac{a+b+c}{2}$.